

Worcester Polytechnic Institute

Digital WPI

Major Qualifying Projects (All Years)

Major Qualifying Projects

2020-05-14

Design and Optimization of an FSAE Vehicle

Avery M. Ingegneri

Worcester Polytechnic Institute

Erika H. Sanborn

Worcester Polytechnic Institute

Jarred O. Measmer

Worcester Polytechnic Institute

John Paul Williams

Worcester Polytechnic Institute

Maxwell J. Pellerin

Worcester Polytechnic Institute

See next page for additional authors

Follow this and additional works at: <https://digitalcommons.wpi.edu/mqp-all>

Repository Citation

Ingegneri, A. M., Sanborn, E. H., Measmer, J. O., Williams, J. P., Pellerin, M. J., & Duff, R. B. (2020). *Design and Optimization of an FSAE Vehicle*. Retrieved from <https://digitalcommons.wpi.edu/mqp-all/7440>

This Unrestricted is brought to you for free and open access by the Major Qualifying Projects at Digital WPI. It has been accepted for inclusion in Major Qualifying Projects (All Years) by an authorized administrator of Digital WPI. For more information, please contact digitalwpi@wpi.edu.

Author

Avery M. Ingegneri, Erika H. Sanborn, Jarred O. Measmer, John Paul Williams, Maxwell J. Pellerin, and Robert B. Duff

Design and Optimization of an FSAE Vehicle

A Major Qualifying Project Submitted to the Faculty of
Worcester Polytechnic Institute
in partial fulfilment of the requirements for the
Bachelor of Science Degree in
Mechanical Engineering and Computer Science by:

Robert Duff, ME

Avery Ingegneri, ME

Jarred Measmer, ME

Pedro de Vasconcellos
Oporto, ME/CS

Maxwell Pellerin, ME

Erika Sanborn, ME

John Williams, ME

Date: May 14th 2020

Approved By:

Professor David Planchard

Table of Contents

Table of Contents	1
Abstract	4
Executive Summary	5
Table of Figures	6
Units	9
Units (SI and US)	9
Frame	11
Powertrain	19
Intake Plenum	19
Exhaust	25
Engine Mounts	27
Shifting	32
Next Steps	35
Fuel Pump and Injector	36
Fuel Tank	37
Cooling System	40
Next Steps	44
Intake System	44
Cooling System	44
Brake System	45
Calipers	46
Master Cylinders	47
Pedal Ratio	47
Pedal Box, Brake Pedal, and Balance Bar	48
Rotors	51
Next Steps	56
Suspension	57
Tires	57
Wheels	59
Linkage Layout	61
Steering System	63
Control Arms	65

Rockers	67
Next Steps	69
Bodywork.....	70
General Design Choices.....	70
Design	71
Nosecone.....	71
Side Pods.....	71
Manufacturing.....	71
Next Steps	75
Finish Nosecone Mold	75
Assemble Side Pod Mold(s).....	75
Vacuum bagging layup of all components.....	76
Fastening Panels to Frame	76
Ergonomics	77
Firewall	77
Digital Sensor System.....	79
Objectives	79
State of the art	80
Objectives for each subsystem.....	84
Conclusion & Results - Digital Sensor System.....	102
Appendix A: SOLIDWORKS Studies	103
Pedal Box Version 1	103
Drilled Brake Rotor.....	105
Appendix B: Status of Components.....	109
Intake System.....	109
Exhaust System.....	109
Engine Mounts	109
Brake System	109
Suspension	110
Bodywork.....	111
Appendix C: Calculations	112
Brake System: Front	112
Brake System: Rear.....	114

Appendix D: References:	115
-------------------------------	-----

Abstract

The purpose of this Major Qualifying Project was to design and build a race car for the Formula SAE Michigan Design Competition. Each year, WPI prepares a new car for this competition, with the intention of improving the team's overall performance in the competition. After the 2019 event, a number of design changes were identified to be applied to this year's vehicle. These were the result of design judging at competition, as well as in-house analysis from both performance and manufacturing perspectives.

For this year's team, the focus was to transition the car from 13 inch diameter wheels to 10 inch diameter wheels, while maintaining current powertrain output and drivability of the previous car. The reasons behind this were to reduce unsprung mass of the vehicle and to transition to Hoosier's LC0 tire compound, a tire compound with a theoretically better temperature range for the type of driving done in FSAE. In order to do this successfully, a new suspension system, braking system, frame, and accompanying parts needed to be designed. The team focused on carrying over the powertrain system, while improving packaging and reducing weight of other systems. The final goals of this car were to achieve a reduced or similar weight to the 2019 car, have improved drivability and handling, and maintain the power output and delivery from the 2019 car.

Executive Summary

To achieve a design that will theoretically perform and score better in competition, each subsystem of the 2019 vehicle was first revisited to determine what improvements would need to be made. This analysis indicated that the primary areas for improvement were the cornering performance of the vehicle, and the team's performance in the design event.

The first step taken to address these issues was a redesigned suspension system, designed around a new model of tier. The team partnered with a consortium of other schools to gather tire data from the CALSPAN Tire Performance Testing Laboratory in Buffalo, NY. Using OptimumK kinematics software, the linkage layout and pickup points were determined. These points were then used as the basis to design a new frame for the vehicle. The frame was based upon the 2019 car's geometry, while incorporating these new pickup points as well as making the cockpit larger and lower to the ground.

In parallel, a new brake system was designed to suit the smaller wheels using the car's estimated weight to calculate load transfer and size brake system components. To provide enough stopping force with smaller rotor areas, properly sized ISR calipers and Tilton master cylinders were selected.

The ergonomic components of the car were designed with simplicity in mind. The steering wheel, steering box, and steering rack have been carried over from last year's car, where they proved to be effective. The pedal box is a new design, utilizing a flat plate to incorporate modular pedal and master cylinder mounts for different driver heights. The seat of the car was to be constructed from expanding foam to guarantee a proper fit for different driver sizes.

The powertrain components of the car also saw some development with both intake and exhaust. Building upon the developments of previous years, this year saw a larger and improved intake manifold, along with improved routing of the intake to lower the overall center of gravity. Development of the exhaust was also performed with the routing also being changed to accommodate the new suspension set up while also improving the center of gravity.

New bodywork was also designed to optimize airflow around the radiator and accommodate the new control arm and suspension geometry.

Lastly, the team began development of an onboard cloud based sensor and data logging system. The goals of this system are to deliver real time performance data about the car while on track and during testing.

Table of Figures

<i>Figure 1: The comparison model used to determine geometry.....</i>	<i>11</i>
<i>Table 1: Loads Used for Frame FEA Studies</i>	<i>12</i>
<i>Figure 2: First New Frame Iteration.....</i>	<i>12</i>
<i>Figure 3: FSAE Cockpit Entry Template.....</i>	<i>13</i>
<i>Figure 4: Second Frame Iteration with rules compliant side impact members highlighted.....</i>	<i>14</i>
<i>Figure 5: Final Frame Design Iteration.....</i>	<i>16</i>
<i>Figure 6: Front Impact Study Factor of Safety.....</i>	<i>17</i>
<i>Figure 7: Longitudinal Axis Torsional Rigidity Study.....</i>	<i>17</i>
<i>Figure 8: Horizontal Axis Torsional Rigidity Study</i>	<i>18</i>
<i>Figure 9: Restrictor Rule from the 2020 FSAE Rulebook.</i>	<i>19</i>
<i>Figure 10: Simulation Representation and Results from 2018 validated in 2020</i>	<i>21</i>
<i>Figure 11: Bellmouth design and model for intake runner bellmouth.....</i>	<i>22</i>
<i>Figure 12: Intake Pulse Simulation Input Data Representation</i>	<i>23</i>
<i>Figure 13: Representation of Flow Trajectories in 2020 Intake Plenum</i>	<i>24</i>
<i>Figure 14: 3D printed intake system.....</i>	<i>25</i>
<i>Figure 15: Preliminary Exhaust routing example</i>	<i>26</i>
<i>Figure 16: Exhaust Mounting Solution.....</i>	<i>27</i>
<i>Figure 17: Front engine mount topology study</i>	<i>28</i>
<i>Figure 18: Front engine mount simulation fixed connections</i>	<i>29</i>
<i>Figure 19: Front engine mount displacement under load (mm).....</i>	<i>29</i>
<i>Figure 20: Front engine mount factor of safety plot</i>	<i>30</i>
<i>Figure 21: Rear engine mount factor of safety</i>	<i>31</i>
<i>Figure 22: Rear engine mount displacement under load.....</i>	<i>32</i>
<i>Figure 23: Shift Drum.....</i>	<i>32</i>
<i>Figure 24: Servo</i>	<i>33</i>
<i>Figure 25: Servo Mount.....</i>	<i>34</i>
<i>Figure 26: Shifting Assembly Side View</i>	<i>35</i>
<i>Figure 27: Shifting Assembly Isometric View</i>	<i>35</i>
<i>Figure 28: Suzuki RMZ 450 Pump Assembled with CNC Machined Adapter</i>	<i>37</i>
<i>Figure 29: New Fuel Tank Design.....</i>	<i>38</i>
<i>Figure 30: New Fuel Tank Packaging.....</i>	<i>38</i>
<i>Figure 31: Fuel Tank Baffle</i>	<i>39</i>
<i>Figure 32: Fuel Tank Manufactured and Mocked Up Prior to Welding.....</i>	<i>39</i>
<i>Figure 33: Mishimoto YFM660R radiator.....</i>	<i>41</i>
<i>Figure 34: Side pod analysis 1</i>	<i>42</i>
<i>Figure 35: Side pod analysis 2</i>	<i>43</i>
<i>Figure 36: Side pod analysis 3</i>	<i>43</i>
<i>Figure 37: Side pod analysis 4</i>	<i>44</i>
<i>Figure 38: Test procedure for determining maximum braking force</i>	<i>45</i>
<i>Figure 39: ISR 22-048 Caliper (Right) and ISR 22-049 Caliper (Left).....</i>	<i>46</i>
<i>Figure 40: The Wilwood Remote Fixed Master Cylinder Used on the 2019 Car (Left) and the Tilton 78 Series Used on the 2020 car (Right)</i>	<i>47</i>

Figure 41: Pedal Ratio Calculation Diagram	48
Figure 42: Iteration one of the pedal box design.....	49
Figure 43: Pedal Box FEA	50
Figure 44: Tilton 600 Series Balance Bar (Left) vs. Tilton 900 Series Balance Bar (Right)	50
Figure 45: Iteration Two of the Pedal Box Design.....	51
Figure 47: Slotted Rotor Thermal Simulation and Temperature vs. Time Plot.....	54
Figure 48: Rotor Temperature vs. Time of Solid vs. Drilled Rotors.....	55
Figure 49: Tire Testing Consortium Test Rig.....	58
Figure 50: Braid Roadwheel.....	60
Figure 51: Four Basic Modes of Vehicle Behavior	61
Figure 52: Basic Linkage Layout, from Milliken 17.5.....	62
Figure 53: The relationship between wheelbase, toe angle, and corner radius	63
Figure 54: Rudolph Ackermann's Race Car.....	64
Figure 55: Ackermann's Steering Effect.....	65
Figure 56: Control Arm FEA Studies	67
Figure 57: Front Rocker Assembly.....	68
Figure 58: Damper Rod-End Assortment (Front, Rear, Original)	68
Figure 60: Contours printed on poster paper.....	72
Figure 61: Contours glued to foam board	72
Figure 62: Hot wire cutting setup.....	73
Figure 63: Foam cut for nosecone mold.....	74
Figure 64: Mold sanding in progress (left) and complete (right).....	74
Figure 65: Nearly complete nosecone mold	75
Figure 66: Firewall solid model and accompanying flat pattern template	78
Figure 67: Firewall and Seat in Frame	78
Figure 68: Arduino UNO microcontroller.....	80
Figure 69: RaspberryPi4 microcomputer.....	81
Figure 70: Qualcomm Snapdragon microcontroller & BeagleBone Black microcontroller	82
Figure 71: Printed Circuit Board of a DVD player.....	82
Figure 72: Sensor Wiring Diagram.....	85
Figure 73: MPU 9250 Sensor Board.....	86
Figure 74: ADS 1115 Analog to Digital Converter Board	87
Figure 75: Infrared obstacle detection sensor.....	88
Figure 76: DHT11 Temperature and humidity sensor	89
Figure 77: 10K NTC Thermistor with 50cm	89
Figure 78: SP2800 Steering position sensor / potentiometer	90
Figure 79: HiLetgo Piezoelectric Sensor Analog Ceramic Vibration Sensor Module	90
Figure 80: Connection layout between Raspberry Pi and LTE Modem Board	92
Figure 82: Server architecture for Google Cloud Platform instances	93
Figure 83: Partial screenshot of user interface.....	95
Table 2: Data points for raw and processed API endpoints	96
Figure 84: Acceleration / G force plot.....	97
Figure 85: Tilt plot.....	98
Figure 86: Steering position display.....	99

<i>Figure 87: Three instances of the throttle position display</i>	<i>99</i>
<i>Figure 88: Two instances of the Gear display</i>	<i>100</i>
<i>Figure 89: Screenshot of the path driven plot</i>	<i>100</i>
<i>Figure 90: Two instances of the speed display</i>	<i>101</i>
<i>Figure 91: Slip angle graphic</i>	<i>101</i>

Units

Units (SI and US)

Quantity	Name	Symbol(s)
Length	meter	m
	inch	in
	foot	ft
mass	kilogram	kg
	pound-mass	lb,lbm
time	second	s
	minute	min
	hour	hr
temperature	kelvin	K
	celsius	C
	fahrenheit	F
Specific heat capacity	Kilojoules per kilogram*Kelvin	(kJ/(kg*K))
angle	degree	deg, °
angular velocity	rotations per minute	RPM
	radians per second	rad/s
speed, velocity	miles per hour	mph
acceleration relative to gravity	g-force	G
area	square inch	in ²
	square meter	m ²
volume	cubic centimeter	cc
	liter	l
	cubic inch	in ³
	cubic meter	m ³
density	kilogram per cubic meter	kg/m ³

energy	joule	J
power	watt	W, J/s, kg-m ² /s ³
	cubic meter per second	m ³ /s
volumetric flow rate	cubic feet per minute	cfm
mass flow rate	kilogram per second	kg/s
pressure, stress	pounds per square inch	psi, lb/in ²
	pascals	Pa, N/m ²
	inch-pound	in-lb
torque	foot-pound	ft-lb
	Newton-meter	Nm
force, weight	Newton	N
	pound-force	lb, lbf

Frame

The frame for this year's vehicle was completed during the prior school year as an independent study project by three members of the Major Qualifying Project team. The following section contains excerpts from the report of this project.

Frame Design

WPI's Formula team has always been more successful with iterating and improving previous cars as opposed to starting from scratch. As such, we set out to design a frame based on the previous year's overall geometry with the following design goals:

- Allow for the use of 10 inch wheels
- Accommodate redesigned suspension to allow for these wheels
- Package large components such as engine and differential with ample room for mounting and routing wires, hoses, chain, and other connection items
- Feature improved rigidity over previous frame iterations
- Feature a similar weight to previous frame iterations

Frame Comparison

Once the design goals were established, we began the background research phase of the project. In order to get a better idea of previous frame iterations, we overlaid the three most recent designs in a SolidWorks model. The suspension pickup points designed in OptimumK software were also added to the model to see how they aligned with previously designed frame nodes. This gave us a better idea of where frame nodes may need to be moved to.

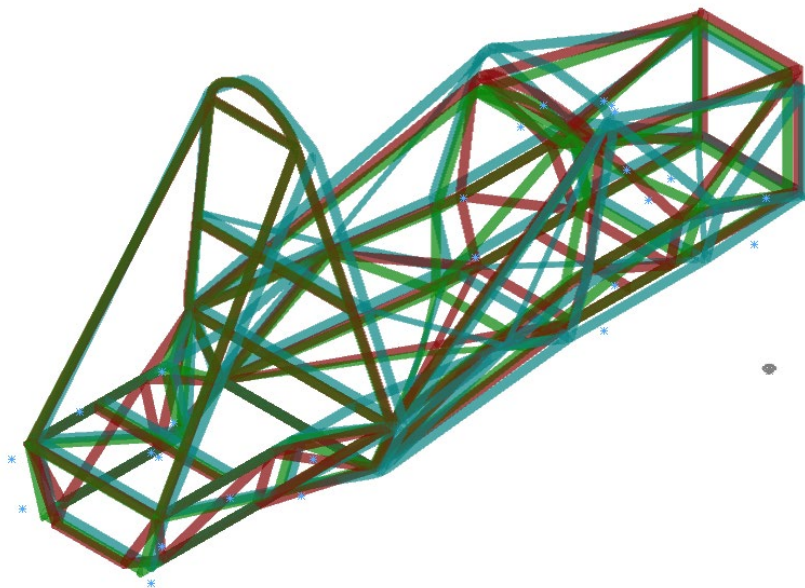


Figure 1: The comparison model used to determine geometry

From overlaying these designs we were also able to brainstorm how various frame member changes may impact the performance of the frame. These included the placement and direction of the way certain members were oriented in our frame.

To gain an accurate comparison of the effects these various configurations would have on overall frame structure and torsional rigidity, a standardized SolidWorks FEA study was created with which to test each case with. Torsional deflection about the X and Y axes were measured. The following loads were applied for each study:

X	4000N
Y	2500N
Z	2500N

Table 1: Loads Used for Frame FEA Studies

A detailed description of all the FEA cases tested can be seen in the Appendix A. Once torsional rigidity data was synthesized for each possible case, it was compared such that the optimal member locations were chosen. The resulting geometry is shown in figure 2.

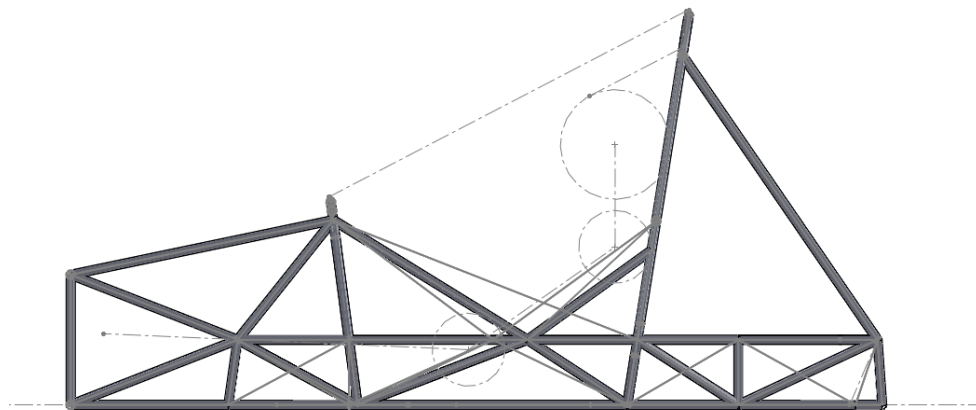


Figure 2: First New Frame Iteration

The largest geometry change between the first iteration produced and the year before's frame comes with the addition of two side bracing members which extend from the side impact structure to the main roll hoop. In addition, the rear engine compartment box design was changed to be simplified from the previous year's. While the 2018-2019 frame had more complicated geometry in this location, it was due to packaging a toe link mount which has since been repositioned with the new suspension design.

Another change that was made was moving up the harness bar member. This member is located above the driver's shoulders and is what the shoulder harness is secured to. This was moved up two inches in comparison to the previous year's frame as it was resting below the drivers' shoulders, resulting in discomfort caused by the seatbelts.

While this change makes the mounting of our harness safer, it prevents the newly added side impact members from being triangulated at the harness bar member. This is due to the cockpit entry template prescribed by the FSAE rules which each frame must pass. The template is inserted from the top of the frame, into the entry of the cockpit.

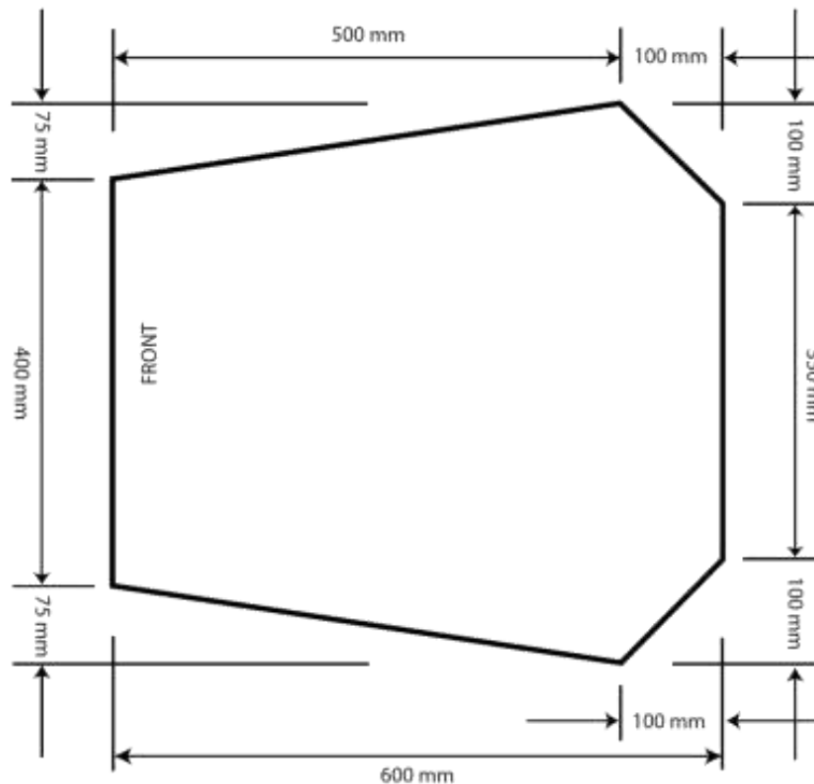


Figure 3: FSAE Cockpit Entry Template

After consideration of the rules and a thorough rules review, a second frame iteration was deemed necessary after it was found that the upper side impact member of the frame would be too low. Although not a complete redesign, many changes are required to the F20 frame in order to accommodate the smaller tire package selected for the new year. The most significant of these was the placement of the upper side impact member. The rules stipulate that the entirety of this member must lie between two planes 300mm and 350mm from the ground. The F18 and F19 cars had a member in approximately this configuration, which was easily aligned with the upper frame rails, without compromising the location of the suspension pickup points. The previous vehicles were able to achieve this because of the larger wheel diameter, which ensured that this frame member was higher than it is on our newly designed frame.

The solution in the rear of the frame is much simpler than the front. Our frame uses a rear box design that simultaneously accommodates the desired pickup points and properly triangulates the upper side impact member.

Such an easy adjustment was not possible in the front in order to maintain both the desired suspension geometry and comply with competition rules. This forced a solution that is not quite as clean as in the rear, which led us to asking for a rules clarification. Eventually, it was confirmed by FSAE staff that this design would be legal.

The upper side impact member, which is shown in teal in figure X below, was moved up in the frame so that its centerline lies on a plane 325mm above the ground. This is the exact halfway point of the allowable range, so that the car's ride height can be adjusted if necessary. Additional members were added to the front box to provide proper triangulation to the upper side impact member. These members are shown in purple in figure X. The tube intersects its green neighbor with a very long fish mouthed weld.

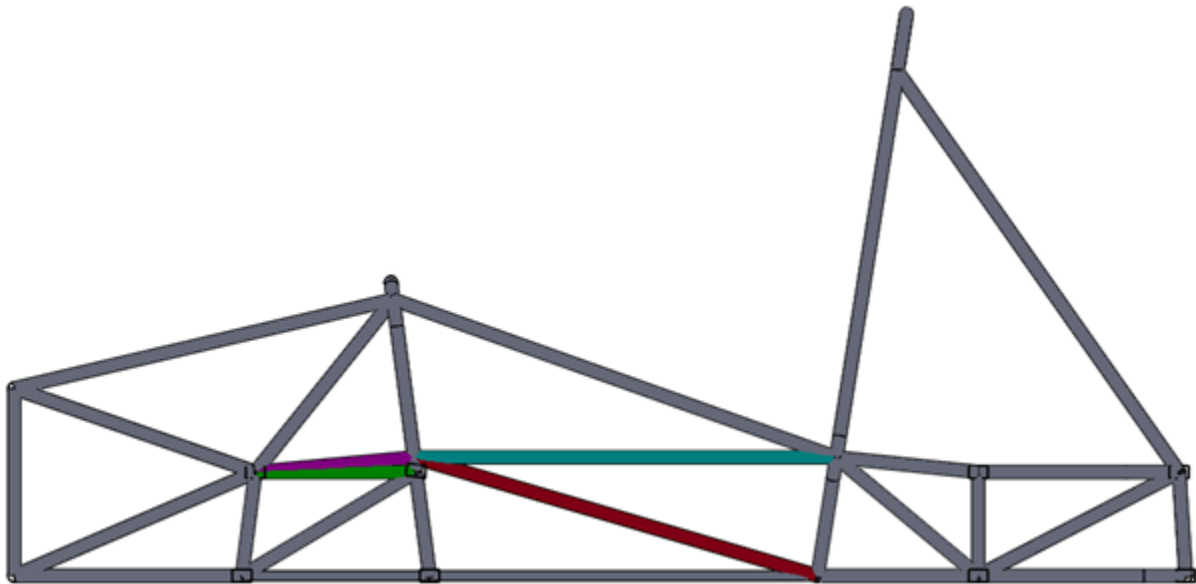


Figure 4: Second Frame Iteration with rules compliant side impact members highlighted

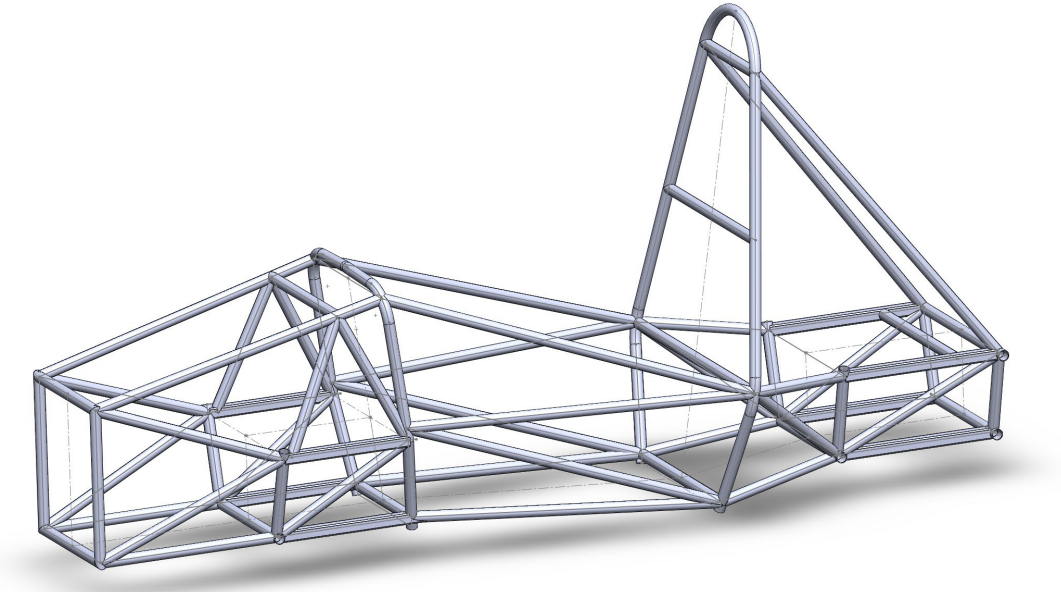
Upon confirming that this frame configuration did pass rules compliance, we decided to revisit the project throughout the summer of 2019 in an attempt to create a third iteration that would be a much cleaner and better solution. Having just attended the 2019 FSAE competition, we also decided to revisit certain aspects of the frame design based on this year's feedback from the competition judges as well as reconsidering manufacturability of suspension components.

Overall, the feedback from the judges was centered around the 2019 frame being a rules compliant frame, but not much else beyond that. In other words, WPI's FSAE team has never really

focused on important performance aspects of frame design. These include center of gravity of the car as a whole and the weight of the frame. Taking this information into account, we came up with additional design goals to those previously mentioned:

- Lower driver position to improve the car's center of gravity
- Ensure that thinner/lighter tubing is used for non critical members
- Design the suspension components to overcome previous manufacturing tolerancing issues

These new goals led to a third design iteration.



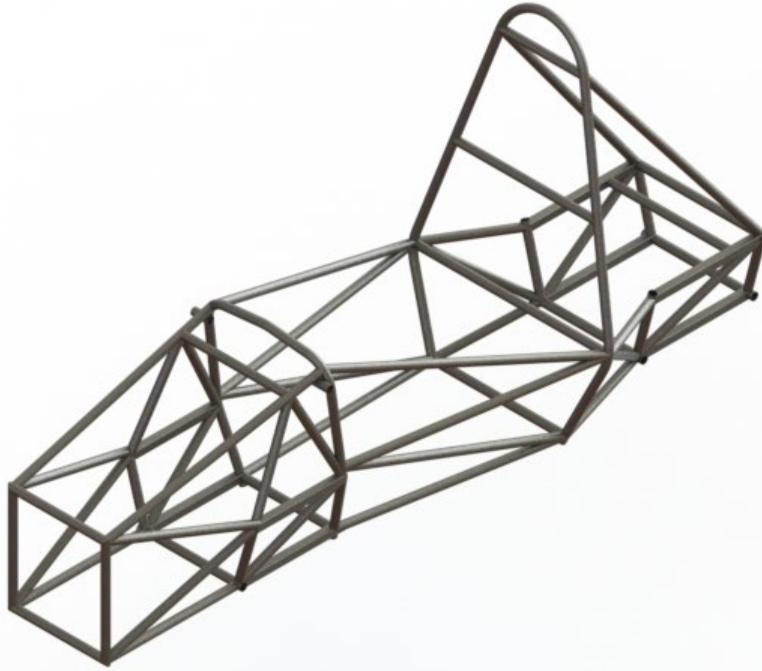


Figure 5: Final Frame Design Iteration

In order to ensure that rules compliance was maintained while making the above improvements to our design, we designed the third iteration in conjunction with following the FSAE Structural Equivalency Spreadsheet (SES). The SES ensures that a frame is “structurally equivalent” to FSAE’s minimum frame design standards. This is accomplished by demonstrating where various sections of the frame are, what thickness tubing they are made out of, and their position and orientation within the frame.

Overall, this new design features a sloped bottom which will allow the driver to sit 2 inches lower in the car than the previous iteration, improving CG. It also features square tubing along where suspension nodes sit, allowing for the manufacture of a suspension system which will better maintain tolerance than previous designs. This is explained in detail in the section, “Suspension Design”.

Finite Element Analysis:

In order to ensure that our final design was strong enough for competition, several FEA studies were conducted using SolidWorks to simulate the conditions of competition. The boundary conditions were utilized to be the same as the 2018 frame such that a direct comparison could be made. The first of these was a frontal impact study. This simulates the conditions of the car facing a 20g impact per rule T.2.25.2. The rear of the car was fixed, and a load of 59 kN was applied to the four front nodes (at 14,750 N per node). The resulting minimum factor of safety was 1.451 which is higher than that of the 2019 frame which had a minimum of 1.34. This means that the frame should be able to withstand the rules-required specified impact.

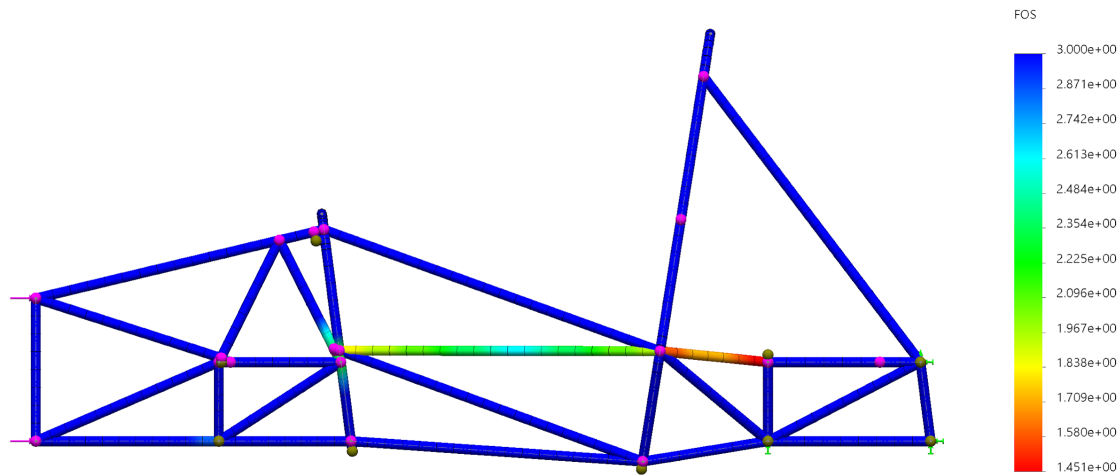


Figure 6: Front Impact Study Factor of Safety

The next study which was conducted was a torsional rigidity study about the longitudinal axis of the car. This study measures a torsional stiffness goal of having approximately 1 degree of twist per 1200 Nm applied. For this study, the frame was fixed at the rear suspension nodes and the 1200 Nm was divided amongst the front eight suspension nodes. The below figure shows that for this loading, the frame will twist about 1.152 degrees. This indicates that our frame will resist twisting under various cornering loads and that the drivability and suspension characteristics should stay predictable.

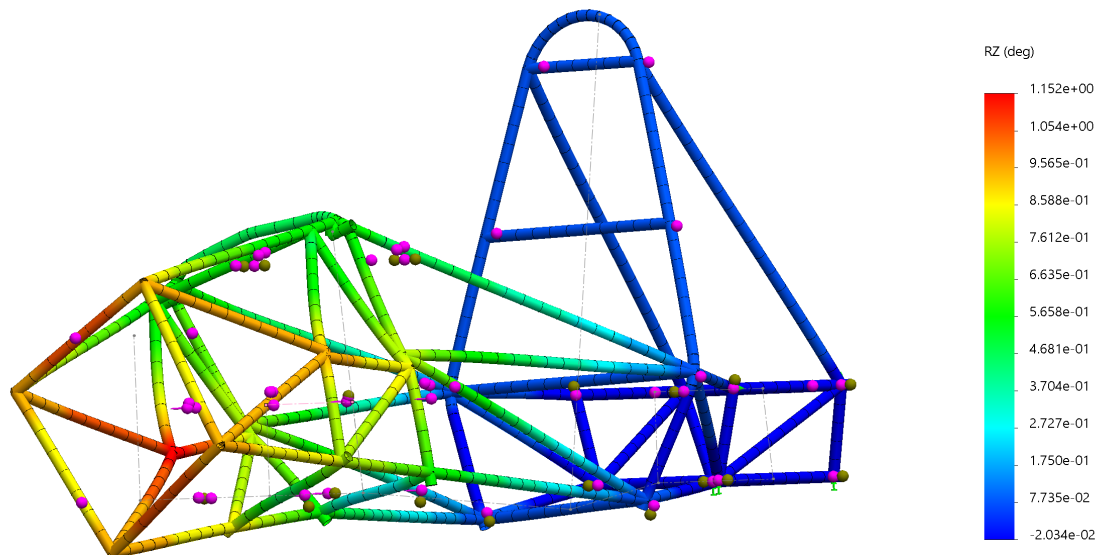


Figure 7: Longitudinal Axis Torsional Rigidity Study

Next, the same torsional rigidity study was conducted about the X axis to simulate conditions under a heavy braking load. A maximum rotation of about 0.175 degrees was observed in this study. This number is very small, indicating that the frame will resist any significant twisting even under heavy braking and acceleration loads.

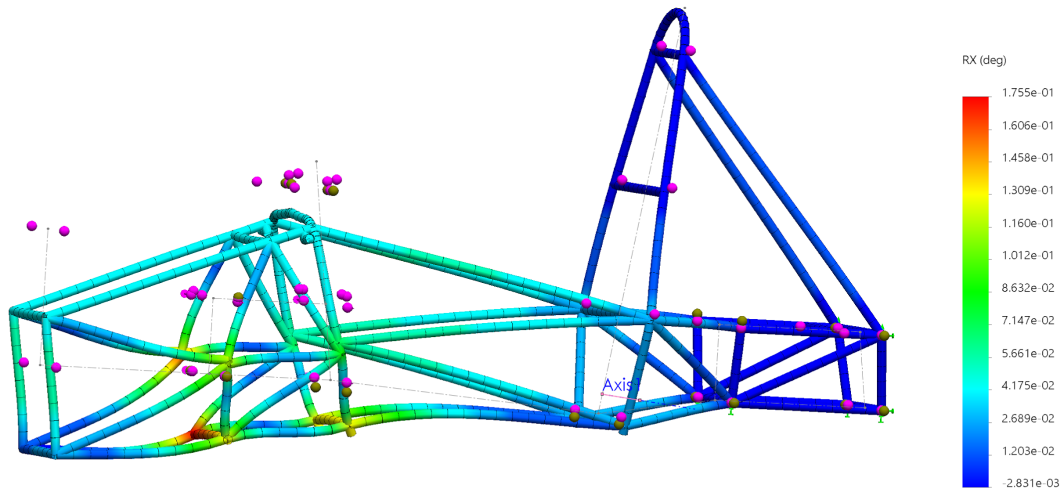


Figure 8: Horizontal Axis Torsional Rigidity Study

Powertrain

Intake Plenum

In previous years, intake design has been an area where points have been lost at competition. While ample analysis has been performed and decent results have occurred, some major details have been overlooked. Fortunately the average score has risen from year to year as our research and development for this particular subsystem has improved. The development for the intake side of engine development started 2 years ago when a previous powertrain head really got a deep understanding of the flow simulation parameters of SOLIDWORKS and how to accurately simulate our choice of engine. The following year the use of 1D engine simulation was introduced and doubled the output of our current engine. This year the focus was to verify that the previous findings produced accurate results and to adjust the packaging such that the overall center of gravity of the vehicle will be improved.

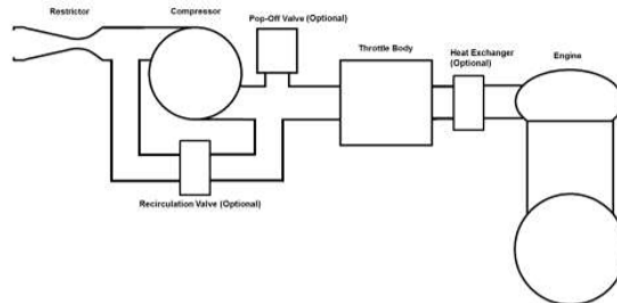
The challenge when it comes to designing an intake plenum for this application is the 19-20mm restrictor required in the Formula Society of Automotive Engineers (FSAE) rule book. The exact rules and requirements can be seen in the figure below.

IC.2.4 Intake System Restrictor

IC.2.4.1 All airflow to the engine(s) must pass through a single circular restrictor placed in the intake system.

IC.2.4.2 The only allowed sequence of components are the following:

- For naturally aspirated engines, the sequence must be: throttle body, restrictor, and engine.
- For turbocharged or supercharged engines, the sequence must be: restrictor, compressor, throttle body, engine.



IC.2.4.3 The maximum restrictor diameters at any time during the competition are:

- Gasoline fueled vehicles 20.0 mm
- E85 fueled vehicles 19.0 mm

IC.2.4.4 The restrictor must be located to facilitate measurement during Technical Inspection

IC.2.4.5 The circular restricting cross section must NOT be movable or flexible in any way

IC.2.4.6 The restrictor must not be part of the movable portion of a barrel throttle body.

Figure 9: Restrictor Rule from the 2020 FSAE Rulebook.

As can be seen all intakes require some type of restrictor depending on its modifications. The purpose of these restrictors is to limit most of the engines used in the competition (less than 700cc's) to a maximum rpm of 10000. The horsepower that an engine produces is simply a function of the torque that it produces and the rpm that it produces that torque at. So, if an engine was to produce a flat amount of torque over the whole rpm range, the horsepower would simply increase as you move into higher and higher rpms. This restrictor limits this number and therefore limits the amount of power that one engine could possibly

produce. This makes the role of the intake plenum in these cars to negate the effects of these restrictors and maximize the area under the horsepower and torque curves up to the 10000 rpm limit.

Starting 5 years ago, the Worcester Polytechnic Institute (WPI) Formula SAE (FSAE) team decided to switch their main style of power plant to be the Yamaha series of 450cc engines. This started with the introduction of the Yamaha YFZ 450cc ATV engine into the 2016 year of competition (build cycle starting in 2015) FSAE car. This engine was chosen due to the fact it can still produce a decent amount of horsepower for our application while also being 40-50lbs lighter than the more powerful 600cc four cylinder engines. Due to the one year build cycle, ample analysis of the intake plenum was not performed in the 2016 year, resulting in the car producing approximately 25 horsepower which is less than the stock rating of 45. The next engine choice was that of the WR450r Yamaha dirt bike, which is the choice that we have continued to use to this day. In 2018, our plenum and exhaust combination produced an improved 29 horsepower due to an improved restrictor and plenum design. However due to the plenum being only 450cc's in volume, this 29 horsepower is all it would ever achieve. Finally in 2019 with the improvement of a 1D engine simulation, a variety of plenum volumes ranging from 2500cc's to 4000cc's, a horsepower of 47 was achieved with the 4000cc intake plenum. The results of the improved restrictor and 4000cc intake plenum have proved to be two necessary components of the plenum and ones that were carried over into the 2019-2020 build cycle.

Arguably the component with the most complicated development is the intake restrictor. Its purpose is to limit the engines that are legal in the competition (less than 710cc) to about 10,000 rpm. This results in less horsepower as smaller displacement engines usually need to spin to a higher rpm in order to produce relatively high amounts of horsepower. Horsepower is a measure of the amount of work an engine is able to over a given time period. In terms of internal combustion engines horsepower is a function of the torque an engine produces and the rpm that torque figure exists. By limiting rpm to 10,000, these restrictors greatly reduce the engine's ability to produce torque at the normal 12-16,000 that they normally do which greatly reduces its ability to reach its original power figure. With regards to the restrictor, it has to meet the rules requirement of only being 20mm in diameter while also being able to supply the engine with adequate airflow to still make the required horsepower.

To accomplish this, development from the 2018 year car was continued. In this year, development started with the assumptions of air at 25 degrees Celsius at sea level. These are accurate assumptions seeing as the time of year when competition can have changeable weather where temperatures can range from just a few degrees or exceed the 25 degrees celsius that was assumed. At 25 degrees this is a data point that is a little higher than the average temperatures for this time of year. When ambient air increases in temperature, the air charge that enters the throttle body which then proceeds through the restrictor tends to become less dense meaning there will be fewer oxygen molecules to burn in the combustion process. This results in a lower horsepower figure since the engine must maintain a strict air fuel ratio while operating at wide open throttle and less oxygen means less fuel that will be burnt and less energy. So assuming a relatively high temperature allows for the creation of a restrictor that will work across a spectrum of temperatures that the car will have to experience. Also the simplification of atmospheric pressure to be that of the atmospheric pressure at sea level is also accurate as Brooklyn Michigan where the track is located is only 991 feet above sea level where the difference in atmospheric pressure is less than one psi.

These assumptions are important due to the fact that they affect the pressure drop that occurs in the restrictor as the intake charge passes through. The speed of sound varies depending on the state of a gas and the intake charge will travel at this speed at the smallest point (Mach 1). With these assumptions

you are able to get the following values; $k=1.4$, $R=286 \text{ J/kg}\cdot\text{K}$, and $T=298 \text{ K}$ (converted from the 25 degrees C). You then can use the following equation to get your maximum mass flow rate at the 20mm section of the restrictor.

$$\dot{m} = \frac{APk}{\sqrt{kRT}} \sqrt{\left(\frac{2}{k+1}\right)^{\frac{k+1}{k-1}}}$$

In this equation, A is the cross sectional area of the 20mm restrictor and P is the atmospheric pressure at the inlet. Atmospheric pressure at the inlet is equivalent to $P=101325 \text{ Pascal}$, and plugging in these values (sin temperature) allows this equation to be simplified to the following.

$$\dot{m} = 3222.135 * \frac{D^2}{\sqrt{T}}$$

In this equation you use the 20mm converted to meter (0.02m) as “D” and T is the 298K from earlier. From this you can get an ideal flow rate (assuming no friction at the boundary layer) to be 0.075 kg/s. To validate this a SOLIDWORKS flow simulation was performed to compensate for the friction along the actual surface of the manufactured aluminum and abs restrictor piece .

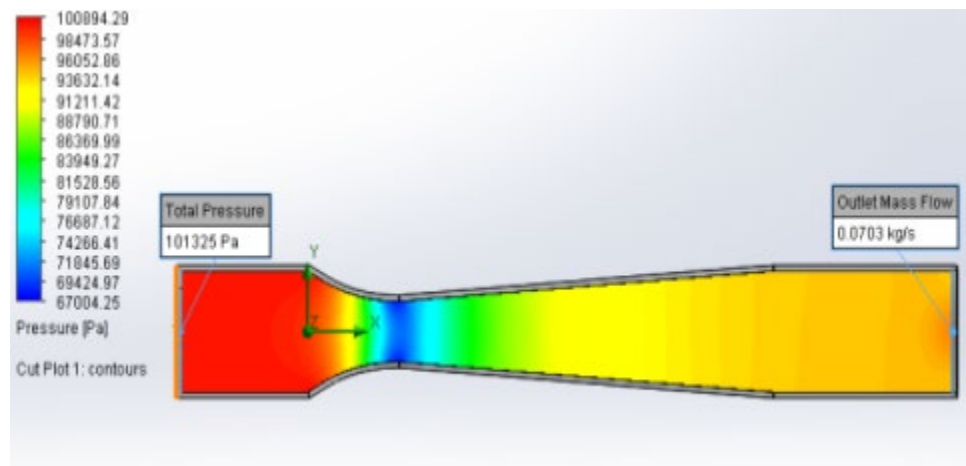


Figure 10: Simulation Representation and Results from 2018 validated in 2020

From the figure it can be clearly seen that a mass flow rate of 0.0703kg/s was possible which is close to the 0.075kg/s from the original calculation. If the displacement of the engine is taken (450cc) and is then converted to cubic meters (0.00045m³) and the RPM/120 cycles per second for the four-stroke cycle, with a standard air density of $\rho=P/RT=1.19 \text{ kg/m}^3$ you can calculate the air demands. With the assumption of a peak power at 12,000 rpm, multiplying these numbers yields a required flow rate of 0.05355 kg/s of air, which is well within the abilities of the restrictor.

The next part of the intake design is the bellmouths contained within the plenum itself. The most important component is the volume of the plenum itself as it acts as a capacitor for air, but how the air

enters and exits the plenum is all dependent on the bell mouth design at the base of the restrictor and at the entrance to the intake runner. One of the most respected papers about this particular component is “Airflow Entering Plain Pipe and Elliptical Bellmouth” by Blair & Cahoon. This paper details all of the necessary bell mouth design parameters with regards to a given pipe inner diameter. This turns out to be “an entrance area 2.13 times the inlet diameter, an axial length equal to the diameter of the inlet, a radius of 0.08 times the inlet diameter outside the entrance area, and an elliptical profile connecting the two” based on the paper itself. This method matches how the bellmouths were designed in the 2017-2018 car and has been carried over to the 2018-2019 build year and my plan is to incorporate the same style of bellmouth on this year’s engine. To accomplish this, just a simple modification of the existing bellmouth model is needed as the dimensions of the intake runner and restrictor exit vary approximately 1mm from previous years designs. One bell mouth was created for both the restrictor exit and intake runner entrance.

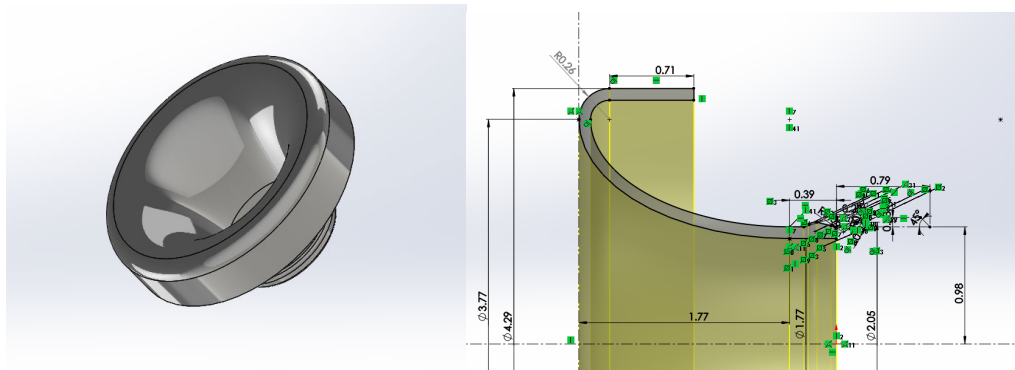


Figure 11: Bellmouth design and model for intake runner bellmouth

The next components to be created are the plenum itself and the intake runner. From the 2018-2019 intake development and dyno testing, the best results were produced with an overall plenum volume just under 4 liters and a runner length of approximately 16 inches. It was found that increasing the plenum size increased the peak power and runner length had no effect on this other than making the curve more erratic. With a single cylinder engine the plenum itself is designed to act as a capacitor for air, where it flows to encompass the whole volume and “store air” for when a wide open throttle condition happens. As a result volume is more important than the actual shape, where the bellmouths determine the flow shape. At the 2019 competition, SAE International added in a much longer endurance course where even our larger plenum was struggling towards the end of large straightaways. To address this I added plenum volume based on the points at which drivers could feel a slight dip in the performance of the vehicle. This would require an approximate 5-10 percent increase in plenum volume. Assuming the previous volume was 4 liters, and this volume was attempted to be matched.

Packaging was also always another issue as the larger plenums tended to cause other components to stick above the roll hoop. To address this a shorter wider “tear drop” shape was decided on. A maximum height of 11 inches was decided on and the teardrop shape was created as a thin revolve feature in SolidWorks. The closest achievable volume with the given shape was found to be 4.2 liters exactly and this was the plenum model to be tested.

From here positioning in the car was decided based on the already existing restrictor and throttle body components and the 16 inch intake runner was routed. The 16 inches referenced includes the already existing injector mounting tube resulting in approximately 11 inches of total runner to be manufactured.

Once all of the components were designed, they were placed in an assembly, where a flow simulation of the complete unit could be performed. As the intake pulses of any engine are not constant, a spreadsheet to make data points for this is required. To accomplish this, a spreadsheet was created a few years back to accurately simulate this condition with a different engine. This takes into account the displacement of the engine, compression ratio, intake cam duration, runner length, volumetric efficiency, atmospheric conditions and finally the desired rpm to test at. For this engine, an rpm of 7500 was chosen to test at, since this is where the engine spends most of its time in an autocross. Below can be seen the input conditions and the start of the results.

Displ. (m3)	0.000449393048						
Comp. Ratio	13.5						
TDC Cyl. Vol. (m3)	0.00003595						
Bore (mm)	95						
Stroke (mm)	63.4						
Ideal Powerband	6000	6500	7000	7500	8000	8500	9000
Integral Intake Runner Vol. (m3)	0.000014	139800 mm ²					
Shortest Integral Runner (mm)	80	appx lin distance					
Longest Integral Runner (mm)	105	appx lin distance 3rd runner 92mm					
Cyl SA (m ²)	0.007088218425						
Plenum Pressure (Pa)	101325						
Assumed Volumetric Efficiency	0.85						
Universal Gas Constant (J/K mo	8.3144598						
PRESSURE CALCULATION							
Engine RPM	7500	VE Guess (0-1)	0.85				
Piston f (Hz)	125						
Piston rad/s	785.3981634						
7500rpm Pressure Calc							
Time (s)	Stroke (m)	Piston Vel (m/s)	Intk Vlv Opn?	Displaced Air Vol	Tot Vol (m3)		
0	0.00000000	0	1	0	0.00003595		
0.000125	0.00015264	2.440344679	1	0.000001081975	0.00003703		
0.00025	0.00060911	4.857187505	1	0.000004317480	0.00004027		
0.000375	0.00136499	7.22725296	1	0.000009675356	0.00004563		

Figure 12: Intake Pulse Simulation Input Data Representation

This spreadsheet produced a wide variety of values, however for the simulation only the pressure drop at the intake and the time interval is needed. At the 7500 rpm data point, SolidWorks is able to repeat test the six engine cycles provided. To Test these two columns of data were copied into the transient flow analysis inputs in SolidWorks, with all other assumptions being the fluid as air and the ambient conditions being 25 degrees celsius at 1 atmosphere atmospheric pressure. The resultant flow trajectories can be seen below for the 7500 rpm test. At slower rpm's the orange component widens out showing that the plenum once again performs its purpose of storing air when it's now needed. The study will be included in the respective appendix.

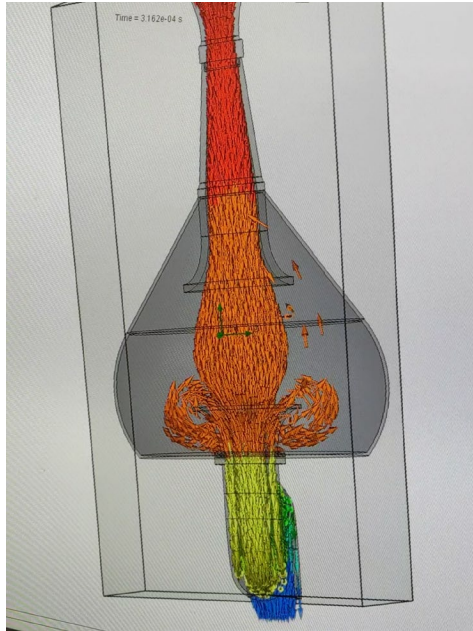


Figure 13: Representation of Flow Trajectories in 2020 Intake Plenum

To manufacture the intake plenum and accompanying bell mouths, 3D printing was chosen. In the 2019 car, a 3D printed intake system proved to be very effective. This method of manufacturing is by far the cheapest and most convenient way, given that WPI has easy access to many printers. The system was designed so that the plenum would be split in half, with the bell mouths locating themselves on the flat surfaces of the plenum.

In order to get adequate strength from the 3D printed parts, we needed to print the parts with increased infill and wall thickness. Both of these add time to the print, though, and meant that the two halves of the intake plenum would take ~18 hours each with the maximum layer height of the .5mm nozzle Lulzbot Taz 6 printers that WPI has. To fix this issue, we chose to use a larger 1.2mm nozzle for the Taz 6 printers. This is a special unit that the school allows use of for special projects. With this nozzle, we were able to achieve a layer height of .9mm, meaning that both halves of the plenum were printed in 8 hours total.



Figure 14: 3D printed intake system

A drawback of using 3D printing as the method of manufacturing is that the parts must be sealed with a special coating to prevent leaks. There is a chance that the part has small gaps between layers due to under-extrusion, so this coating is used to fill in the gaps between layers. We used XTC-3D by Smooth-On to achieve this airtight finish.

Exhaust

When it comes to exhaust development, the previous years design showed no issues with restriction, only the sound level that it produced. This showed that the lengths were correct for the assumed 6000 rpm torque peak but only needed added baffling for noise reduction. These lengths were calculated with formulas from “A. Graham Bell’s Performance Tuning in Theory and Practice, Four-Stroke” and the results can be seen below. Keep in mind most of these values were rounded to adapt to

$$P = (850(ED) / \text{RPM}) - 3$$

P= Pipe Length (in.)

$$P = (850(254) / 6000) - 3$$

ED = Angle range in which exhaust valve is open.

$$P = 33 \text{ in.}$$

$$ID = (\sqrt{(cc / (P+3)25)}) * 2.1$$

ID = Inner Exhaust Pipe Diameter

$$ID = (\sqrt{(449.3 / (32.98+3)25)}) * 2.1$$

cc = Cylinder Volume (cm,3)

ID =1.5 in.

Working with a 1.5 inch inner diameter, the exhaust was then routed forwards instead of backwards. The reasoning for this is with the addition of the spring and damper assemblies in the rear, the exhaust would be too high from a center of gravity perspective. To keep the same routing the exhaust would have to be more than 4 inches higher than previous years. With routing it forwards, it gives the ability to place the muffler at a much lower height and also take up room that was previously wasted. Since the exhaust was previously too loud and required modification at competition, a resonator needs to be added at the end of the 33in length but before the muffler. The resonator in mind is the powerbomb from FMF which the team is in possession of in the left over exhaust from the 2017-2018 car.

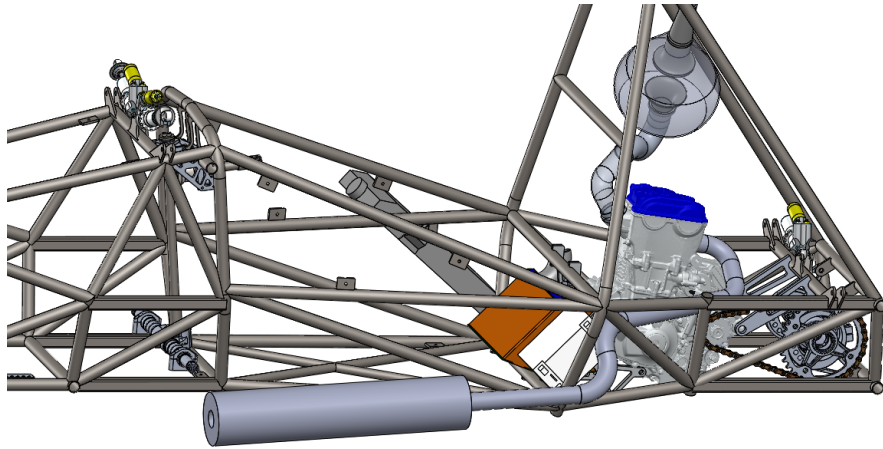


Figure 15: Preliminary Exhaust routing example

When it comes to mounting the exhaust, part availability was the primary focus. To accomplish this universal 1.5 in exhaust hangers from Summit Racing are being used in order to add simplicity and also insulate any kind of heat transfer to the frame from the exhaust. In addition to these mounts, custom tabs to interface with the existing exhaust tubing were laser cut. The full assembly in its intended mounted position can be seen in the figure below.

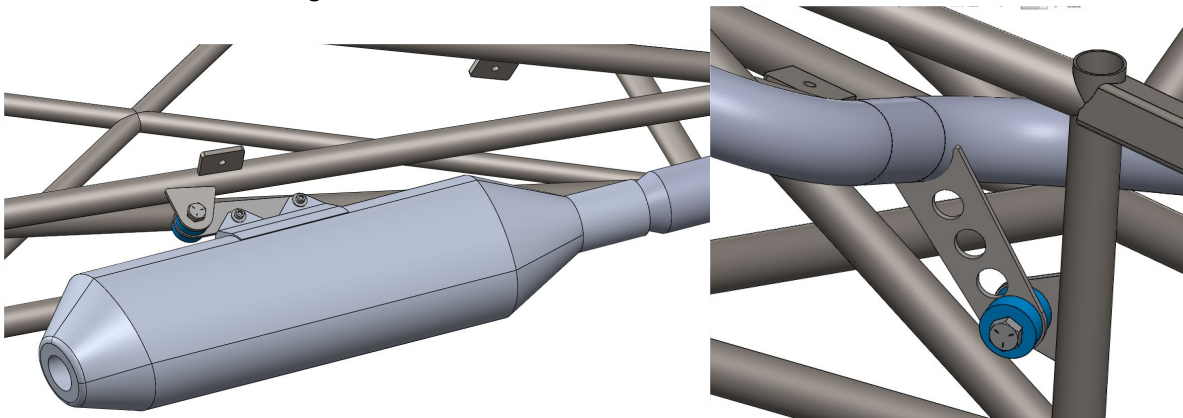


Figure 16: Exhaust Mounting Solution

While most of the exhaust components have been decided on and ordered, nothing aside from the mounts has been manufactured. The following are the necessary steps to complete the exhaust. First the resonator out of the 2017-2018 exhaust needs to be cut out. Next all of the bends in the exhaust (modelled as individual pieces) need to be cut. Then, the original header flange needs to be reused and the new tubing welded to it. The model should then be followed to weld all of the mounting tabs in place. Finally with the engine in the mounts in its final position should the tubing be run and welded into place.

Some other considerations in order to be rules compliant are a heat shield that mounts to the outside of the frame that blocks the direct heat of the muffler, and a 180 degree bend that comes from the exit of the muffler and runs to behind the driver's head. At the final exit the exhaust should have a bend that turns to the outside and up to help prevent sound waves from amplifying as they bounce off the ground. Finally, replace the muffler with the new one that should be in the shop. The amount of time this engine has run on the 100 octane leaded race fuel has eaten all of the old muffler packing material away, causing the effect of the muffler to be reduced.

Engine Mounts

In designing the engine mounts, the loads that would be applied to them had to be calculated. The 2019 car produced a peak of 50 lbf*ft of torque. This torque is multiplied through the gearing of the transmission. First gear has the most aggressive gearing, with a ratio of 2.42. Therefore, the maximum torque applied from the engine on the mounts is 121 lbf-ft, or 1452 lbf-in. The weight of the engine also had to be considered for design purposes. Our WR450F engine was estimated to weigh 70 lbf.

The engine is mounted with 2 front mounts and 2 rear mounts. To allow for the easiest manufacturing method while still having adequate strength, the mounts are waterjet from $\frac{3}{8}$ " 7075-T6 plate.

The first step in designing the engine mounts was creating a sketch of the mounting holes and tubes on the engine and frame, respectively. The engine mounts are attached to the frame tubes via shaft collars, so knowing their location is important. Once the locations were determined, a very general shape of the front mount was designed around the engine to run a topology optimization simulation in SOLIDWORKS. The goal for the topology optimization was to maximize stiffness (for best responsiveness and minimal flex in the powertrain), while decreasing weight. To guarantee that the mounts can support the forces in all situations, the entire torque value and weight are applied to each engine hole on the mount. Therefore, if all the forces shift to one single hole on the mount, it will still be able to support these forces. The results of the topology optimization for the front mounts are seen below (the black outline is the original shape):

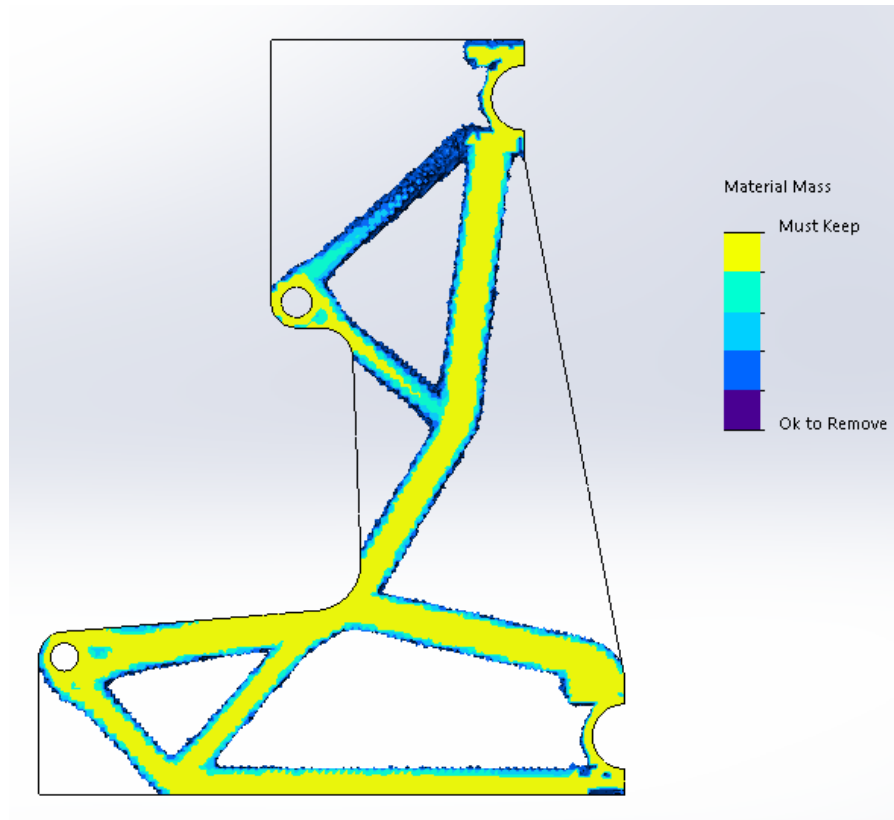


Figure 17: Front engine mount topology study

This generated shape was used as inspiration for the actual design in determining which areas required material. The front mount final design has a weight of .54 pounds each, with a FOS of 20. This factor of safety is very high, but minimizing deflection in the mounts was an important factor. The deflection under engine torque and weight loads is only .1mm.

Additionally, the size of the mount is greater than last year's car due to the spacing of the frame tubes for attachment. However, equal strength and weight were achieved when compared to last year's car, despite the larger size. The final design and deflection results for the front mount are seen below:

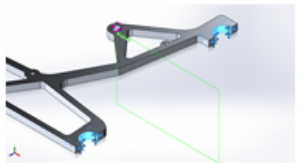
Fixture name	Fixture Image	Fixture Details			
Fixed-1		Entities: 6 face(s) Type: Fixed Geometry			
Resultant Forces					
Components	X	Y	Z	Resultant	
Reaction force(N)	-391	0.0143016	858.449	943.3	
Reaction Moment(N.m)	0	0	0	0	

Figure 18: Front engine mount simulation fixed connections

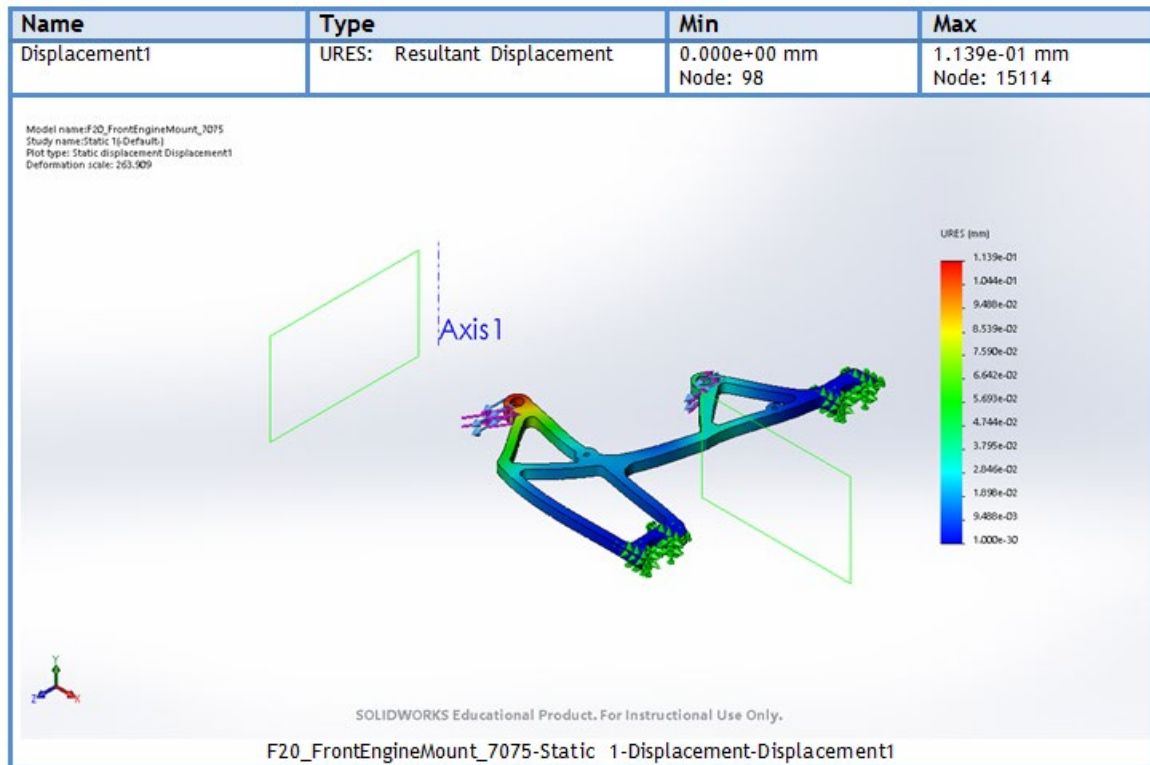


Figure 19: Front engine mount displacement under load (mm)

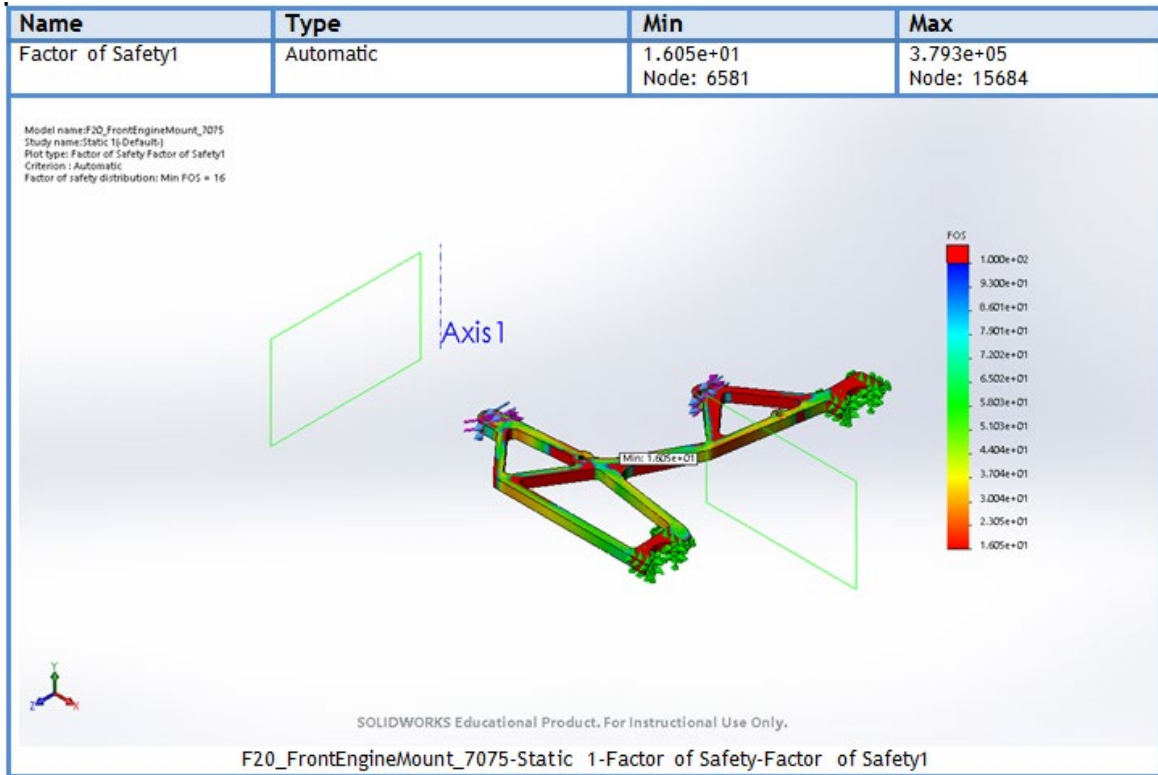


Figure 20: Front engine mount factor or safety plot

The rear engine mounts were designed with the same loads in mind. These mounts only have one attachment point to the frame, so are less rigid. However, a FOS of 1.6 was still achieved with a mass of .28 pounds. The final design and displacement of the mounts can be seen below:

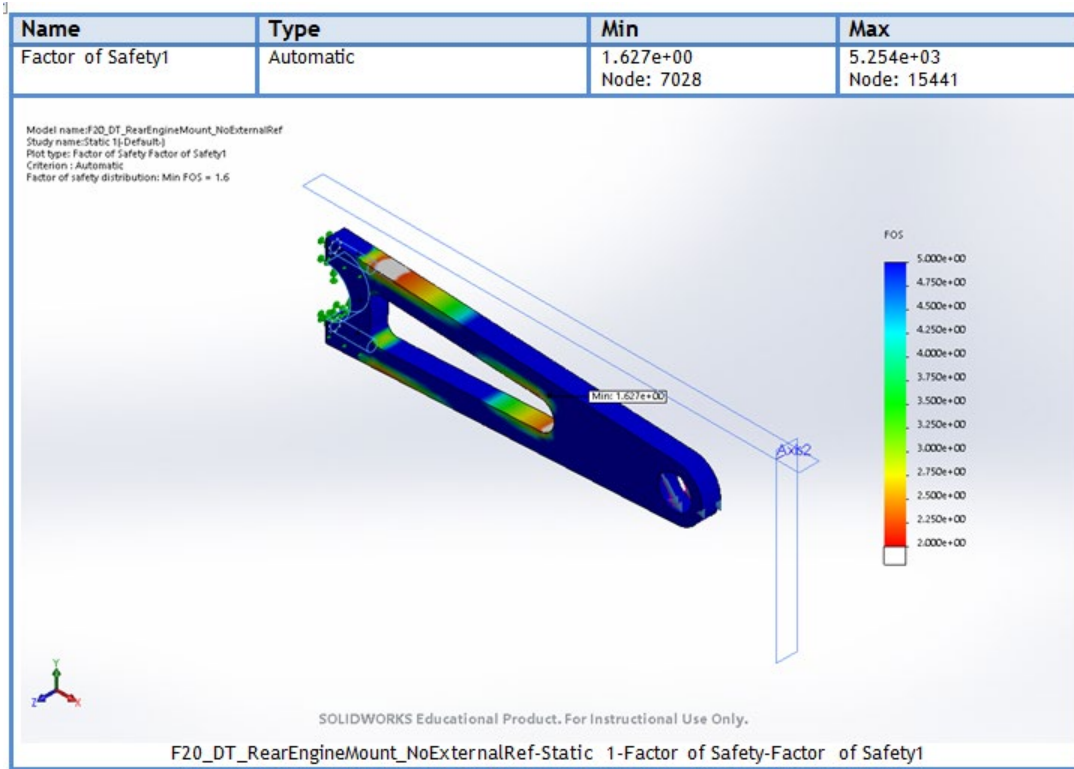


Figure 21: Rear engine mount factor of safety

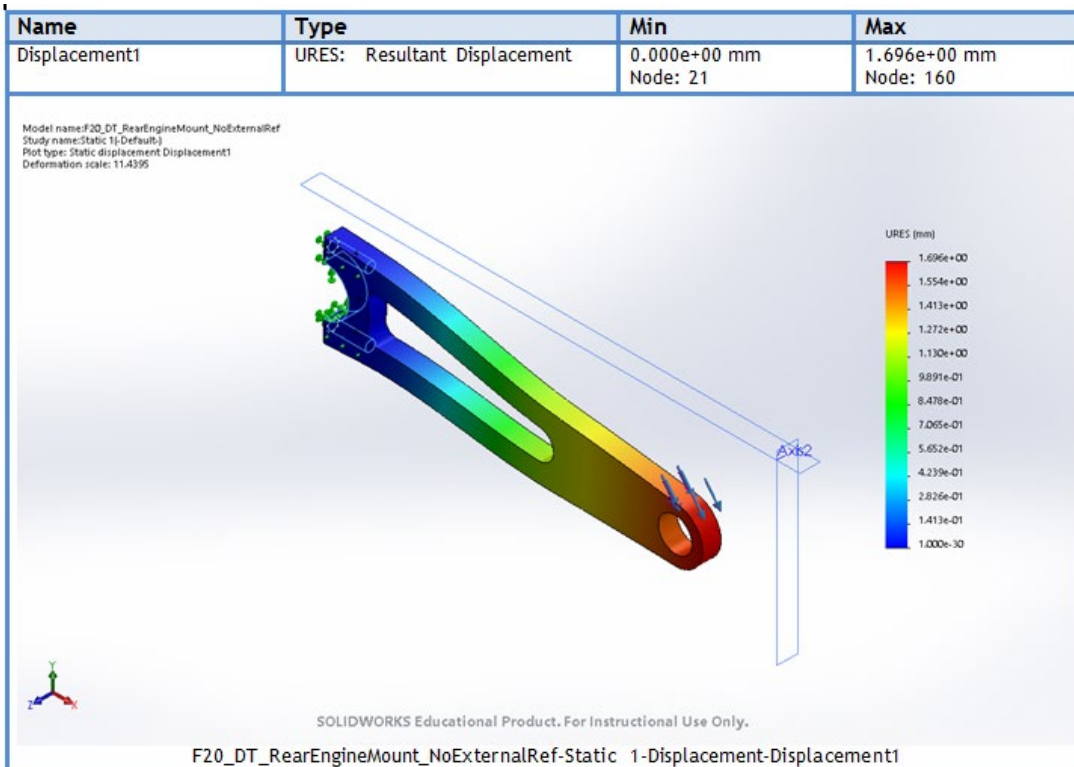


Figure 22: Rear engine mount displacement under load

Shifting

The FSAE car runs a WR450 engine with the stock transmission. With the engine mounted in the rear of the car it is not desirable to have the transmission shifted with the driver's foot, as it would be on the motorcycle. The last iteration of the car used a set of paddle shifters to control a linear actuator to 'kick' the kick shifter. The linear actuator turned out to be unreliable at actually completing the shift to the next gear. This makes it a challenge for the driver to smoothly control the car.

A motorcycle transmission is shifted by use of a shift drum shown in Figure 23. As the drum rotates the shift forks slide in the slots to shift the gears. Therefore, if the shift drum could be rotated directly to the correct positions at the correct time the shifting could be controlled. It follows that if a servo could be attached directly to the shift drum it could rotate the drum to the correct positions.



Figure 23: Shift Drum

There are several challenges that arise from this system. First, the system needs to be packaged in a very small space. Second, in order to be an improvement over the last iteration it should be lightweight. Third, the servo needs to have very high torque for its size to rotate the transmission.

The servo was selected based on two main criteria, its torque output, and its range of motion. Testing was done on the transmission to determine the amount of torque necessary to turn the shift drum. It was determined that it would require 30 kg-cm to rotate the transmission in most cases. It was therefore



Figure 24: Servo

After some basic testing it was determined that three major components were needed to mount the servo onto the engine. The main mount that holds the servo in position and allows it to rotate the drum, the hub that adapts the servo to the drum, and the servo saver that allows the servo to rotate even when the transmission won't without burning out the servo.

Due to the shape of the transmission housing it was determined that the best way to mount the servo is by replacing the back panel of the servo. That mount allows there to be only two small standoffs that come directly in contact with the housing. The mount can be seen in the Figure below.

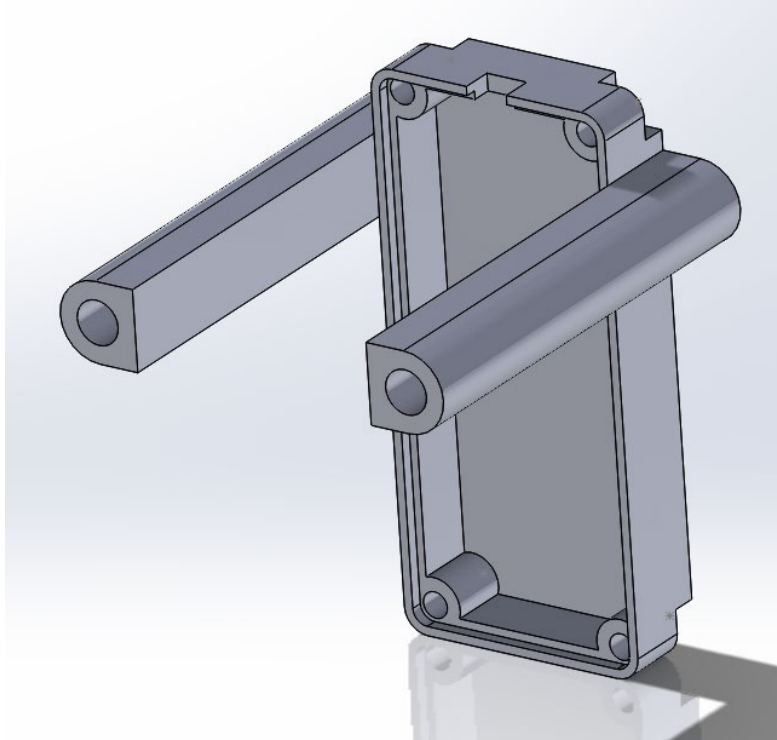


Figure 25: Servo Mount

The final piece of the shifting system that has not yet been completed and tested is the servo saver. There are instances where the servo tries to shift but the transmission resists more than normal because the dog teeth aren't perfectly aligned. This was also a problem with the previous system which was only actively pushing for a split second. Unfortunately, in this case it could also burnout the servo if it is pushing against the transmission for too long. The servo saver allows the servo to transfer its energy into a spring which can then release it later.

The servo saver needs to strike a balance between outputting enough torque to still turn the transmission but not over power the servo. The initial CAD designs are shown below. The springs are placed behind the servo and the misalignment disks fit inside the transmission housing. As the misalignment disks twist against each other the entire servo assembly is lifted away from the transmission, compressing the springs.

The servo turns 45° per shift and the force from the springs should be equal to just a little less than the torque of the servo. The amount that the misalignment hub needs to displace the springs can be calculated using equation (##) below, where τ is the servo torque, r is the radius of the misalignment hub and, k is the spring rate.

$$\text{Servo Displacement} = \frac{\tau}{2rk}$$

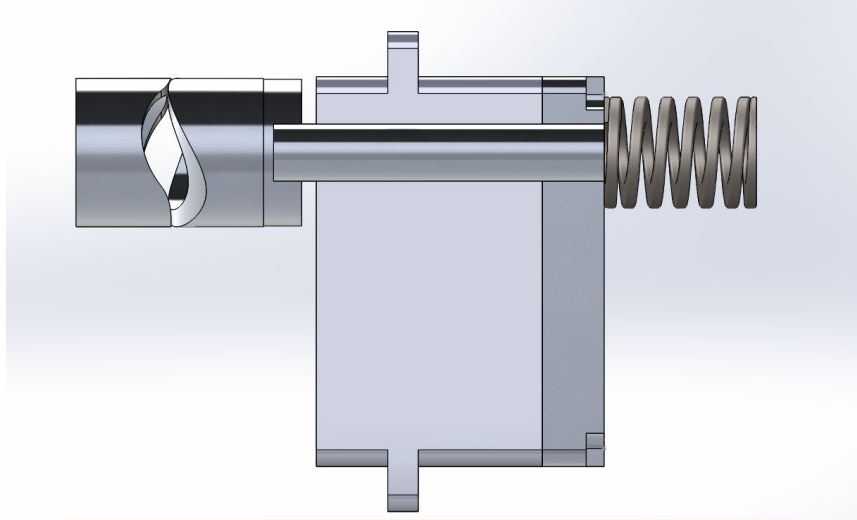


Figure 26: Shifting Assembly Side View

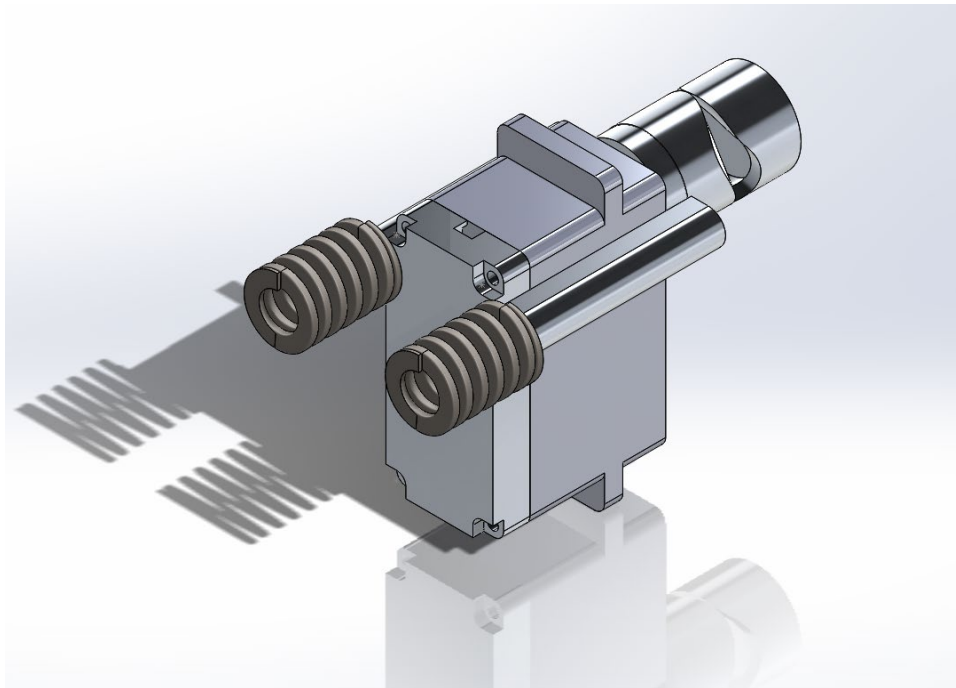


Figure 27: Shifting Assembly Isometric View

Next Steps

Most of the components in this new shifting system were in the prototype phase. Some preliminary testing has provided information on how the system should function but further steps need to be taken to make the system more durable.

Back Panel Mount

The back panel mount needs to be machined. In order to do this it is recommended that the studs on either side of the mount that space it off of the transmission housing be split into separate pieces. With the back panel and the spacers separated it should be a much easier task to machine it. It is also recommended that the pads on the back panel where the springs rest should be expanded. This will give the springs a larger place to sit.

Servo Saver

An example of the misalignment hubs needed for the servo saver is shown in Figure xx. This is just a rough model and doesn't represent a finished design. Two sets of die springs have been ordered for testing. They have different spring rates but both are strong enough to develop the necessary force in the space allowed. The exact displacement can be calculated using equation (##)

Fuel Pump and Injector

For this year's vehicle, a new fuel pump was selected. Previously, WPI FSAE vehicles utilized a Walbro 255 (255 liter per hour) fuel pump. This pump was selected because it is easy to make rules-compliant due to its metal construction. It was also easier to use with existing fuel tanks as it is an inline pump and provisions did not need to be made to mount a pump inside of the fuel tank. While this pump worked well and had no issues supplying enough fuel to the injector, it was one of the main sources of current draw. Being that this pump drew 9 amps, it used over 60% of the engine's stator power output, making it rather inefficient. This led to reliability issues with shifting later on as there was less current available for the actuator.

With all of this taken into consideration, the team switched to a fuel pump from a Suzuki RMZ 450. This pump is designed for a dirt bike with a 450 cc engine, meaning that the current draw will be much less than the Walbro pump designed for full scale automotive engines. This pump is also meant to be mounted in-tank, meaning that a new fuel tank needed to be designed. Another hurdle to overcome with the new fuel pump was to ensure rules compliance. FSAE rules require major parts of the fuel system and its connections to be all metal. While the pump has a metal body, the outlet hose barb is plastic. Knowing this would be an issue, a new adapter was designed to replace this plastic barb and CNC machined. The adapter features pipe thread to accommodate a male 6AN fitting. Because this pump also features an integrated fuel pressure regulator, the fuel hose routing was greatly simplified this year with just a single hose going from the pump to the fuel injector.



Figure 28: Suzuki RMZ 450 Pump Assembled with CNC Machined Adapter

The same fuel injector was carried over from the previous car. This is a 550cc/min Black-Ops M-Series Injector. While it delivers more fuel than the car needs, it has proven reliable and is not a large power draw source like the previous pump.

Fuel Tank

Previously, WPI's Formula SAE team has been using the same student designed fuel tank for the past two cars. With packaging becoming fairly tight for hoses, the battery, and other larger components, it was decided to revisit the design of the fuel tank this year. To begin this process, fuel usage throughout the last two competitions during the endurance event was considered. This data is publicly available through SAE post competition. In 2018, the team did not finish endurance but used 1.466 liters of fuel for 8 laps. Averaging this value per lap, this would have come out to about 2.38 liters for the whole endurance event. In 2019, the team completed the event and used 2.69 liters for the whole event. This comes out to about 0.7 gallons. The previous fuel tank had a 1.5 gallon capacity, or over double of what was used. This results in extra unneeded weight as well as the tank occupying a large volume and making packaging of components difficult. While some extra fuel is needed to prevent fuel starvation due to sloshing and to compensate for potentially different track layouts with more on-throttle driving, it was determined that the capacity could safely be reduced.

A new tank was designed to package between the two front engine mounts, a space previously not used for anything. This freed up more space around the sides of the tank for the aforementioned battery, hoses, etc. The new tank has a capacity of approximately 1.2 gallons, leaving about 0.5 gallons as a safety margin.

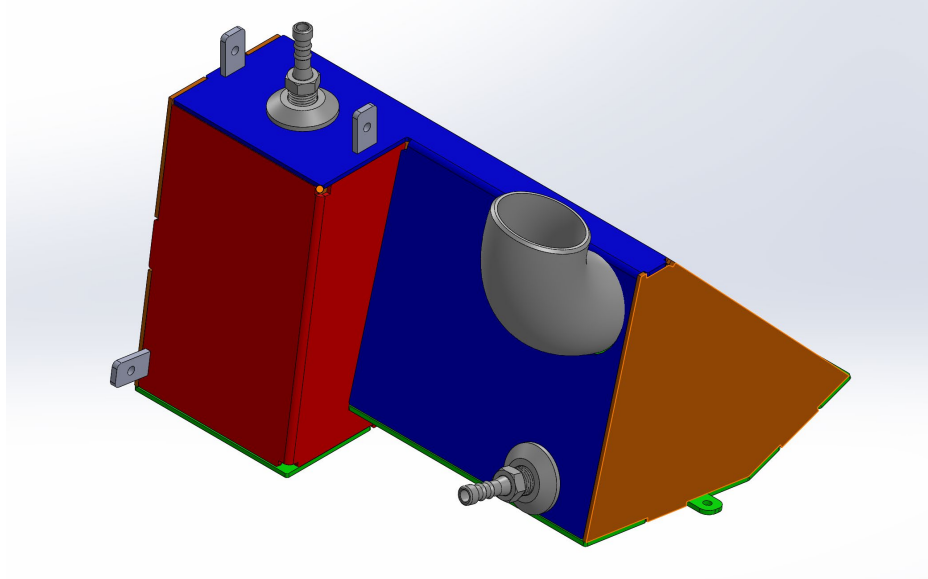


Figure 29: New Fuel Tank Design

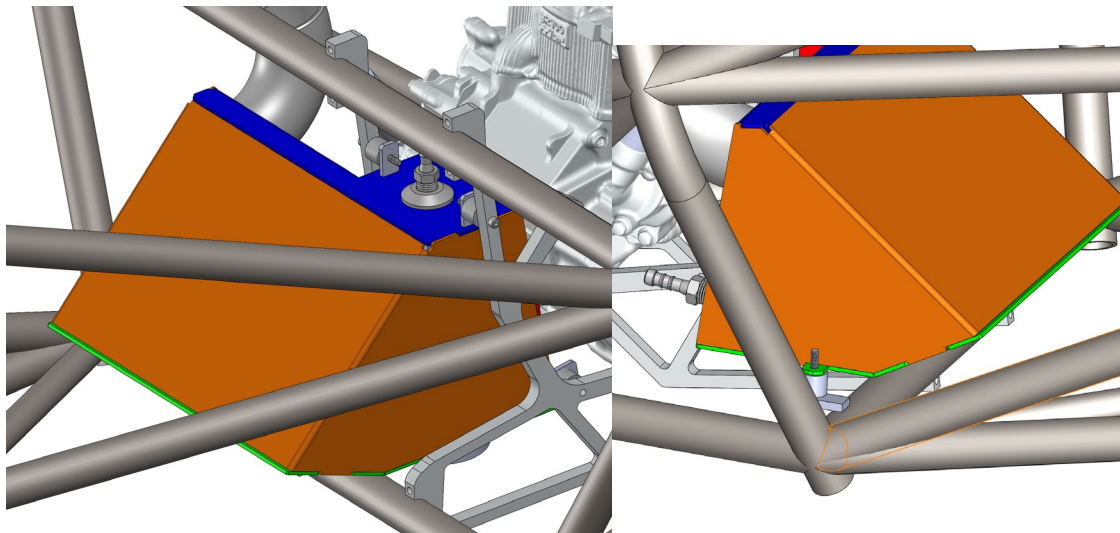


Figure 30: New Fuel Tank Packaging

The fuel tank was constructed from 0.090" thick 5052 aluminum sheet metal. The tank features an internal baffle with a sloped sump where the internal fuel pump mounts into the bottom of the tank. This will minimize fuel sloshing under hard cornering or braking and keep fuel in close proximity to the pump pick up. The tank also features a fitting on top for a breather hose with check valve (required by the rules) and a fitting in the back of the tank for a return line or a plug for a returnless system (as was intended to be used on this year's car).

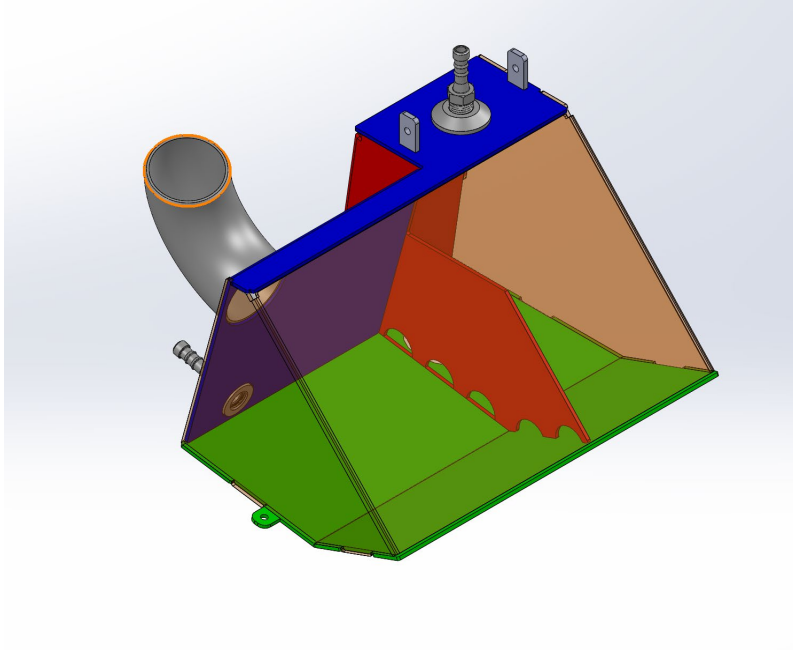


Figure 31: Fuel Tank Baffle

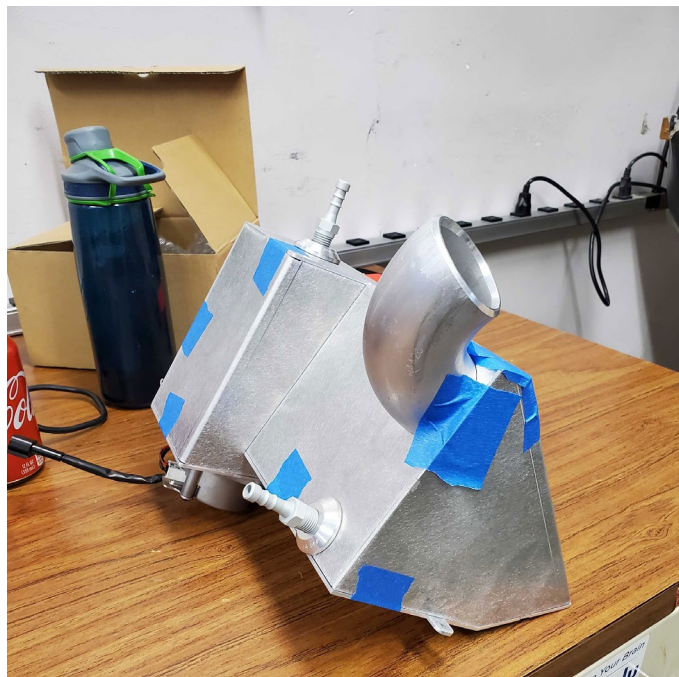


Figure 32: Fuel Tank Manufactured and Mocked Up Prior to Welding

Cooling System

For the 2020 car, we looked to improve the cooling system, as we do with every subsystem of the vehicle. The 2019 vehicle placed the radiator at the very rear of the car with a nearly horizontal orientation. While this is an easy mounting location, as it is conveniently out of the way of most other subsystems, and remains nicely spaced from the driver with the firewall separating the two, it can underperform in cooling the engine. With limited airflow naturally flowing through the radiator at a near horizontal angle in this position, the cooling system relied heavily on the fan to pull air through the radiator.

To reduce the workload on the cooling fan and thus reduce the draw of current from the battery (which was another goal of the 2020 vehicle), we decided to move the radiator to the side of the car, where the flow of air can be more easily directed through the radiator. The airflow on the side of the vehicle is relatively clean along the bodywork; it is only disrupted by the control arms and tie rods.

With the radiator to be placed on the side of the vehicle, we determined it would be best to have the radiator placed vertically (tall way) so that it protrudes less distance from the bodywork. This decreases the chances of the radiator being struck by a cone in the event that a turn is taken too sharply. It also means that more mass will be moved to a central point in the chassis, although the center of gravity will be slightly higher because of the radiator being placed vertically instead of horizontally.

To reorient the radiator to this location meant we needed to purchase a different radiator. A unit where the pressure cap was located at the top, when in a vertical position, was ideal such that the cooling system could have water added without removing it from the car. When purchasing a new radiator, we decided not to proceed with a smaller unit. Although there would likely be more airflow through the radiator in this new location, and thus more cooling capacity, we decided that it would be best to stick with the previous year's size to guarantee that the system would operate properly. If it was determined, during testing, that the radiator was easily capable of handling the necessary cooling capacity then we could downsize to a smaller radiator. The unit we decided on, which has the correct orientation with the pressure cap and is the same core size as the previous year's system, is the Mishimoto YFM660 2001-2005 radiator.



Figure 33: Mishimoto YFM660R radiator

We decided to package the radiator at a 27 degree angle for two reasons: to reduce the height of the radiator in the frame while keeping it a safe distance from the ground, and to maintain efficient cooling. By mounting it at too steep of an angle, excessive pressure is created in front of the radiator because the air has a more obstructed path. At the back of our side pod, we incorporate a cooling fan to help air flow through the radiator when the vehicle is stopped.

To assist in airflow getting to the radiator, a side pod will direct the air through the core. Since the air behind the front tire will be reasonably turbulent, having this duct will make sure that the air will then pass along the side of the car through the radiator. Incorporated in the side pod design will be the cooling fan at the outlet of the duct. By having the fan at the outlet of the duct, the air can freely flow through the fins of the radiator; if the fan were attached to the back face of the radiator core, it could cause an increase in pressure at the radiator face, and restrict the flow through the fins. Also, if the fan were to be attached to the rear of the radiator, it would only pull air through a cross sectional area that is the same size as the fan. By having the fan located at the rear of the duct, it will pull air through the entire core of the radiator, increasing the cooling capacity.

To determine the best shape for the side pod, a 2D analysis was completed in Ansys. To keep the analyses consistent, the same 15 m/s inlet velocity (~34 mph - typical speed driven at competition), as well as the same inlet size, was used for each simulation.

The results for the first simulation are as follows: outlet pressure = 15.6 Pa, mass flow rate = 5.54 kg/s. This simple shape was used as a basis to judge the following designs. A screenshot of the first simulation is seen below:

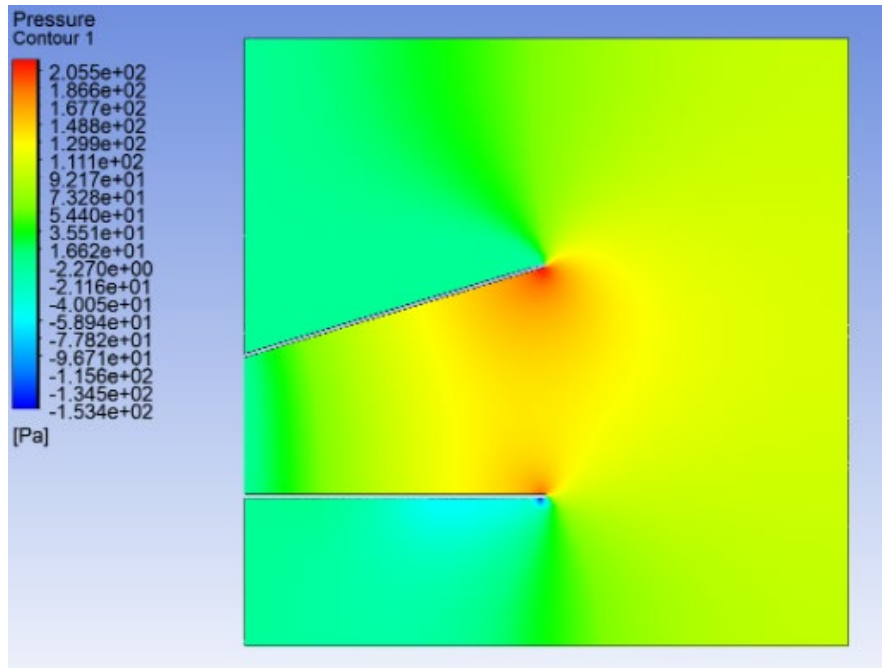


Figure 34: Side pod analysis 1

For the second iteration, a more streamlined shape was used. The pressure at the outlet was 8.8 Pa while the mass flow rate through the duct was 5.44 kg/s. As is seen in the screenshot below, there is a large pressure increase at the bend of the duct. To try and remedy this in the next iteration, a shallower curve was used.

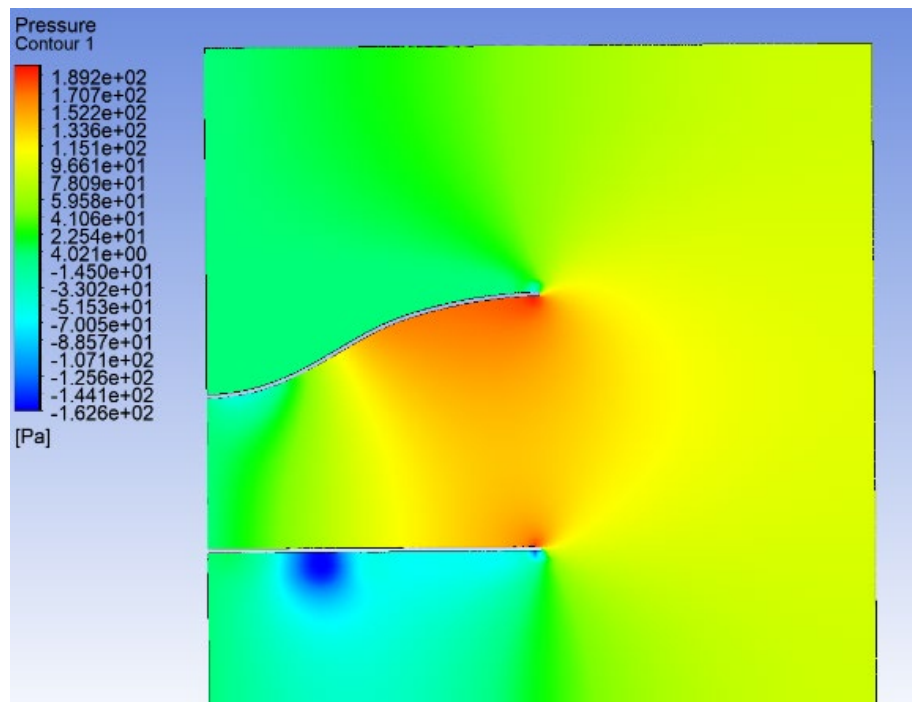


Figure 35: Side pod analysis 2

In this third iteration, a shallower curve was used compared to the second iteration. The pressure at the duct outlet was 8.7 Pa, while the mass flow rate was 5.49 kg/s. The high pressure area at the bend of the duct is slightly better in this case, but could be made even better if the entire duct length was increased. Then, the curve could be made shallower to lower the internal pressure.

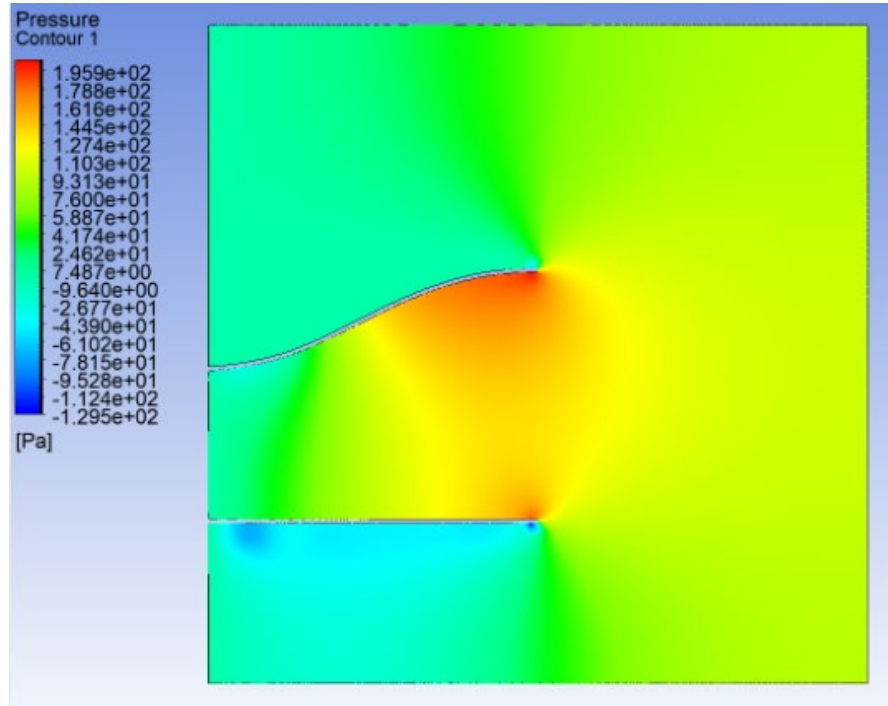


Figure 36: Side pod analysis 3

In this fourth analysis, the entire length of the duct was made longer. Now, a shallower curve is used to reduce the pressure at the outlet to 4.9 Pa with a mass flow rate of 5.48 kg/s. It is clear that lengthening the side pod would decrease the internal pressure because of the shape of the curve used. However, lengthening this piece makes for difficult packaging on the side of the vehicle, so a compromise has to be made.

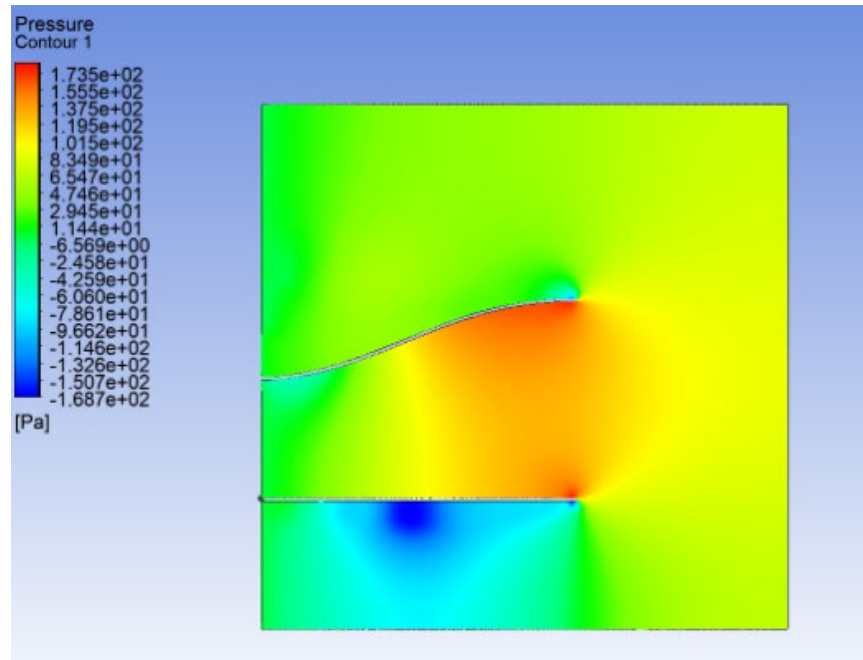


Figure 37: Side pod analysis 4

Next Steps

Intake System

To finish the intake system, all parts must be coated in XTC-3D coating to ensure an airtight seal. Then, appropriate sanding must be done to make sure all parts fit together properly. Use the same epoxy that is normally used for the bodywork to first glue everything together and wrap the entire assembly in a single sheet of carbon fiber to seal all of the different parts together.

Cooling System

Radiator placement has been determined from the side pod design. The radiator must be welded on to the frame. The left 'ear' of the radiator is mounted to the frame via a welded tab. This mounting location uses the OEM rubber grommets to provide some flexibility in the system. The other 'ear' on the radiator should be cut off to allow the side pod closer to the core of the radiator. The bottom mounting of the radiator was not fully designed, but the easiest solution would be to use a tube with a nut welded on the end. The nut will be welded at an angle such that the cylindrical protrusion on the bottom of the radiator sits in the nut. The other end of the rod will be welded to the frame. Longitudinal placement of the radiator is determined from placement in the side pod. A jig should be 3D printed when welding on radiator tabs to guarantee proper placement in the frame.

To finish up the side pod, aside from actually making the piece from carbon fiber (discussed in the bodywork section of this paper), a way to seal the duct to the side pod will have to be determined. If the side pod is not sealed off to the radiator, there is a chance that the air will flow around the radiator instead of through the actual core. This would result in decreased cooling of the engine.

Brake System

With this year's car's change in wheel size from 13" diameter to 10" diameter, a full redesign of the car's braking system was required. This was necessary for both packaging constraints within the new wheels, and to factor in the car's new weight and tire compound utilized. The design of the brake system began with calculations (**See Appendix C: Brake System Calculations**) set up in an Excel spreadsheet to ensure all desired parameters for the system were met. Because two separate brake circuits are required for competition (front and rear), separate calculations were done on separate sheets for both.

Because the car could not be fully designed before the brake system was designed due to time constraints, some assumptions were necessary. These included:

- Total car weight with driver of 550 lb.
- Coefficient of friction between the tire and road of 1.6
- Based of previous cars' handling, design goal of 80-20% front to rear pressure distribution

The overall design goal of the brake system is to have the capability to lock all four wheels (as this is required for competition) while still being able to be effectively modulated by the driver in order to quickly slow down the vehicle. To achieve these design goals, a method was first devised to determine drivers' preference of pedal force required to lock the wheels. A corner scale was placed against a flat surface with potential drivers sitting in the car's seat. The drivers pressed upon the scale with their desired pedal force for lock up. Between five different drivers, the desired force ranged between 90 lb. force and 110 lb. force.



Figure 38: Test procedure for determining maximum braking force

Once this force was known, the calculations could be done to ensure that the wheels would be able to lock with this force applied to the pedal. The overall calculations were done by figuring out the torque per wheel, and determining what size components would be necessary to achieve this. This also depended on the pedal ratio which is discussed later. The next step in creating the braking system was to

determine the calipers to be used. Because of the 10” wheels, caliper size was an important factor, meaning that the calipers would have to be determined before any other components could be determined.

Calipers

In order to properly size brake calipers, their piston area must be known, as this determines how much brake fluid pushes their pistons as well as how much contact area will be pressing on the brake pads. In selecting calipers, one should aim to have the difference in caliper piston areas between front and rear contribute significantly to brake bias. Then, corresponding master cylinders can be selected. On the 2019 WPI FSAE car, a dual piston setup was used in both the front and the rear of the car with different calipers being selected to achieve this difference in piston areas. The 2019 car had a piston area of 2.4 in^2 in the front and a piston area of 0.79 in^2 in the rear. For the 2020 vehicle, the first factor in caliper selection was packaging within the 10 in. wheel. The calipers selected based on the calculated rotor torque needed were the ISR 22-048 for the front (a four piston caliper with 3.04 in^2 of piston area) and the ISR 22-049 for the rear (a two piston caliper with 1.52 in^2 of piston area). The necessity of larger piston areas over the previous vehicle reflects the new tire compound with a higher coefficient of friction as well as the fact that the brake rotors (and thus the effective lever arm stopping the wheel) need to be smaller.

The ISR calipers have a high piston area, low weight, and small size (important for packaging in 10 in. wheels), all while being reasonably priced.



Figure 39: ISR 22-048 Caliper (Right) and ISR 22-049 Caliper (Left)

Master Cylinders

In order for the brake system to function properly, the master cylinders must be sized correctly. The needed size of the master cylinders depends on the brake pedal ratio, rotor diameter, brake caliper specifications, and other vehicle parameters. The master cylinders for the front and rear braking systems must be sized differently as well. Under full braking, the weight shift to the front tires requires more force to be applied to the front braking system to maintain full lockup of all wheels. Therefore, a smaller bore master cylinder is typically required in the front of the vehicle compared to the rear to supply the necessary increased brake line pressure.

In addition to the previous considerations, two main styles of master cylinders can be selected. One of these is a fixed style master cylinder where the cylinder does not move and the brake pedal applies force to it via a bias bar. Another style of master cylinder that can be used involves master cylinders which are mounted on spherical bearings and can pivot. This allows the master cylinders to be positioned at an inclined angle as opposed to perpendicular to the pedal. While the 2019 car used the former fixed style, it was decided to move to the pivoting style for 2020. In addition to being smaller and lighter, the pivoting style master cylinders save space in terms of packaging and are also adjustable in terms of their position. This adjustability was crucial for us this year to ensure that we can fine tune brake pedal ratio based on the position of the master cylinders to ensure proper operation of the new braking system. Based upon the previous calculations involving required torque and piston areas, the following bore sizes were selected: $\frac{5}{8}$ " front (as compared to the 2019 car's $\frac{3}{4}$ " front) and 1" rear (compared to the 2019 car's $\frac{7}{8}$ " rear). The pivoting style cylinder that could accommodate these sizes came in the form of the Tilton 78 Series master cylinders.



Figure 40: The Wilwood Remote Fixed Master Cylinder Used on the 2019 Car (Left) and the Tilton 78 Series Used on the 2020 car (Right)

Pedal Ratio

The pedal ratio is an important factor in the braking system because it changes how the driver foot force translates into stopping force. The pedal ratio can be thought of as the difference in lever arm, from the pivot, between the master cylinder rod and brake pedal. With a pedal ratio greater than one, the brake pedal has a longer lever arm compared to the master cylinder rod, meaning that the force on the master cylinder is multiplied from the driver input on the pedal. The higher the pedal ratio, the more force is transmitted to the master cylinder.

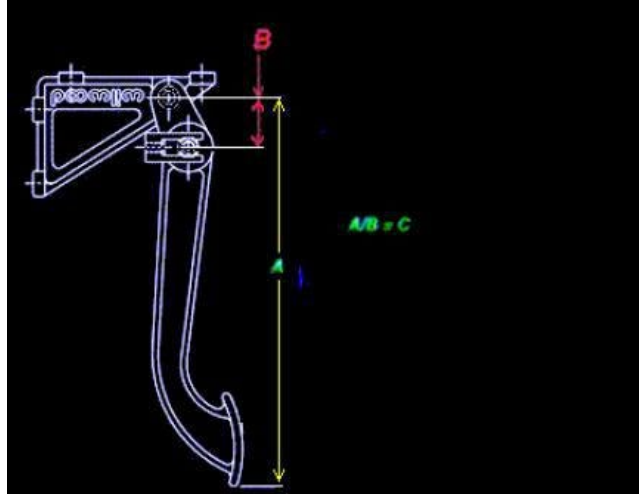


Figure 41: Pedal Ratio Calculation Diagram

Increasing the pedal ratio too much has drawbacks, though. When this ratio is too high, there is an excessive amount of pedal travel needed to get any stopping power. The pedal movement is found by: $Pedal\ Movement = pedal\ length\ from\ pivot * angle$. A high ratio means that the pedal length is high, and thus the pedal must move a lot to compress the master cylinder. Therefore, a good balance must be found between having a pedal ratio that is high enough to allow the driver to apply enough force on the braking system, while also have a responsive pedal that does not require an excessive amount of travel.

For the F20 car, the best pedal ratio was determined to be 2.48. This works well to supply sufficient force to the front and rear brake systems in order to lock up all four wheels. However, different drivers have different preferences when it comes to pedal feel. Some may like a longer travel for more control over the input force, while some may like a short pedal for quick response. It became clear that having some adjustability of this pedal ratio would maximize the performance of our braking system by tailoring to different drivers preferences. This would also allow for final tweaking during testing of the vehicle.

Pedal Box, Brake Pedal, and Balance Bar

Once the calculations were performed to determine the necessary parameters and components for the brake system, a pedal box and brake pedal were able to be designed. The major design goals of this subassembly were adjustability (in terms of pedal ratio and position), minimizing weight, and meeting the FSAE rules requirement that states the entire assembly must remain intact with a 2,000 newton force applied to the face of the brake pedal. In addition with the time constraint of designing and building the car in one academic year, ease of manufacturing was also an important consideration.

The first iteration of the pedal box was designed with a waterjet plate and rails which mount to the frame. The rails have a linear hole pattern which allows the assembly to be translated forward or backward to suit drivers of different leg lengths. On the plate itself, another linear hole pattern allows for the brake pedal itself to be moved along with the master cylinders, which all bolt to the plate with brackets. The first iteration of the pedal itself was designed to be made from a piece of off the shelf square tubing to save on machining time.

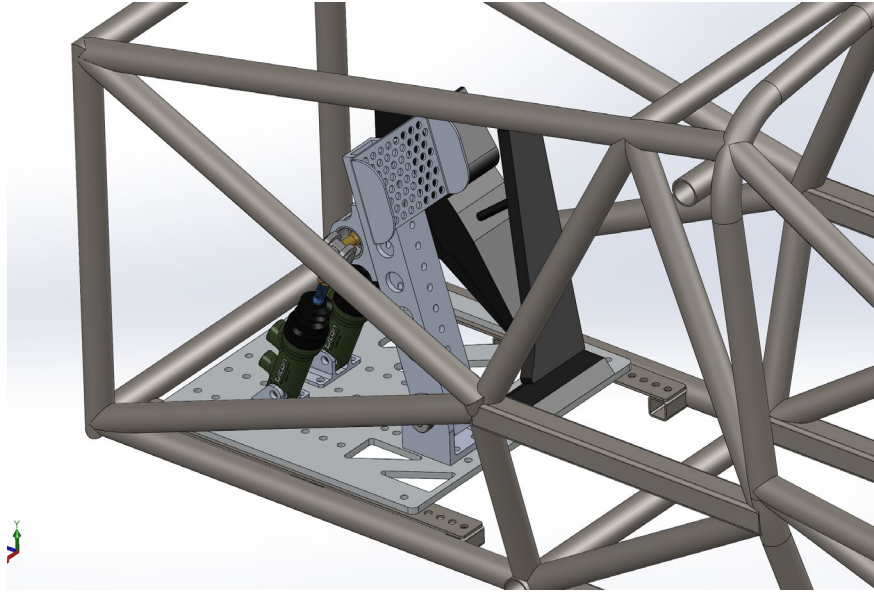


Figure 42: Iteration one of the pedal box design

FEA was also performed on the entire assembly to ensure rules compliance with supporting the required 2,000 N load at the pedal face. This confirmed that the assembly could support the load with all components having a factor of safety of 3 or greater. (See **Appendix A, Pedal Box Version 1**)

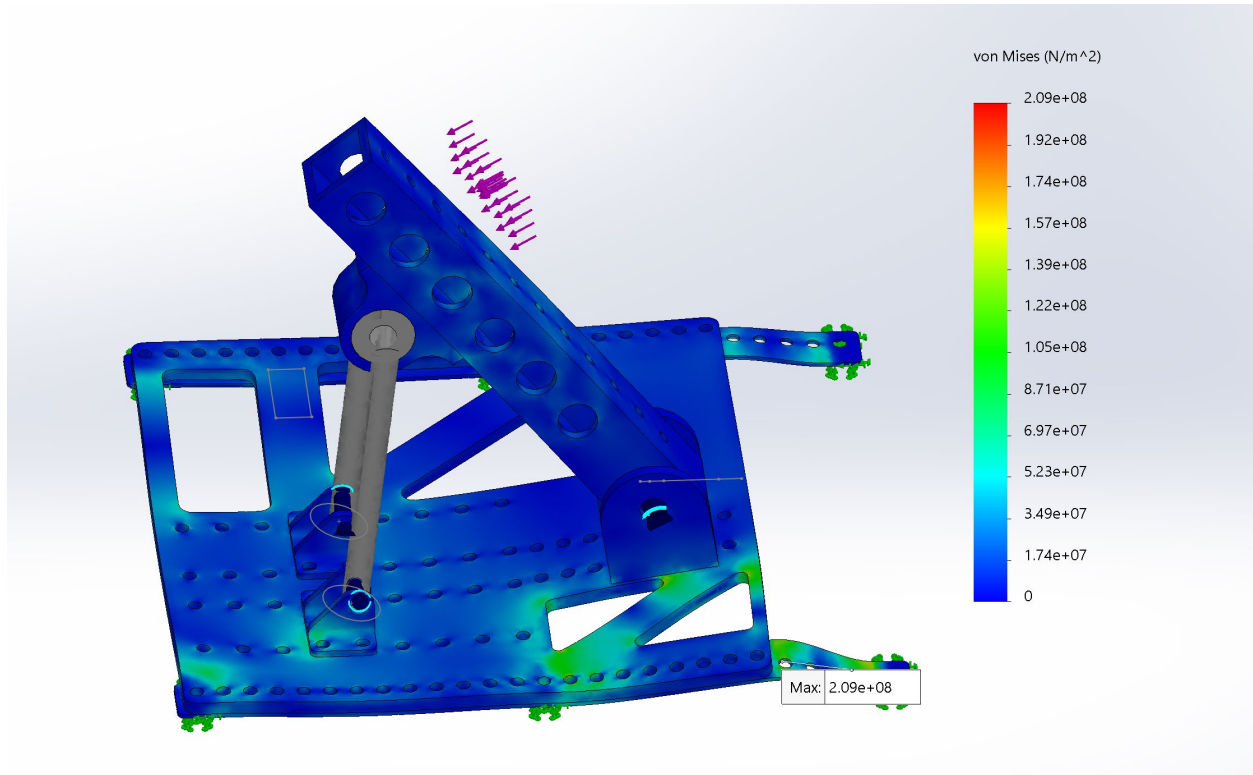


Figure 43: Pedal Box FEA

While this assembly would have performed successfully, concern was raised over the function of the balance (or bias) bar used in this assembly. The role of a balance bar is to fine tune the distribution of force from the brake pedal to the front vs. rear master cylinders, further tuning the brake bias.



Figure 44: Tilton 600 Series Balance Bar (Left) vs. Tilton 900 Series Balance Bar (Right)

This assembly was designed using the tilton 600 series balance bar from the 2019 car which is designed for fixed master cylinders. The problem with this balance bar being fitted to pivoting cylinders is that the spherical bearing in the center provides extra degrees of freedom and causes the pivoting master cylinders to move off-axis, reducing the effectiveness of the applied force on the pedal. Therefore, it was decided to redesign the pedal to accomodate a Tilton 900 Series bar. This bar uses a trunion style design with needle roller bearings to reduce degrees of freedom in the movement of the balance bar. The new pedal design also proved to be 0.2 lb. lighter and is more easily manufactured (waterjet).

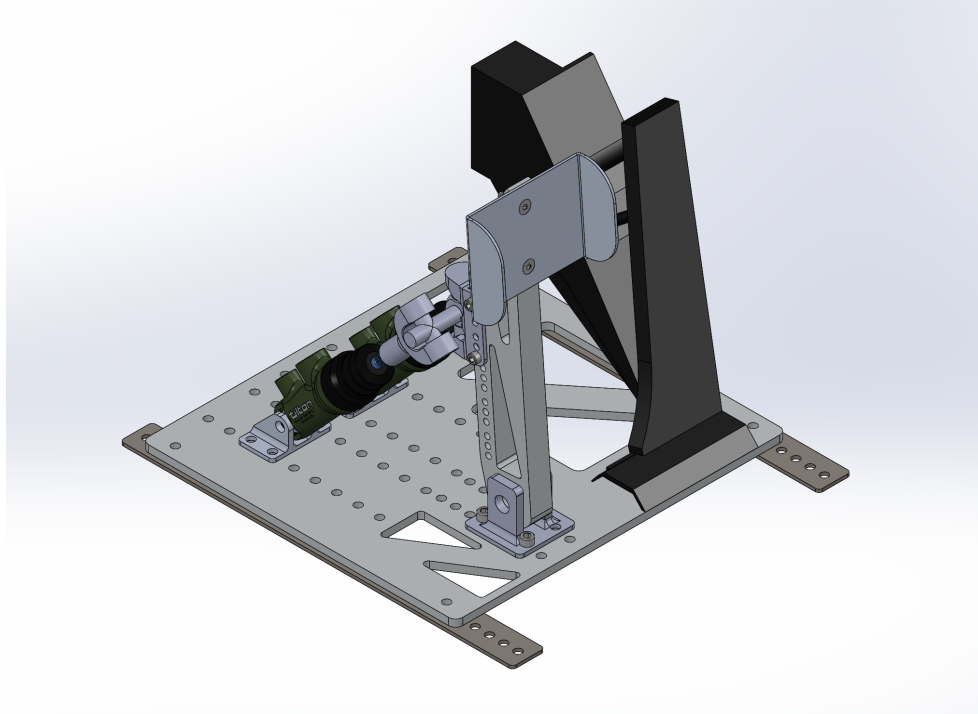


Figure 45: Iteration Two of the Pedal Box Design

Rotors

The role of the brake rotor is to provide a surface for the brake pads to grip in order to stop the vehicle. Because of the design change to move from 13 inch to 10 inch wheels, few rotors were commercially available that would fit the packaging requirements for the smaller wheels. Some off the shelf rotors for motorcycles are available in smaller sizes, but these would need adapters to attach to our RCV hubs rendering them overly complex. Therefore, the decision was reached to design and manufacture the brake rotors in house. From the previous braking calculations and the sizing of calipers, it was decided to use a 194 mm diameter rotor.

The next design variable to consider was material. Most commercially available brake rotors are made from either carbon steel or cast iron. Doing a quick calculation for the change in temperature of each material under braking, it is evident that they are quite comparable with cast iron coming out just ahead of steel with a slightly larger temperature change. Assuming that each rotor equally shares the overall heat transfer:

Kinetic Energy=Thermal Energy

$$\frac{1}{2}m_{car}v_{car}^2 = (4 \text{ rotors}) * m_{rotor}c_p\Delta T$$

Mass of car = 550 lb.=249.5 kg

Velocity of car = 45 mph=20.12 m/s

Solving for change in temperature: $\Delta T = \frac{12,625.149 \text{ Joules}}{m_{rotor}c_p}$

Using masses from SOLIDWORKS and c_p values for both cast iron and carbon steel:

Cast Iron:

$m=0.504 \text{ kg}$

$c_p=0.46 \text{ (kJ/(kg}\cdot\text{K))}$

$$\Delta T = 54.456 \text{ K}$$

Carbon Steel:

$m=0.545 \text{ kg}$

$c_p=0.49 \text{ (kJ/(kg}\cdot\text{K))}$

$$\Delta T = 47.276 \text{ K}$$

The next material property to consider in the design of the rotors was coefficient of friction between the rotor and brake pad. A higher coefficient of friction will provide better braking performance, but will also increase temperature more quickly. While there was unfortunately no test data available to back this up, the sintered metallic brake pad compound for the pads that fit in the previously selected calipers tend to have a higher coefficient of friction between them and cast iron vs. them and carbon steel. KAZ Technologies offers rotor blanks specifically for FSAE made out of Dura-bar G2 cast iron. After further research, it was also determined that we could get rounds of cast iron cost effectively from a local supplier, so it was decided that Dura-bar G2 cast iron would be used.

Once size and material were decided, the next design decision to make was the geometry of the rotor itself. While rotors on passenger cars are often solid, rotors for race applications typically include a circular pattern of slots, drilled holes, or other radially symmetric cut-out. These are used for a variety of reasons including weight reduction, providing a larger surface area for the brake pads to grip, and providing space for gases generated during wear to escape from the brake pad and rotor surface. The downside to these cut-outs is that they induce stress concentrations, increasing the rotor's chance of failure due to cyclic heat and mechanical loading at these points. In order to test the effectiveness of these different types of cut outs, a time dependent transient thermal analysis was set up in SolidWorks. The analysis simulates a period of hard braking for 4 seconds followed by 30 seconds off of the brakes and then back on the brakes for 4 seconds again.

The first round of simulations tested drilled vs. slotted rotors. Overall, there was very little difference in the performance of these designs. The slotted rotor reached a maximum temperature of 524 degrees F whereas the drilled rotor got up to 532 degrees F. Looking at maximum temperature vs. time plots, it is also evident that the slotted rotor cooled at a slightly quicker, but negligible rate. (See **Appendix A, Drilled Rotor**)

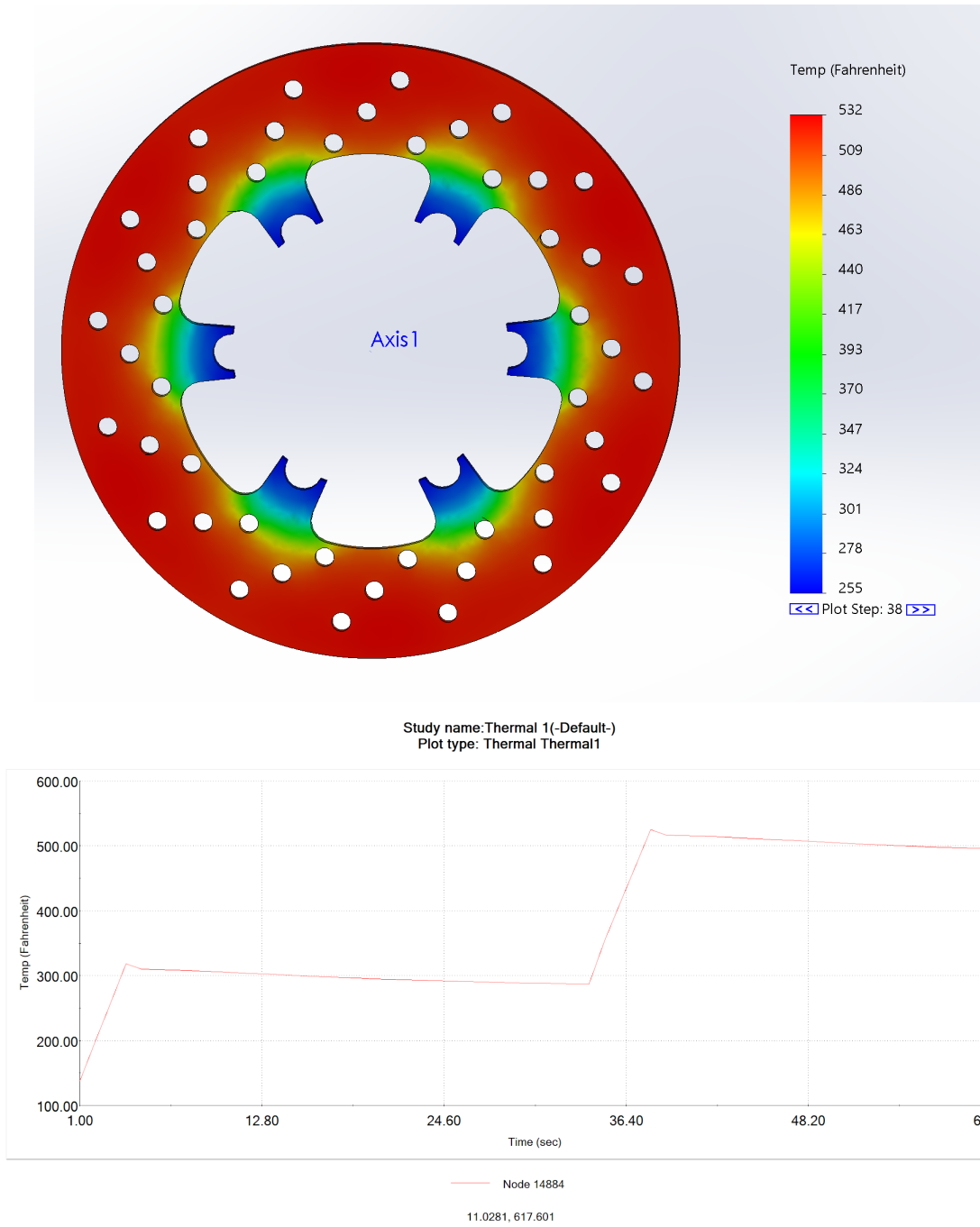
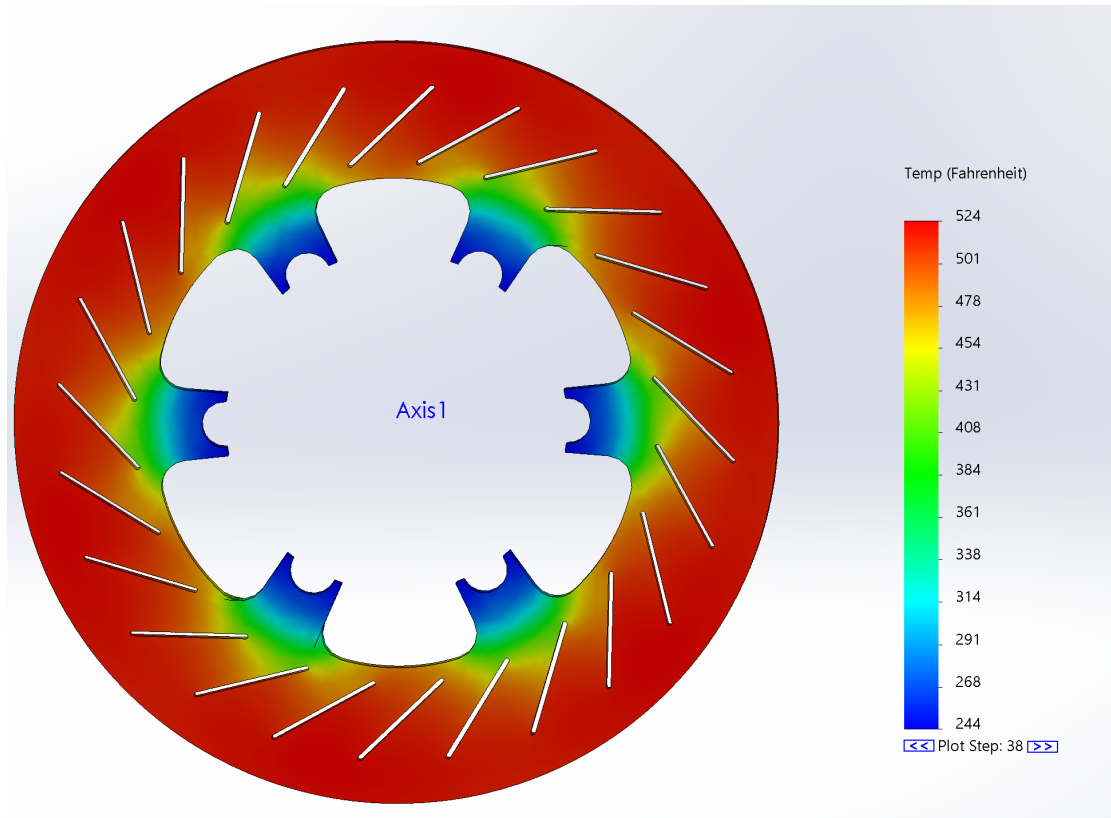


Figure 46: Drilled Rotor Max Thermal Simulation and Temperature vs. Time Plot



Study name: Thermal 1(-Default-)
Plot type: Thermal Thermal1

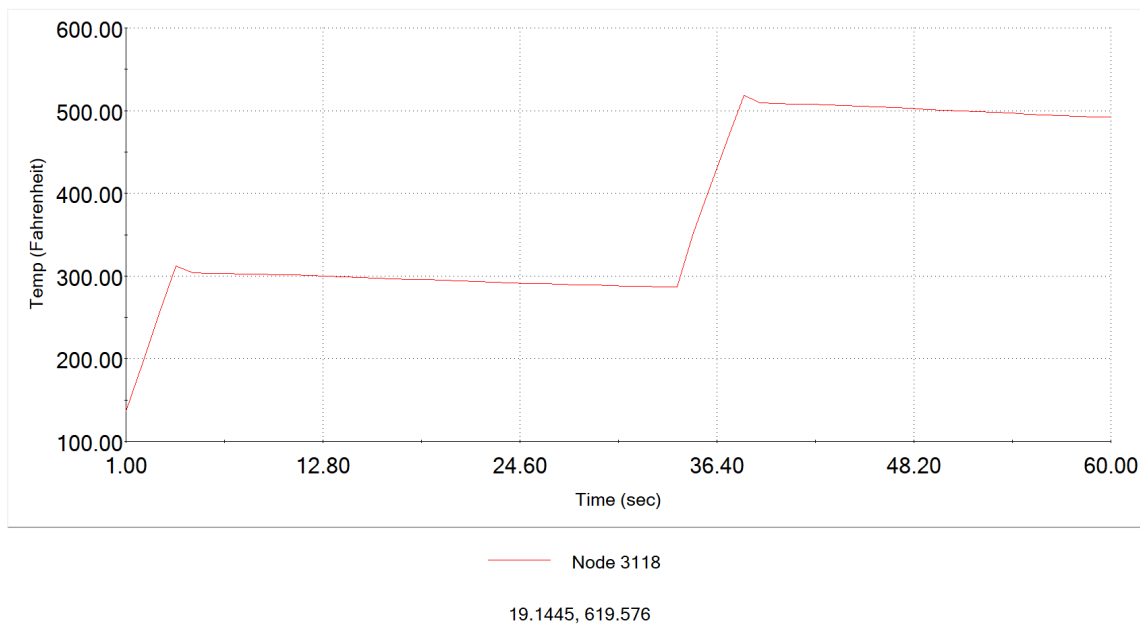


Figure 47: Slotted Rotor Thermal Simulation and Temperature vs. Time Plot

Because the performance difference was so small between these two designs, the drilled rotor was selected as the superior option simply due to ease of manufacturing. It was planned that the rotors would be waterjet out of blanks with minimal machining to achieve the required surface finish, therefore, the drilled design would be more conducive to this process.

Once the drilled design was selected, the next set of simulations tested the theoretical performance of drilled rotors vs. solid rotors. Aside from being lighter, the drilled rotors offered no obvious added benefit. The simulations suggested that the solid rotors may even be better performing. The following graph (Figure X) illustrates that the solid rotors had a lower maximum temperature than the drilled rotors. The rate of cooling was also examined by adding a linear trend line between the data points for both sets of rotors. The slope of the trend line for the solid rotors is ever so slightly steeper, suggesting that they would cool at a faster rate. Possible explanations for this include that the solid rotor has more mass to heat up, causing it to reach a lower temperature.

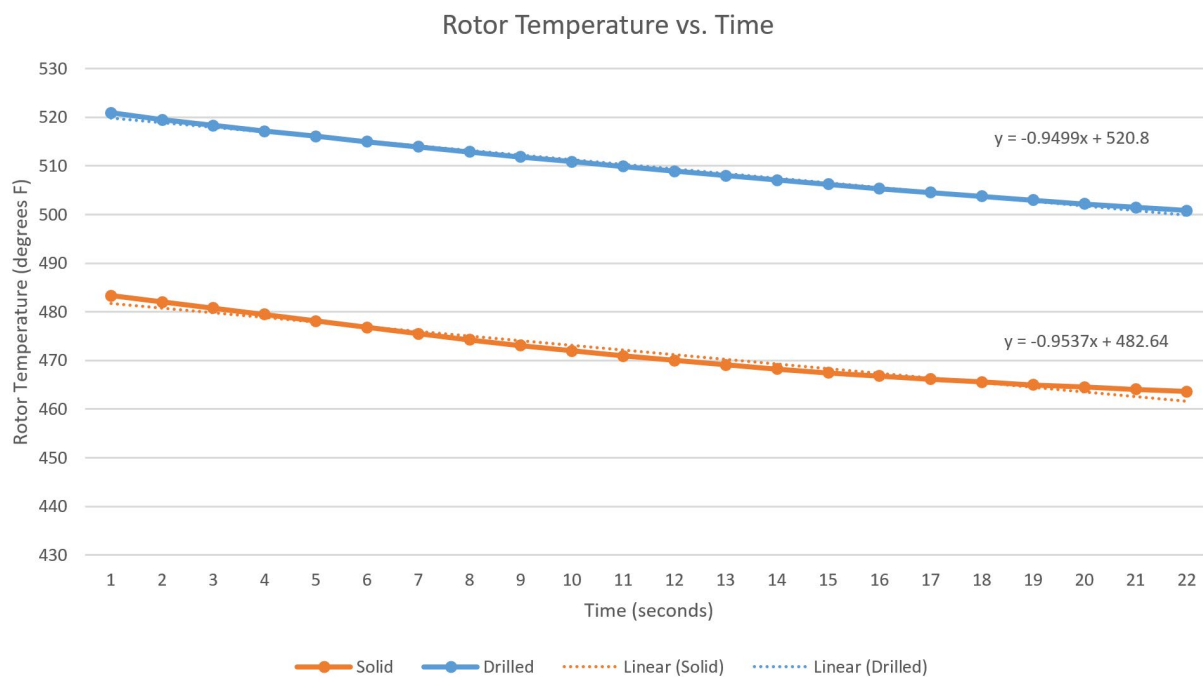


Figure 48: Rotor Temperature vs. Time of Solid vs. Drilled Rotors

These results somewhat agree with SAE Technical Paper 2006-01-0691 [1] which found a 3.2% deficit in cooling performance on drilled rotors vs. solid rotors, beginning braking at around 31 miles per hour (similar to the average speeds reached in FSAE competition). Another potential drawback of drilled rotors offered by this paper is faster pad wear. This is due to the pad material being squeezed inside of the drilled holes under braking, causing more uneven abrasion as compared with a smooth surface.

Because it was cost effective to do so, the team decided to move forward with manufacturing both a solid and drilled set of rotors to compare their performance in the real world and validate the results of the simulations and background research. Unfortunately the manufacturing phase was not reached.

Next Steps

Manufacturing needs to be completed for:

- Rotors
- Brake pedal
- Brake pedal and master cylinder brackets

Suspension

Tires

Throughout most of the existence of the automobile, the biggest hindrance to speed has been tires. This has only changed recently, as the combination of aerodynamics and tire development have made the human driver the biggest limitation in top racing cars. This is because the acceleration levels experienced by the drivers in normal driving (not crashing) are enough to cause blackouts and spinal problems, not because of crash safety at higher speed.

It's very easy to say "I want the best tires to make my car fast", but much harder to know what "better" means. The tires produce friction between the ground and the car, and are where almost all of the forces in the car originate. Tires are really complicated, totally unreliable, and generally a pain for anyone involved with a car. The problem with them of course is that as you know, they are squishy. What a hassle. One of the world's most famous tire modeling engineers, William Cobb, is known for saying (and I paraphrase) "to do it over again, I would make the wheels from asphalt and the roads from rubber." As a mechanical engineer, we are taught how to deal with all sorts of objects that behave in ways we understand. It is difficult to deal with something that few if any people understand completely.

While they are obviously round, think of them as black boxes. Something happens at the bottom, where the tire touches the ground. Something happens in the middle, where it attaches to the suspension of the car. Not one person on the face of this earth understands completely what happens in between. There are many theories. Some models exist to predict the behavior of the tire, but their accuracy is limited. What would be really nice is if there was just some formula some ancient greek brought down from Mt. Olympus to explain how much, and what kind of friction a tire will produce. There isn't, but a professor named Hans Pacejka from Delft, NL kindly made one up. It's not actually one equation, it's really more like 40-70 equations depending on what the engineer is willing to ignore. Pacejka very aptly called this the "Magic Formula."

To use these formulas to even do anything at all, you need a bunch of data you can only get from a giant tire testing machine, of which there are a handful globally. The way these machines work is that they have one surface that simulates the road (ours uses a flat track, others use round drums), and another that holds the tire. The machine squishes the two together in all sorts of ways, pushing, pulling, twisting, rocking, etc and recording the output forces.



Figure 49: Tire Testing Consortium Test Rig

So now that we've done all our tire testing and used a few different metrics to look at the data, which tires are best for the team? I'm still not sure. There are a few options, each with its own ups and downs. When tires are made, there are generally two parts of the project. The first is the chemical compound of rubber used to make up the tire, and the second is the mechanical construction of the tire.

Developing a compound is really expensive as tire companies have to pay a lot of smart kids who did their chemistry homework to figure it out. No tire company will ever develop a compound specifically for Formula SAE competition. Annual sales volumes are just too low to justify the massive expense. Every year our competition has 120 teams, with two sets per team allowed during the event. Most teams barely do enough testing to scrub in their tires, much less use an entire third set. For comparison, an F1 race weekend uses thirteen sets of tires per car. Even though there are only 24 cars, an F1 season consumes over 25,000 tires! FSAE teams are only using a tenth of that, generously, so we are stuck using somebody else's compound. This is undesirable because FSAE cars are much lighter and have much less power than traditional racecars.

Remember above when I told you that we cared about the temperature effects of the tire? Here's why. Rubber compounds only work in a limited temperature range. Imagine the eraser on a pencil. Sometimes it is just so easy to erase, it's like the eraser knows where you want it to go. Other times you get an eraser that's crusty and gross and just kind of smears the graphite around. Tires are just like erasers. When they are fresh and in their operating temperature range they grip the pavement a billion times better. Well, not really, it's more like four times better. One other key detail to know about temperature effects for racing tires is that generally higher the operating temperatures are associated with higher levels of grip.

However, more thermal energy will be required to bring the tire into its ideal temperature range. A tire with a lower operating temperature is expected to produce less grip, but will heat up faster.

There are four compounds that are considered relevant for Formula SAE competition. The hottest compound is probably the Avon A92 compound, which is designed for hillclimb competition in England. These hillclimb events are very short in length, but mostly gather modified street cars and high powered aero formula cars. The problem with this compound is that our car will not be able to generate enough heat to keep the tire in its temperature range. Avon previously offered a softer A45 compound that might have been more appropriate, but no longer do.

The second hottest is the Goodyear D2704 compound. This compound was redesigned by Goodyear for the 2016 model year due to REACH, a set of European chemical safety regulations with which the previous D2697 compound was not compliant. The D2697 compound was used in the 1997 F1 rain tires. F1 cars of this time had easily 800hp and 2000lb total downforce, while our targets for next year are 50hp and 400lb. An F1 race is over an hour long, while the longest event in FSAE is 22km. Even though it was initially developed as a rain tire, it is likely the grippiest compound in contention when used properly. I say likely as for some reason the world's most sophisticated tire testing machine has no direct capability to control tire temperature, and thus no capability to test it. Useless really. Both of these tires are very fast but unforgiving, requiring proper temperature management, and fast recovery.

The last two options come from the specialist company Hoosier Tire. Hoosier does not make any products for street driven cars, and is focused exclusively on racing tires. Their two softest dry compounds are called the R25B and the LC0. The R25B compound is native to lightweight formula style road racing cars. These cars are largely similar to Formula SAE cars in terms of construction methods, but are designed to run on much more open courses. The R25B compound is the tire the team has run for the previous three seasons, with good success. We have won multiple regional autocross events and had good results at competition using this compound. The R25B compound performs best when track temperatures are above 75F, which is a problem in Massachusetts in April and in Michigan in May.

The tires are the single most important part of the vehicle when optimizing for performance, and as such must be chosen first in the suspension design process. Based on Calspan TTC data, discussions with tire company representatives, and interviews with other teams, the Hoosier 43075 LC0 model of tire was selected.

Wheels

With the tire choice made, the next component to define is the wheel. In industry this is commonly referred to as the roadwheel. This term is used specifically to resolve confusion caused by saying "steering wheel." When the car turns both the roadwheel and the handwheel turn, and it quickly becomes bothersome to clarify between the two. There are several factors at play when determining ideal wheel geometry. The lip diameter of the wheel should be very close to the inside diameter of the tire, to ensure the tire does not leak or become distorted when mounting on the wheel rim. The next design choice is the rim width. Tires are typically molded with a tread width that is very similar to the intended rim width, although there are exceptions such as cantilevered tires, which are popular in racing series that restrict rim

width. Formula SAE has very few restrictions regarding roadwheel design. The most significant rule restricts the minimum outside diameter of the wheel to be eight inches. Materials, fasteners, and geometries are otherwise unregulated.

Tire test data from the Tire Testing Consortium indicates that the Hoosier 43075 model of tire performs best with a rim width slightly larger than the molded tread width. Obviously, this is a generalization, as there are advantages and disadvantages to both stretching, as described above, and to pinching, where the rim width is narrower than the tread width. Generally, as a tire is “stretched”, a reduction in sidewall deflection is experienced, as well as a reduction in the change of the wheelprint shape as the vehicle maneuvers. The disadvantage of a stretched tire configuration is a reduction in steady state performance. This is related to the lateral sidewall stiffness as mentioned above. Since the sidewall is more aligned with the direction of loading as the car corners, the tire has a higher effective lateral stiffness, which results in a geometrically smaller wheelprint area. In order to extract this transient performance benefit, an eight inch rim width was selected. This is 0.7in wider than the measured tread width of our tires of 7.3in.



Figure 50: Braid Roadwheel

There are a number of choices out there when it comes to wheels, our team selected Braid wheels as they were readily available in the custom sizes required, and offered a one-piece construction, increasing the stiffness to weight ratio of the wheel. Many designers do not realize that the wheel displays significant elastic deformation under load when maneuvering, potentially resulting in undesired toe and inclination angles. During the skidpad event at competition, deflection of the metal wheel rim has been measured to be over three degrees, a huge change considering the car is aligned to the nearest tenth of a degree.

Linkage Layout

The purpose of the suspension system is to transmit loads from the tires to the frame of the vehicle. There are a large number of designs that have been used throughout history, and there is still not a global consensus on which one is best, even on which is best for one specific application. The system employed by the WPI F20 is by far the most common in modern racing cars, unequal length double wishbones. This style of suspension was selected because of the simplicity of tuning it, as well as the high stiffness to weight ratio relative to a multilink layout. The geometry of these wishbones is determined by a set of studies, each designed to ensure proper operation in a certain circumstance. When we consider the entire vehicle's suspension system, there are four distinct scenarios it experiences. These are Bounce, Pitch, Roll, and Twist modes of operation.

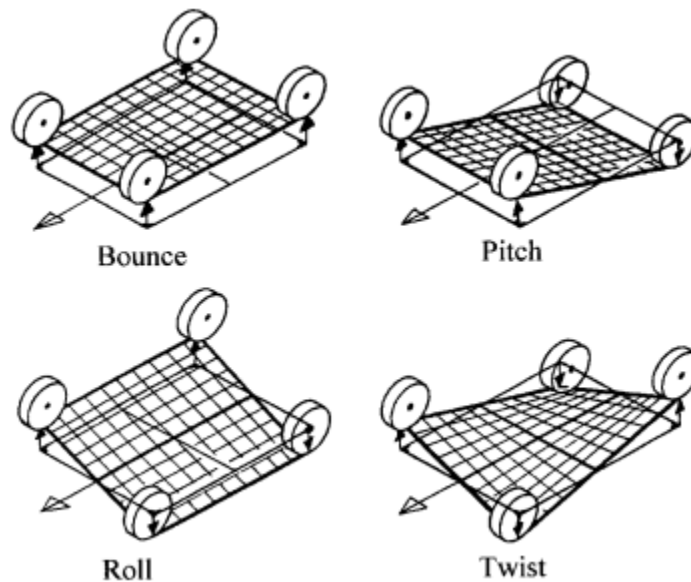


Figure 51: Four Basic Modes of Vehicle Behavior

In Formula SAE, we are most concerned with the roll and twist modes. The car will experience roll every time it corners. A roll moment is an inevitable consequence of having a center of mass above the ground. Even the fastest cars ever made have some mass, and hopefully all of it is above the ground. This roll moment is reacted in as many as four ways. The four places a roll moment can be reacted are through the springs and dampers, through the control arms, through anti-roll bars, and through aerodynamic effects. Most likely, all of these mechanisms will be at play, and each of them results in a component of the total load transferred from one side of the vehicle to the other. When this load is transferred through the springs and dampers, it is referred to as elastic load transfer. When load is transferred through the control arms, it is called kinematic, or geometric load transfer.

The suspension system of the WPI F20 is designed to maximize the portion of elastic load transfer, and minimize the portion of geometric load transfer in roll maneuvers. This is to allow the engineering team to make effective setup changes during testing. When designing the car, I knew that I did not know what the ideal wheel rates and Total Lateral Load Transfer Distribution (TLLTD) for the car would be, so I

needed to leave myself room to change them during testing. There are many guides, equations, and rules of thumb for determining values for spring rates, damper rates, and bar settings, and many of them were used. With that said, all simulations are wrong, and even though some of the ones used in designing the WPI F20 may be useful, simulation is never a replacement for physical testing. By using a data logging system to record vehicle accelerations, steering angles, and spring positions, empirical decisions about car setup can be made.

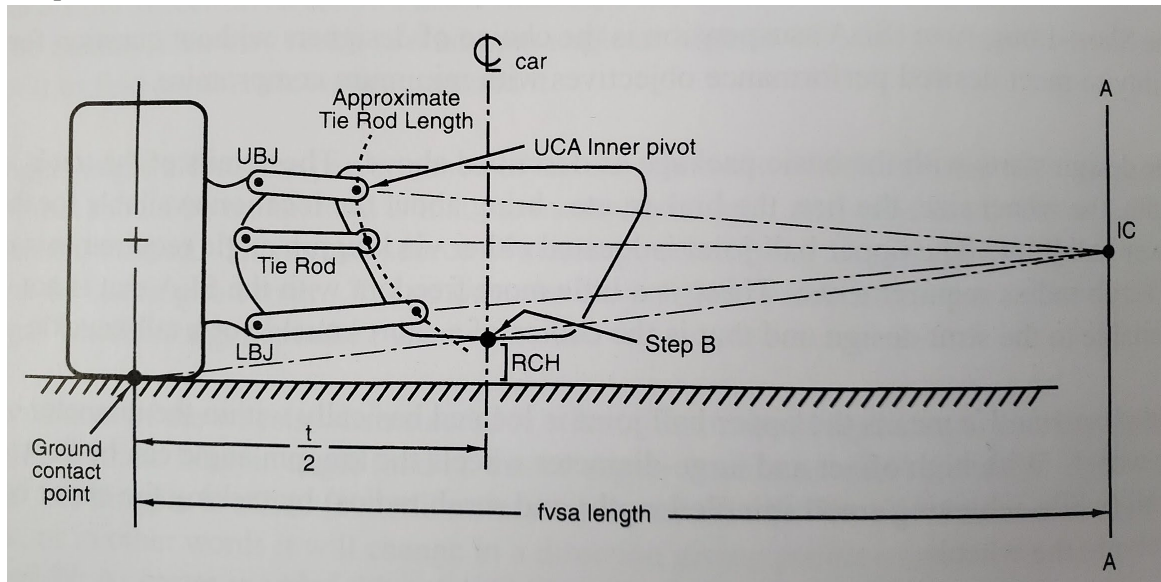


Figure 52: Basic Linkage Layout, from Milliken 17.5

This reduction in geometric load transfer was achieved by designing the linkage system to have roll centers very close to the ground. Throughout the kinematic design of the suspension system, a software package called OptimumK was used. With the wheels selected, the front view geometry will be examined. A four bar linkage model is used, the bodies being the unsprung mass, the sprung mass, the upper control arm, and the lower control arm. This method is described in literature by the Millikens in Chassis Design, which details the work of Maurice Olley. Olley worked at GM beginning in 1930, and is considered by many to be the pioneer of independent front suspension.

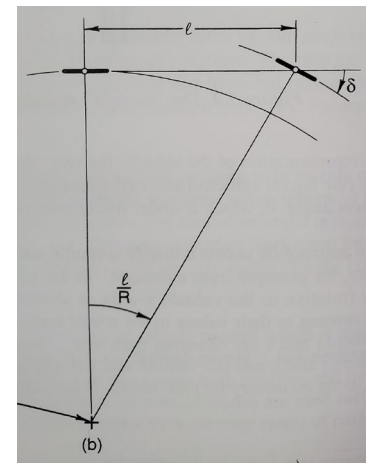
One of Olley's observations was that roll center migration created undesirable responses during cornering, and that an easy way to resolve this is to set the ratio of the lengths of the links equal to the ratio of the heights of the outer ball joints. The lower ball joint is positioned as low and close to the brake rotor as packaging constraints allow, and must be considered at the same time as the side view geometry. Specifically, the caster angle and steering offsets affect how low in the wheel the ball joint can be packaged. These values were 8° and 10mm respectively. A large caster angle results in improved steering response due to steering camber effects, and also in a large mechanical trail, which increases steering effort. This is dealt with in modern passenger cars by using a power steering assist system, but in a formula style car a steering axis offset is used to bring the mechanical trail closer to the target, which was 24mm for this design. The same process is used to place the upper ball joint, except now the kingpin inclination must also be considered. Where caster is the side view projection of the steering axis, kingpin

is the front view projection. For this design, the kingpin angle and offsets are outputs of maintaining roll geometry and tire scrub radius. When measuring scrub radius, tire deformation under static camber and race weight were estimated based on data from the Calspan TTC. The effect of this deformation is a slightly reduced tire radius, and a wheelprint that is slightly offset towards the vehicle centerline, a result of the static camber setting.

Steering System

The steering system of the WPI F20 is very similar to that of the F19. It features a rear steer configuration with approximately 50% of Ackermann steering. The primary objectives of the steering system were to ensure the vehicle could navigate all portions of the course without excessive tire slip, and to reuse the existing steering rack and steering gearbox from the WPI F19.

The first consideration in the design of a car's steering system is the layout of the course it will be driven on. The car must be able to turn a tighter circle than the tightest circle on the course. Failure to adhere to this will require the driver to slide the car across the top of the pavement. This poses a number of problems such as tire wear, driver fatigue, and off course penalties, but worst of all it makes the car slower. This is because it requires operating the tires at a slip angle much higher than is ideal. To accomplish this, a simple calculation is used to define the required toe angle of the roadwheel. This analysis is performed on a simple bicycle model of the car. A steering system exhibits nonlinear response due to the geometry of the linkage system, but this is something to be dealt with later. For now, start with



the figure below, which can be found on page 128 of Milliken, where it is figure 5.3.

Figure 53: The relationship between wheelbase, toe angle, and corner radius

The total steer angle required to navigate a given course is given by $\delta_{rad} = l/R$, where l is the wheelbase and R is the corner radius. There are two things to think about when you choose a value for R . The first is the configuration of the endurance course at competition. Obviously, you won't know exactly what this is, but Rule D.12.2.2 in the Formula SAE rules states that the minimum diameter of the sharpest turn in the endurance event will be 9m. When designing a steering system, don't forget that this is a diameter not a radius, and also consider that the ideal racing line will not be all the way around the outside of the corner.

The second factor to consider is the steering effort of the car. Formula SAE head design judge Claude Rouelle recommends a steering torque of no more than 5Nm of handwheel torque maximum, whereas road cars commonly require below 1Nm. The geometric factors that affect this are the length of the steering arm, the linkage geometry and the steering rack c-factor. Geometrically, higher (“faster”) steering ratios will require larger handwheel torques, and lower (“slower”) steering ratios will have a reduced handwheel torque requirement, but will require larger angular displacements of the handwheel. In road cars it is common to turn the steering wheel more than a complete turn in either direction when maneuvering, but this is undesirable in motorsport applications. The biggest reason small handwheel displacements are desirable are biomechanical. The handwheel rim force in a formula style racing car is dramatically higher than in a road car. Road cars typically have high steering ratios, on the order of 20:1, as well as hard, narrow, relatively gripless tires and power steering assist systems. A Formula SAE car has the opposite, low steering ratios on the order of 5:1, soft, sticky tires, and no power steering system. In a road car, the handwheel can generally be rotated to both extremes with one finger at any speed. Even Arnold Schwarzenegger would be unable to do that in a Formula SAE car. Designing the steering system to allow for smaller handwheel displacements allows the driver to engage more muscles as they steer, such as the rotator cuff and tricep, as opposed to only using muscles in the forearm, which is what most drivers on the road do.

The next aspect of the steering system to be designed is known as the Ackermann steering effect. It is named after Rudolph Ackermann, who patented its use in England, but it was not his design. The concept we know today as Ackermann was coined in 1878 by french engineer Charles Jeantaud. The design Rudolph Ackermann



Figure 54: Rudolph Ackermann's Race Car

contributed to the world of vehicle dynamics is the double pivot steering system, as opposed to single pivot steering systems commonly seen today on radio flyer wagons and the like. Except it wasn't, he in fact somewhat dubiously used his own name when applying for the patent rights to the same invention by german carriage designer Georg Lankensperger, who had hired Ackermann to acquire the patent in the UK.

Ackerman steering effect is the difference in the toe angles of the roadwheels when negotiating curves. As the vehicle travels around a circle, the inside and outside wheels are travelling on circles of different radii, different by the track width of the vehicle. In order for each tire to operate in its ideal slip angle range, the tires must assume different toe angles. When Jeantaud devised the solution, his objective was to reduce the size of the ruts his rigid carriage wheels made in gravel driveways. The first pneumatic tire similar to what we use today wasn't produced until 1888, by John Dunlop. When discussing

ackerman effects, ackermann is referred to as a percentage of “Ackermann” steering. For a given corner, this is defined such that lines drawn through each spindle axis converge to the same point. Another way to visualise it is that the two front spindle axes converge to a point, and that point is on the centerline of the car’s rear axle.

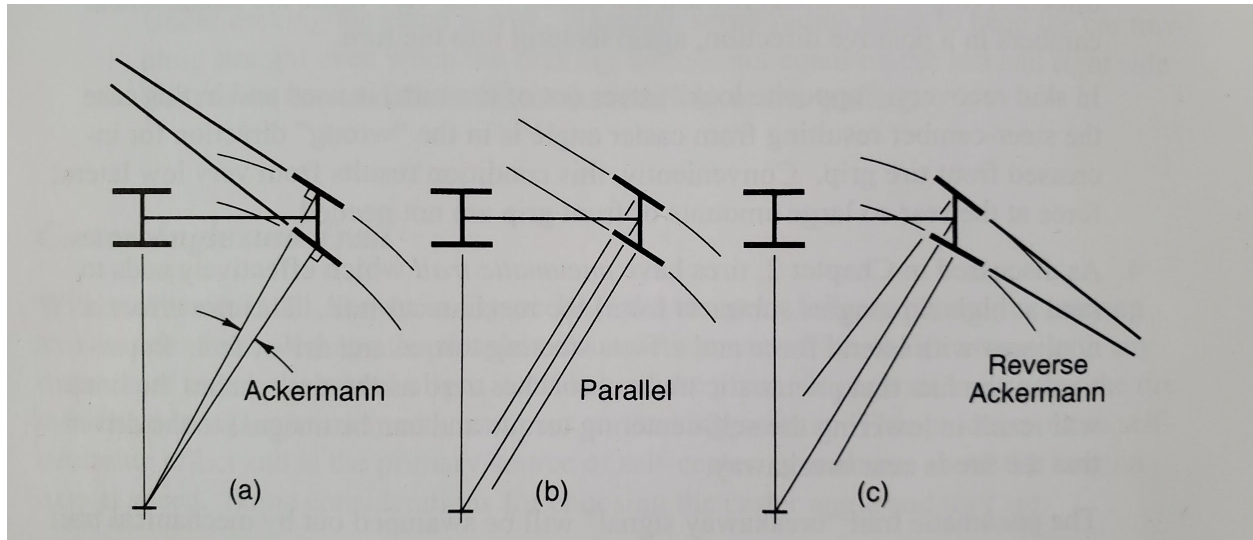


Figure 55: Ackermann's Steering Effect

Finally, the effects of bump steer must be considered. Bump steer is toe change that results from the suspension actuating vertically. In most applications it is generally undesirable. Even though the courses Formula SAE cars run on have few if any “bumps,” the cars suspension will move during all dynamic maneuvers. The F20 front toe links are designed to give a maximum of 0.1° of toe in the vehicles range of bump travel. This slight amount of toe in will improve the car's stability in braking efforts. The rear toe links are designed to have no toe change at all. OptimumK is used to create an iterative solution the position of the toe link pickup point on each upright, and define the toe link lengths.

In future years, it is the recommendation of the team to design a front steer suspension geometry with an angled rack and no u-joints, apex joints, gearboxes, or any other kind of articulation between rack and handwheel. This type of setup has been employed by many teams, notably including University of Connecticut, in Storrs, CT. The advantages of this setup are the ease of manufacture, reduced weight, reduced steering compliance, and reduced steering effort. Additionally, front steer designs are recommended (by me, but also by Milliken and Milliken in section 19.2) as they place the more highly loaded toe link in tension as opposed to compression, allowing for a weaker toe link due to lack of buckling effects, as well as reduced steering compliance.

Control Arms


The control arms of the car are generally responsible for only two things. These are camber control and reaction of brake torque, for cars with outboard brakes, which includes most cars. These forces can both be quantified using tire data, as they are both reactions of forces that originate at the wheelprint.

There were several important design choices that went into this year's control arms. One of the major problems with previous iterations of this car has been the freedom of movement in the linkages.

This has led to binding in the suspension linkage so that it doesn't operate as designed. The cause of this problem is difficulty maintaining the necessary tolerance between the frame nodes for the control arms and the connection points on the control arms themselves. Both components are welded and are fitted together with spherical bearings. While spherical bearings are good for components that must move freely in multiple directions they have minimal tolerance in misalignment normal to their axis. In the 2019 car it was observed that when the control arms were removed there was as much as 7mm of misalignment between the control arm and its mounting point.

It was decided to make the transition to machined, instead of welded, control arms. This was determined to be the best option because the necessary furnaces to normalize welded components or the necessary fixturing to make the components more accurately were not available. Machining the control arms will allow the distance between the mounting points to be made with much greater accuracy.

The main function of the control arm is to prevent the wheel from moving laterally with respect to the frame. It's highest load case occurs when the vehicle is braking. In that load case the control arm effectively acts as a beam in bending parallel to the ground plane. One of the strongest and most weight efficient geometries for a beam on bending is the I beam because of its high moment of inertia.

Fixture name	Fixture Image	Fixture Details
Fixed-1		Entities: 2 face(s) Type: Fixed Geometry

Resultant Forces				
Components	X	Y	Z	Resultant
Reaction force(N)	1,415.28	-323.345	-4.53549	1,451.75
Reaction <u>Moment</u> (N.m)	0	0	0	0

Load name	Load Image	Load Details		
Force-1		Entities: 1 face(s), 1 plane(s) Reference: Lower Control Arm Plane Type: Apply force Values: 1,415, 324, --- N		

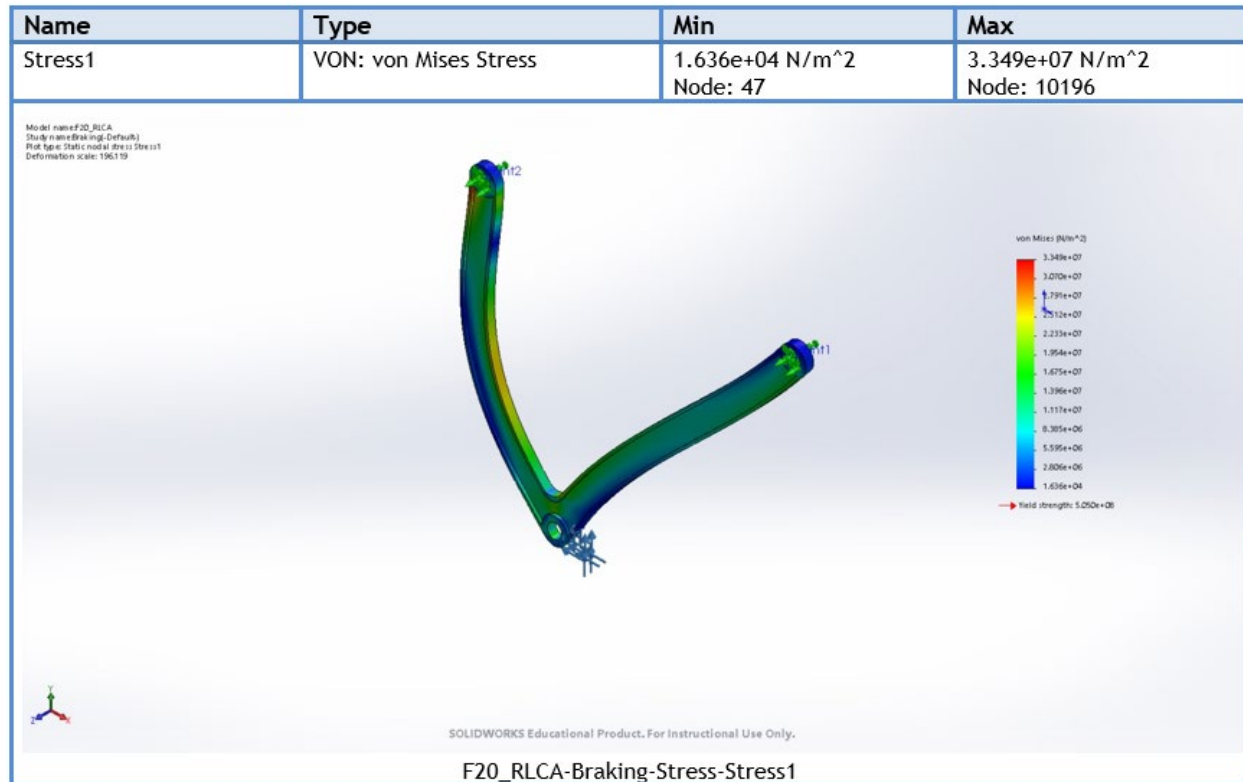


Figure 56: Control Arm FEA Studies

Rockers

The suspension rockers serve to redirect jounce and rebound forces from the wheel from the pushrod to the springs. The hardpoint geometry was determined using Optimum K as explained above. This section will discuss the mechanical design of the rocker itself.

A pushrod and rocker system is employed on the car for a number of reasons. First is the desire to adjust the installation ratio of the coil spring and damper. This means that the rocker geometry is designed to give the desired wheel rates using springs that are actually available. While springs in custom rates are available in the sizes required, they are very costly and have a long lead time. An added benefit of remote mounting the dampers using rockers is the ability to incorporate rising or falling motion ratios into the design.

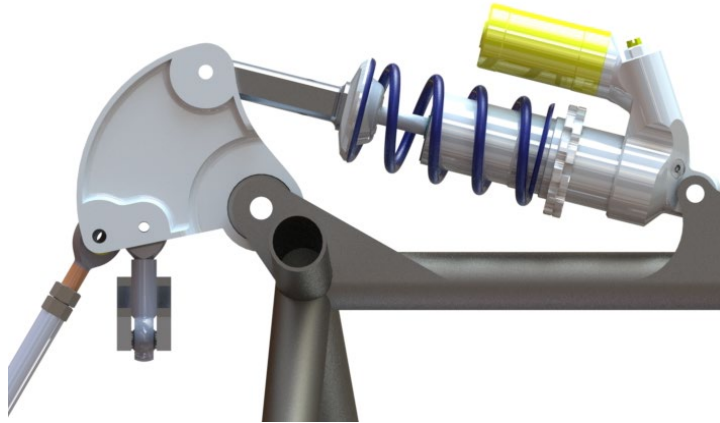


Figure 57: Front Rocker Assembly

When modifying rocker geometry to give ideal motion ratios and ramp rates the length of the shock must also be changed. To accomplish this quickly, in house rod ends were fabricated to increase the length of the spring and damper assembly. This is nice because the spring does not need to be removed in order to adjust the shock length, only the rod end. The team made two different lengths of rod end, one for the front and one for the rear.



Figure 58: Damper Rod-End Assortment (Front, Rear, Original)

The main pivot bearing selection for the suspension rockers posed an interesting challenge. The main function of the rocker is, as the name suggests, to rock back and forth on a pivot access. While pivoting is the main function the bearing also needs to be able to withstand a certain amount of side

loading without binding. The suspension geometry is designed so that in an ideal case the rocker will see primarily radial load but there will still be flex in the structure in which case the wheel forces will come out of line from the axis. Additionally, kingpin inclination effects result in longitudinal migration of the wheel center and therefore load the rocker off-axis. Those constraints must all fit within a confined space, the width between the rocker tabs is only about 15mm and optimally the bearing diameter would be as small as possible to save weight. After discussing with multiple bearing suppliers, a single double row angular contact ball bearing is used in each rocker, to ensure the stiffness of the assembly, as well as to reduce the binding moment in the rocker's pivot point. In the current IndyCar, manufacturer Dallara uses a stack of two thrust bearings and a needle roller bearing. This solution was evaluated and deemed not necessary for our application. IndyCar is a minimum weight series, so any weight gain can be taken out of the cars ballast, without sacrificing a lot of performance. The three bearing combination offers slightly increased stiffness and reduced friction, but at a cost of over 200 grams per corner and increased size they were determined to be undesirable for Formula SAE. Formula SAE is one of very few high level motorsports where there is no minimum weight.

Next Steps

The designs of all of the suspension components are complete and the material has been ordered. This section will layout the plans that were made for manufacturing.

Uprights

The main body of each on the rear uprights has been machined, leaving the mounting holes for the ball joints, toe bar, and brake caliper to be drilled. The next step will involve using a rotary positioning chuck clamped on the center bearing bore to rotate the upright to the necessary angle.

With the front uprights it is recommended to do the first operation in a vise and to bore a hole through to the other side of the stock centered in the middle of the bearing bore. The hole allows for easy location on the second side. The upright can then be clamped by the bearing bore using the rotary positioning chuck. The flat bottom of the ball joint pocket can then be indicated into the y axis of the machine. Step over distance of the roughing tool should be reduced on the second side to prevent the part pullin off the chuck.

Control Arms

The intention of the control arm was to have the outside profile cut to size on a waterjet and have the spherical bearing bores cut under size for final machining. The blank could then be clamped down to a fixture plate to machine the h-beam. Finally the spherical bearing holes could be machined to size.

Once the control arms and there mounting clevises are complete the clevises should be put in place on the square tube of the frame using the control arm as a spacer. The hole positions for the clevis should then be marked on the frame. There is a hand drill alignment press in the shop, this should be utilized to drill the holes through the frame. It is critical that these holes are correct!

Bodywork

This section covers the design and manufacturing of the vehicle's bodywork. Design choices will be discussed first, followed by the design and manufacturing processes. Lastly, the section is concluded with a detailed guide for completing the unfinished manufacturing steps. Units for this section are listed in imperial instead of metric because manufacturing materials were sold in imperial dimensions.

General Design Choices

The bodywork design features a nosecone, side panels, side pods, and a floor panel. The main objective for the bodywork was function, with appearance being a less critical but still important factor. The largest goal for this year's car was to incorporate functional side pods, which will be discussed in their own section later.

One consideration was whether or not to make an engine bay cover. However, it was deemed unnecessary because it would take a lot of time to design the shape around the contents of the engine bay and the benefits of having one would not sufficiently outweigh the potential downsides. The benefits would be a more complete appearance and (potentially) better aerodynamics. However, the extra aerodynamics would likely not play a significant role since previous teams have reported the average speed at endurance to be about 40 mph. The potential downsides to an engine bay cover are engine cooling problems, reduced ease of access to the engine bay, and a significantly longer design and manufacturing phase. For these reasons, when prioritizing the functionality of the bodywork, it made much more sense to not include an engine bay cover and instead spend extra time refining the side pods to be as beneficial as possible.



Figure 59: Bodywork render

Design

The design process began with sketching up a concept on paper. This was just a simple sketch to get a rough idea for how the components would be shaped and placed as a whole. Next, the components were modeled in CAD software. Originally, Autodesk Fusion 360 was used for both the nosecone and side pods because of its soft modeling functionality that made modeling of “freeform” objects easy. However, this ended up being less preferable for the side pods as they were more dimension driven - they had to fit around a radiator and exhaust. Flow simulation was also challenging because the bodywork had to be exported as a STEP file to be usable in SolidWorks, and SolidWorks does not allow for editing of STEP files. This meant that a new file had to be created and exported to SolidWorks for every change made to the design. Therefore, the side pods were later redesigned in SolidWorks to make dimensioning possible and facilitate the flow simulation process. The nosecone was still modeled in Fusion 360 and was later imported to SolidWorks as a finalized STEP file.

It should be noted that even though side panels and a floor pan were to be included in the finished product, these components did not require any significant design work because they would be flat or nearly flat. Instead, dimensions could be measured directly off of the frame and a sheet of carbon fiber fabric could be simply cut to size for manufacturing.

Nosecone

The nosecone was designed to minimize drag and fit snugly around the frame. It covers the section of the car from the front roll hoop forward. Flow simulations were run to make sure airflow around the car was as smooth as possible. This resulted in a nosecone that was very long and slender, extending far enough beyond the front end of the frame so as to leave ample room for the impact attenuator. It measures about 48 inches long.

Side Pods

The side pods were the main focus of this year’s bodywork design. On the left side of the vehicle, one side pod surrounds the exhaust to allow it to be routed outside the engine bay. On the other side, the side pod serves as a cooling duct for the radiator. The radiator is placed towards the front of the side pod, which narrows down to a cooling fan. Flow simulations were run on initial mock-up models and the actual part models to ensure the desired airflow dynamics were achieved. A more detailed discussion of the radiator side pod is covered in the cooling section above. As for the exhaust side pod, the goal was to fully shroud the exhaust to protect the driver and anyone standing near the vehicle from heat and hot surfaces. However, no finalized design was achieved because the shape is dependent on the exhaust routing, and the exhaust design was not completed until just before the COVID-19 lockdown.

Manufacturing

Molds for the bodywork were to be assembled using foam board and body filler. Large sheets of insulation foam board would be cut according to templates, stacked to form the approximate shape, and then sanded down and sealed with body filler for a smooth, non-porous surface. This section discusses the creation of the nosecone mold, which is a male mold.

First, the finalized CAD model was sliced at 1.5 inch intervals to create a series of contours. These contours, originally saved as DXF files, were converted to PDF at 1:1 scale, and numbers were added to each contour to keep track of their order. They were then printed on poster paper. Next, the contours were cut out and glued to sheets of foam board as templates. Two foam board sizes were purchased: 4 foot by 8 foot and 2 foot by 2 foot. Both sizes were 1.5 inches thick to match the slice intervals. Spray adhesive was used to glue the paper to the foam.



Figure 60: Contours printed on poster paper



Figure 61: Contours glued to foam board

The foam was then cut to shape using a hot wire. A horizontal wood beam was mounted to the side of the large table outside the SAE shop and a nichrome wire was strung vertically between the beam and the table. Both ends of the wire were held by screws. The wire could be tightened or loosened by turning the screws, as the wire was wrapped around the shank of the screw. A power supply provided a

constant current. The leads were attached to the wire-fastening screws. See Figure X below for a diagram representing this setup.

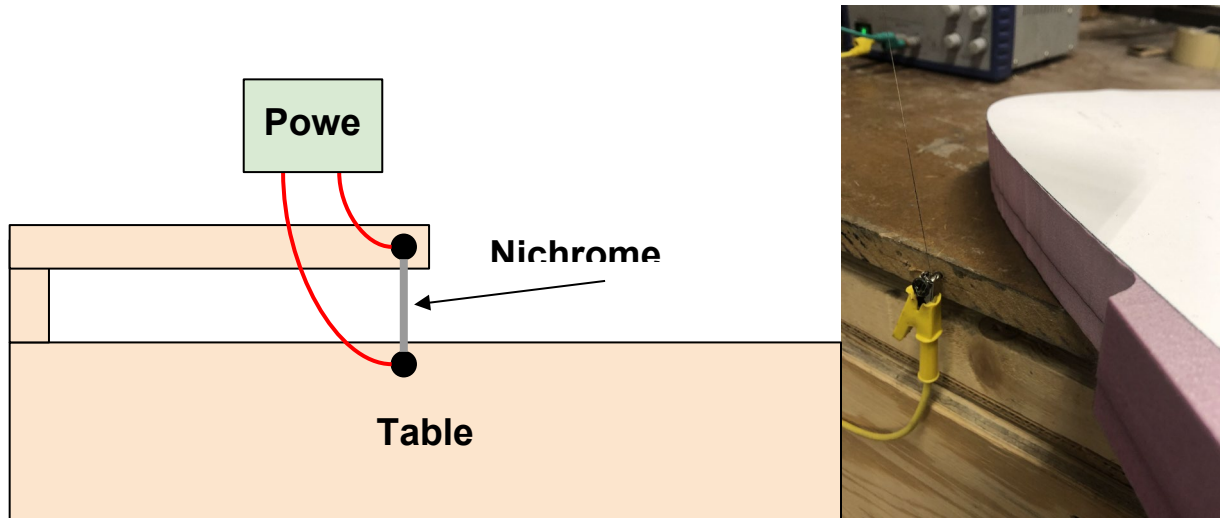


Figure 62: Hot wire cutting setup

This setup was very effective for achieving a clean and even cut with foam. The wire easily sliced the foam but the paper was much more resistant, making it easy to follow the template. It should be noted, however, that setting the wire perfectly vertical and keeping it vertical is extremely difficult. As a result, there was a slight chamfer to the foam pieces. This was only problematic towards the bottom where there was minimal change between cross-sections. Towards the tip, there was enough change in size between layers that this chamfer was not an issue and was sanded away regardless.



Figure 63: Foam cut for nosecone mold

The layers were stacked paper side down so that the slightly smaller face was pointed toward the tip. The mold was assembled by gluing the layers together using the same spray adhesive that was used to attach the paper to the foam. This was mostly effective, but a stronger adhesive would be recommended for future mold-making as some smaller layers separated and had to be re-glued during sanding.

The next step was to sand the “stepped” edges of the foam between paper contours to get a smooth, continuous surface. This was accomplished by sanding with 60 grit sandpaper by hand. Although it was significantly slower to work by hand compared to using a powered sander, hand sanding was chosen out of caution to avoid over-sanding or otherwise damaging the mold. 220 grit was used at the very end to smooth out the rough surface left by the 60 grit.



Figure 64: Mold sanding in progress (left) and complete (right)

The final step was to coat the mold in body filler to seal it and create a smooth surface finish. This was done in the loading bay in the basement of Higgins Labs where the bay door could be partially opened to give appropriate ventilation. Body filler was applied to the full surface of the mold, but was particularly necessary towards the bottom where the chamfer created in the foam cutting process created some concavities. During this process, it was observed that the body filler very slightly melted the foam underneath. Although this was not a problem in terms of shape, the fact that the paper templates did not shrink accordingly left some subtle waviness. Therefore, a second coat of body filler was required to smooth this. Sanding with 220 grit was done using a power sander after the first coat was finished.

Figure 65 below shows the extent of progress reached before campus was closed. The nosecone mold is nearly complete, but needs a couple more areas touched up with additional body filler before final sanding.

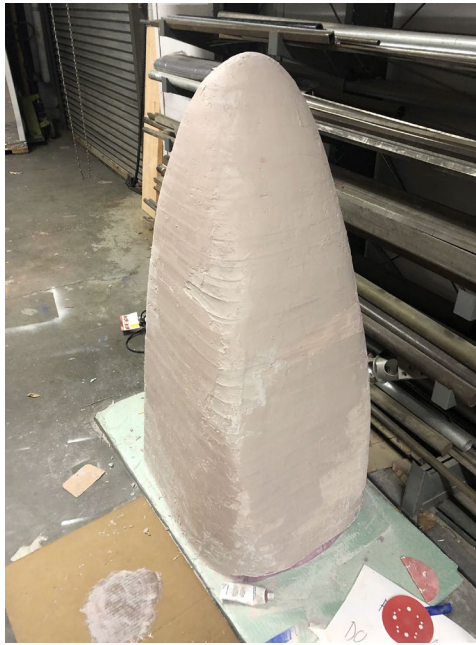


Figure 65: Nearly complete nosecone mold

Next Steps

The next steps for completing the bodywork are covered in detail below. For a summary of the progress made and next steps required, see Appendix B.

Finish Nosecone Mold

The nosecone mold is mostly complete as is; however, there are a few more final steps to finish. First, a few sections still need to be filled with a second coat of body filler. Some sanding will be necessary to smooth out rough patches before applying the second coat. This is only required where concavities remain: smooth sections of the mold already coated with body filler do not require another coat. Lastly, after the body filler is fully hardened, the entire surface should be sanded down with 220 grit to ensure everything is even and free of imperfections.

Assemble Side Pod Mold(s)

It was briefly discussed towards the end of C term whether or not a full side pod should be assembled to shroud the exhaust. Given that the extra time required to make two side pod molds instead of one was likely not available, we determined that a basic sheet metal shroud or other thermal barrier would be sufficient. However, given that the car will no longer be competing at the end of this academic year, this gives ample time to create the second side pod in full. The recommendation is to create a full second side pod if time allows as the car will look far more complete, although a basic heat shield or shroud is preferable in the case of limited time and/or resources.

As for the assembly of the side pod mold(s), the same process used for the nosecone mold is recommended, except with using a female mold instead of a male mold. It was recommended by previous teams that female molds create a better surface finish and are easier to work with for this shape and size of component. Additionally, finding an alternative sealant for the foam that does not cause the slight shrinkage observed with the nosecone mold would be ideal.

Vacuum bagging layup of all components

Although the composite layup steps of the manufacturing process were never reached, this area was heavily researched and a lot of useful information was found that the next team will want to take into consideration. First, there was the choice between vacuum bagging and vacuum infusion. The difference between these two is that vacuum bagging requires epoxy to be applied to the composite fabric before pulling a vacuum on the part, whereas vacuum infusion uses the vacuum force to pull epoxy into and through the fabric. Vacuum infusion was used by the 2019 FSAE team. The team found that the pumps available in the SAE shop were not able to pull and hold a sufficient vacuum, leading to challenges with epoxy not fully saturating the fabric. This is why vacuum bagging was recommended, as it only requires enough pumping capacity to remove air instead of pulling epoxy through fabric. Still, it is recommended to use both pumps in parallel to effectively double the pumping capacity. Each pump is rated for about 2.8 cfm, which would be 5.6 cfm when used together, and the recommended flow rate for vacuum bagging of large components is 4-5 cfm.

The vacuum bagging of the nosecone and side pod(s) will be done with their respective molds. For the side panels and floor panel, these do not require molds as they are almost entirely flat. Instead, it is recommended to use the procedure that the 2019 FSAE team used, which was to simply cut a sheet of composite fabric to the appropriate size and do the vacuum bagging procedure on a large, flat surface. The table outside the SAE shop works well for this. For the side panels, they should be curved to fit around the frame when the epoxy is nearly cured - this will create a slight curve in the panel that will harden in place. The epoxy should be mostly cured about 24 hours after mixing, assuming the epoxy hardener's pot life is 2 hours. This is the longest pot life option generally, and is recommended to maximize working time. When working with the panel, it should be stiff enough to be handled (while keeping it in the bag) but pliable enough to change shape if bent around the curvature of the frame.

Fastening Panels to Frame

After all the panels have been completed, they must be fastened to the frame. The preferable method is quarter-turn fasteners because these allow for quick attachment and removal of panels while still providing a sturdy connection. Quarter-turn fasteners would require tabs welded to the frame for mounting the fastener hardware. The fastener would fit through a hole in the tab and clip to hardware on the back of the tab. This fastener type appears to be a popular choice among other FSAE teams, given the ease of use and low cost. Rough tab placements are currently added to the cumulative SolidWorks model - these locations are not final because they will need to be adjusted to work around any other components.

Ergonomics

Firewall

The firewall is a component required by the rules to protect the driver from the passage of any flame or fluids between the engine bay and the cockpit of the car. For our vehicle, it was designed to serve this purpose but also to provide a rigid place for the foam seat to sit. The firewall was designed out of 0.040” thick aluminum sheet metal in SOLIDWORKS. Once designed, a flat pattern template was derived from the model and printed at 1:1 scale. This allowed for the metal to be cut to shape with electric shears, and then bent to properly fit into the frame on a manual bending brake.

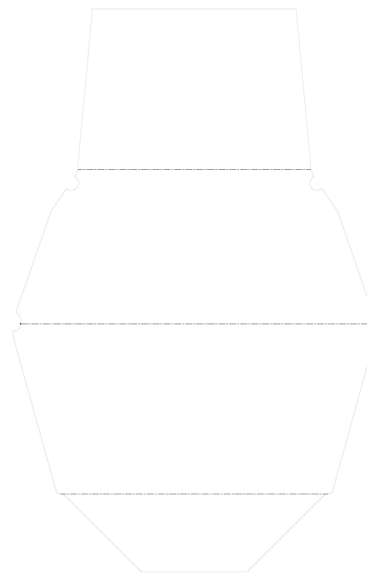
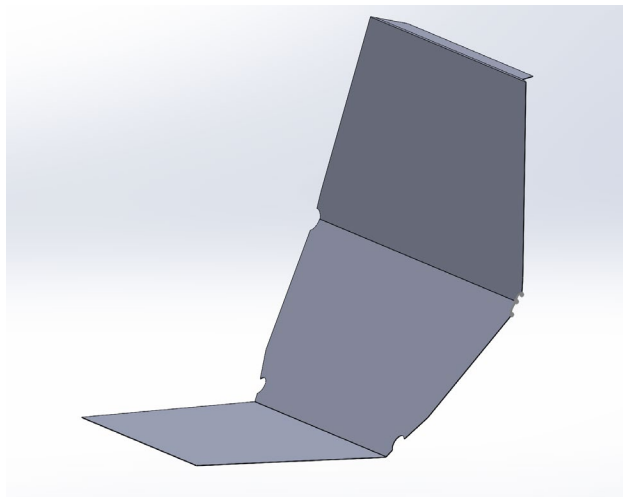


Figure 66: Firewall solid model and accompanying flat pattern template

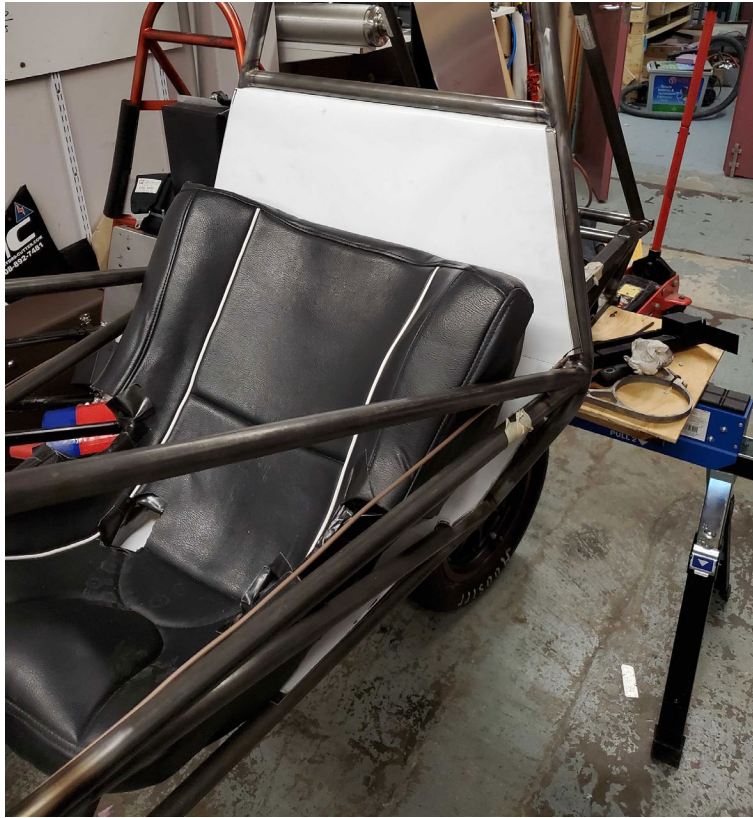


Figure 67: Firewall and Seat in Frame

Digital Sensor System

Looking ahead in the future of the automotive industry, it is undeniable that cars have increasingly developed a digital component. This goes beyond the smart gadgets and features that are selling points today, but it is a crucial aspect of understanding how each car component is performing and could be optimized, along with designing “active” systems with AI and/or controls. With all these things in mind, SAE international is pushing for innovation and digital technologies in the car designed by the universities. The WPI team does not want to stay behind and is integrating computer science in the MQP by developing our own computational capabilities in the car. The long term process of making the car fully digital can be distributed over several projects on multiple MQPs. To start, there needs to be a well-developed collection of data from sensors all over the car, and a reliable way to store and distribute it. This also enables the development of a live-streamed team-view program, in which the engineers can watch and monitor the car as it races. This feature is commonly seen in professional racing teams and it is of high interest to the MQP team and competition judges. The data gathering, streaming, storage and displaying are the critical components for this year's MQP's *Minimum Viable Product* on the Computer Science side.

Objectives

1. Provide accurate and live information about the car and each of its subsystems

The first objective of the digital sensor system on the Formula SAE race car is based on collecting and organizing data from multiple sensors distributed around the car. The car computer needs to individually gather calibrated data from each sensor but also maintain concurrency between each sensor. This means the computer needs to gather synchronous blocks of data from all sensors and stream them in the order they were collected. This is crucial for correlating behaviour of different systems later on.

2. Supply thorough test data to validate design decisions

With access to accurate and live information from the car, the engineering team is able to understand the effects of design decisions and validate testing done from Finite Element Analysis or Computational Fluid Dynamics. There are several subsystems of the car, such as the radiator, that can't be accurately designed to requirements without testing it on a running car. The digital sensor system aims at supplying such a test and validation tool, which not only helps us improve the car's design, but perform better against competition judges.

3. Build a platform where future teams can expand sensing and actuating capabilities of the car's computer

The goal of the platform this year is to focus on key subsystems and on sensing only. For safety and regulation issues, we refrain from controlling any aspect of the car with it. This does not mean it cannot be done in the future. The path for more programmable control systems has to be taken slowly, and base itself on a reliable source of data. The third goal of this year's digital system is to provide that platform.

State of the art

Microcontrollers

The core of the digital sensor system is the car's computer and its sensors. To understand the options available for our project, the most used and supported microcontrollers were analyzed. Those are key attributes as it is our goal to have this system be built upon in the future. To evaluate these microcontrollers, we also looked at the sensors we will use and their compatibility with them.

The Arduino



Figure 68: Arduino UNO microcontroller

The Arduino is a commonly used development board based on open-source technology. It allows for both digital and analog input and output. It is known for its flexibility by being able to interface with a variety of sensors easily and thus building prototypes in fast-paced environments. In contrast, the Arduino does not have a lot of flexibility on its operation system and programming structure. Programs are written in C/C++ and uploaded from another computer. This restricts the variety of sensor drivers to be used, and possible multi-threading. Lastly, fewer options were found for connecting it to the network on its own than in some other options.

The Raspberry Pi

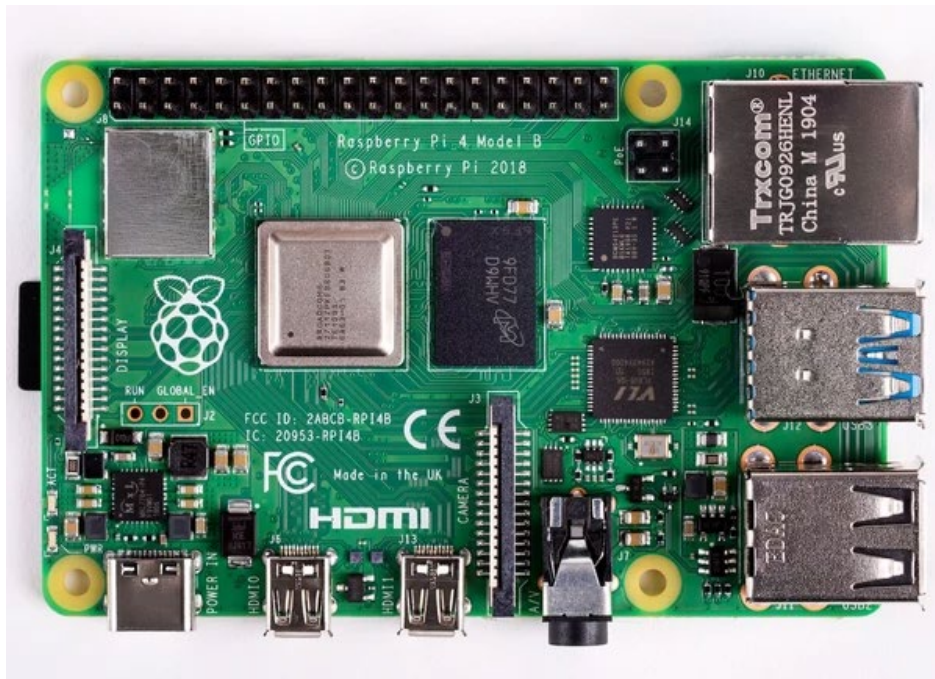


Figure 69: RaspberryPi4 microcomputer

The Raspberry Pi is a low cost powerful minicomputer. It not only can run on multiple operating systems, many based on Linux, but it also can hold its own as a computer with 6 USB, 2 HDMI, and 1 Ethernet ports, as well as Wifi. It is also based on open-source programs which means it has access to a constantly improving list of public libraries and sensor drivers. Because of the multitude of operating systems based on linux, programs can be written on almost any desirable language, such as Python, C/C++, Rust, and C#. It also allows for distributed programs and multi-threading with ease. It supports numerous types of digital input and output like the arduino, but it does not have analog pins. To counteract that however, analog-to-digital converters can be used without any issues.

Other Embedded Systems Development Platforms

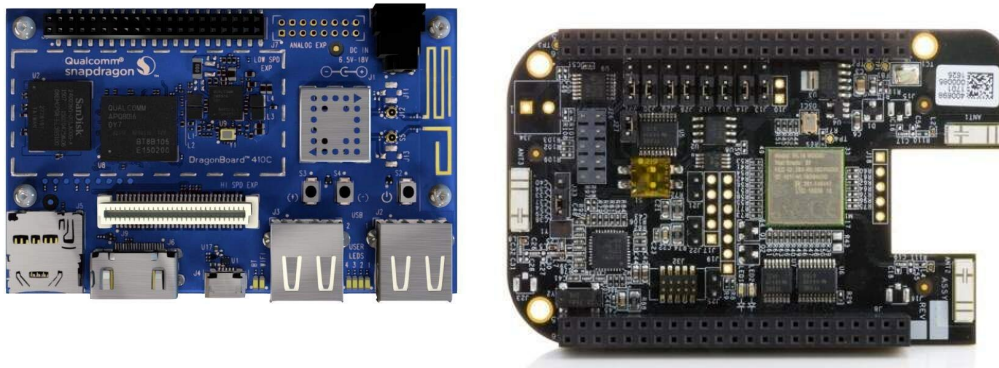


Figure 70: Qualcomm Snapdragon microcontroller & BeagleBone Black microcontroller

There are other interesting options besides the Arduino and Raspberry Pi when it comes to embedded development platforms. A few examples are Qualcomm Snapdragon and the BeagleBone Black, which provide similar hardware and interface specs as the Raspberry Pi and support different operating systems. Their main downside is support and availability of drivers for sensors because their usability worldwide and access to open-source projects is not near the Raspberry Pi or Arduino.

Printed Circuit Boards



Figure 71: Printed Circuit Board of a DVD player

Printed circuit boards are non-programmable and thus not usable for development of the system itself, as a new board would have to be made for every change in program logic. In contrast, it might be an option to consider when looking at controlling certain aspects of the cars with actuators, which require redundancies for risk and safety concerns. A printed circuit board would allow for a reliable behavior that does not depend on a program to work.

Streaming data

The next piece of the digital system is the streaming of the data from the car's computer to the cloud platform. This is summarized to providing constant and reliable internet connection to the car's system.

Wifi

The first option for connecting the car to the internet would be to directly connect the computer to available wifi networks, as most have that capability. That would mean it would require to be within range of routers for the entire time, in a location such as on campus. When moving to other locations, such as the competition racetrack, there is no way of knowing how available a wifi network would be.

Local computer interface

Along with the wifi option, the team could set up a laptop or computer near the car to connect to it via its own broadcasted wifi or bluetooth. The computer then could interface the streaming of data to the server. While wifi range is typically around 150 feet, bluetooth range jumps to 328 feet at its highest capacity. Considering the scale of a racetrack, this could be a viable option only for testing purposes at a small facility.

Cellular Network

Lastly, the majority of the microcontrollers and computers looked at can be expanded with cellular network shields, which can provide 3G and LTE data. After consulting with the main provider's network maps, it was found that AT&T has full coverage of campus and the competition race track in Michigan, thus allowing any network shields compatible with AT&T to be a viable option for the car.

Storing and distributing the data

On-premises server

Servers for storing data and serving as an application host have been around for decades, and for our project there are direct examples the team could build upon, of other racing teams using such. The structure is based around a computer with high memory running an instance of SQL server and configuring its network ports to receive data from the car, and hosting the visualization platform on other computers. These systems require dedicated computers to them, and require a significant amount of work to configure all ports and secure them. It also presents a bottleneck of processing power, as the entire data processing, storage, and streaming is done through the same computer.

Cloud virtual machine

A more recent evolution of the on-premises server is the use of a similar setup with virtual machines in the cloud. The management of the instance is handed off to the cloud provider, which simplifies the configuration of network ports depending on the product. On top of that, it provides a much more flexible access to computational power, as offerings for virtual machines can provide significantly more memory than what an on-premises computer could. The ultimate downside of this option is cost, as the user pays for the hosting of the virtual machine non-stop.

Cloud NO-SQL database and container application

In recent years, cloud technology to take the place of many virtual machines has surged. The term Platform as a Service (PaaS) refers to the approach to hosting applications, databases, etc, with no server or virtual machines. It works based on clusters fully managed by the cloud provider, that provide computational power to applications on demand. That also means the user pays for what they use only when they use it. The variety of products available in this format has also been increasing, which includes NO-SQL databases. These are flexible forms of storage, suitable for development needs. While SQL databases require one to define the structure of data from the beginning, NO-SQL does not.

Visualizing the data

D3.js

D3 is a data driven visualization tool written in Javascript. Instead of drawing graphs and shapes over and over, it creates such within an SVG (Scalable vector graphic). Although the steep learning curve, it allows immense flexibility of what is built and is able to bind its elements to datasets. For our project, the key aspect is that as data changes, the graphical elements can be animated to change as well. It does so without redrawing each element as any static plotting or chart library would, leading to a faster and smoother interface. The most most important advantage of D3.js is its flexibility and adaptability to different website frameworks. It is capable of doing so with the large community supporting it, the vast number of examples one can get online, and the fact it is based on a non-proprietary framework. It's flexibility can also come as a challenge however, as it comes with a steep learning curve for learning how to structure and build complex graphics.

HighCharts

HighCharts is a close competitor of D3 in the market, also having a variety of dynamic graphs available and good support online. It is, however, built on a more template style, which limits the flexibility of making very customized graphs. On top of that, it is a commercial option blocked by licenses. This is an obstacle for using it in this project but also means there are less users and good examples to build upon in the community.

Objectives for each subsystem

Car Dynamics

The objective of the digital sensor system, when it comes to general car dynamics and driving, is to improve the car's overall performance and driveability. The key metrics within the car to understand performance are speed, acceleration, slip angle, gyroscope angles, and gear shifting along the racing path. These ought to be correlated with driver's actions described by throttle position, steering angle, and brake pressure, as they are the main forms of input and control they have. The main challenge associated with this objective is the fine tuning of allowed engine power, and sensibility of the brakes and steering. The goal in the end is to improve our performance in competition phases such as the endurance (22km timed trial), skid-pad (cornering ability evaluation), and autocross (maneuverability evaluation).

Aerodynamics and radiator flow

The goal for the digital sensor system when it comes to aerodynamics and radiator flow is to improve the design and validate testing of the car's main body, side-pods, and radiator (both size and position). Computational fluid dynamics cannot be relied on without physical testing to validate it, which is critical when making design decisions about all aero related parts. A significant challenge the team has had in recent years is sizing the radiator appropriately. This means projecting enough air flow to cool down the engine while creating the minimum drag possible through smaller or more angled radiators. We

hope that this testing and validation from the sensor system, mainly via air pressure, humidity and temperature, will allow for more accurate and less oversized radiator designs.

Drivetrain and steering

Similarly to the approach to general car dynamics, the sensor system intends to improve our understanding of the internal aspects of the drivetrain and steering subsystems, with the same performance improvement goals. We hope to understand the correlations between each wheel's speed, steering angle, transmission, braking and traction on the wheels. Observing this will allow the team to identify critical issues and bottlenecks for the system to behave as expected without loss of control or power.

System Layout

RaspberryPi and Sensors

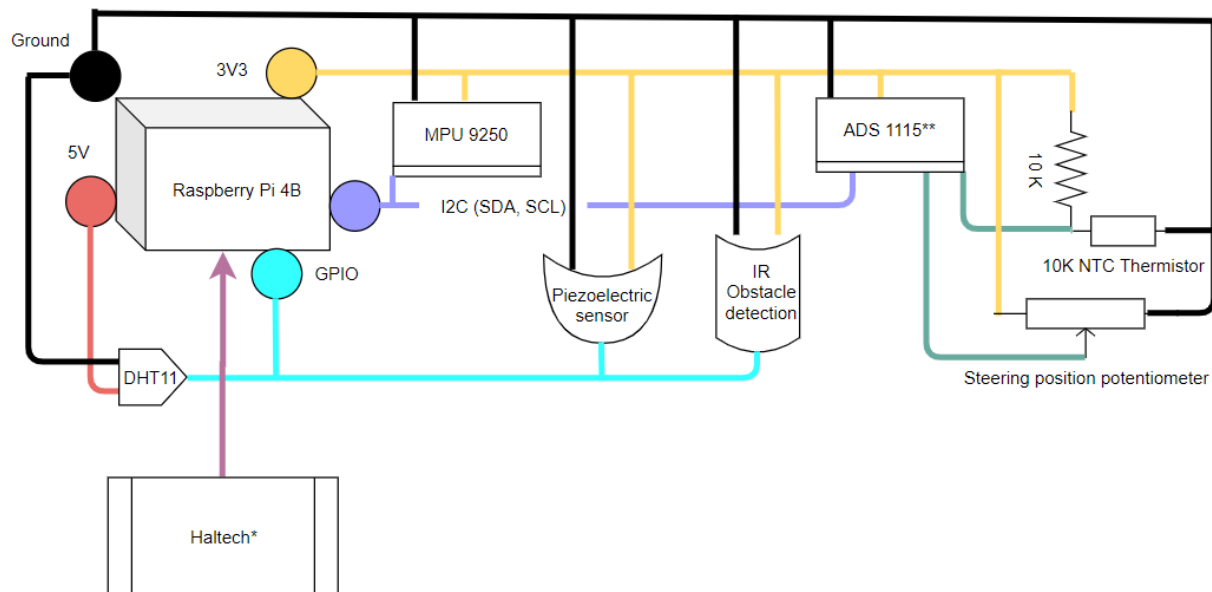


Figure 72: Sensor Wiring Diagram

The RaspberryPi is the core of the sensor system of the car. It provides the common ground for all components, 5V source, and 3V3 source. With all sensors connected to the same source and ground, they interface with the computer's GPIO (General-purpose input/output) and I2C (Inter-integrated circuit) interfaces. These two methods of communication are based on digital signals, which is why the analog signal from certain sensors is converted to digital. The diagram above represents all sensors used and how they are connected. It is important to note it does not represent the exact number of sensors for each type, but how they fit in the system. This is important as the engineering team can fine tune the requirement for, say, thermistors or area pressure sensors with flexibility. Such flexibility is possible as the RaspberryPi has few limitations on the number of pins it provides.

The computer does however, limit the current through all pins to be cumulatively less than 51 mA. In case the system gets near the limit, it can be relieved by moving the voltage source to outside of the RaspberryPi's system, while making sure such source shares the same common ground. Such adaptation would reduce the current through the microcontroller board to the signals received only. It is also important to note another limitation that is already taken into account in this design, which is the maximum voltage allowed in the interface pins. Both GPIO and I2C protocols limit the voltage input to be at most 3.3V, which is why almost all sensors only use a source at that level. Looking at the layout above, there are three main digital sensors, two analog sensors, a digital I2C protocol sensor, and a I2C protocol analog-to-digital converter.

MPU 9250 - Acceleration and Gyroscope

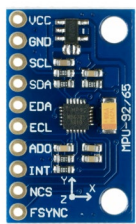


Figure 73: MPU 9250 Sensor Board

Datasheet: <https://invensense.tdk.com/wp-content/uploads/2015/02/PS-MPU-9250A-01-v1.1.pdf>

Register Map: https://cdn.sparkfun.com/assets/learn_tutorials/5/5/0/MPU-9250-Register-Map.pdf

VCC: 3.3V

Signal: Digital/I2C - Uses default slave address of 0x68, with settings and data points in different registers, as defined in the register map.

Library: <https://github.com/FaBoPlatform/FaBo9AXIS-MPU9250-Python>

Output: Acceleratio (X, Y, and Z), and Gyroscope (X, Y, and Z)

The MPU 9250 is an IMU (Inertial Measurement Unit) critical for the car to understand it's movement and orientation. Not only we will be able to analyze its linear acceleration, but also other g-forces that the driver and car experiences. On top of that, not only will we know exactly the orientation of the car on the cardinal system, but we will be able to see its lateral and frontal tilt on actions such as turning and braking. These are often important by directly affecting traction on wheels and risk of an accident. To use this sensor, we connect it to the SDA (Serial Data) and SCL (Serial Clock) ports on the RaspberryPi I2C bus. The sensor can be configured and calibrated using input registers that can take pre-determined values, as determined in the datasheet. For example, the current set-up uses an 8g scale for acceleration and calibrates the gyroscope using the starting magnetometer readings. This sensor allows for multiple discrete readings, based on the design choice. Because the readings are based on a magnetometer, it has little delay in updating its values.

ADS1115 - Analog to Digital Converter

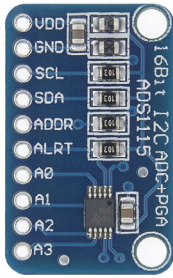


Figure 74: ADS 1115 Analog to Digital Converter Board

Datasheet: <https://cdn-shop.adafruit.com/datasheets/ads1115.pdf>

VCC: 3.3V

Signal: Digital/I2C - Uses default slave address of 0x48, with each analog signal processed to different registers, as well as gain settings.

Library: https://github.com/adafruit/Adafruit_CircuitPython_ADS1x15

Output: Voltage read on each of its analog ports.

The ADS1115 is an analog-to-digital converter critical to processing any analog signal from sensors. It shares the same I2C bus as the IMU, meaning they connect to the same SDA and SCL ports on the RaspberryPi. Each ADS1115 has 4 analog ports (A0, A1, A2, and A3), and multiple of itself can be connected in parallel to the same I2C bus if there are more analog signals to be processed. It can read single signals or differences. While the first will contrast the voltage of a pin to ground, the second mode gives the voltage difference between two pins.

Different gain settings can be used on different pins, as it is specified on each read. These will vary by reducing the voltage scale it reads while increasing accuracy. This converter outputs a 15-bit number, with the lowest 15-bit number (-32767) corresponding to the lowest voltage in the gain setting, and the highest (-32767) to the highest voltage in the gain setting. The gain settings available are the following:

- Gain of 2/3: +/- 6.144 V (Lowest accuracy)
- 1: +/- 4.096 V
- 2: +/- 2.048 V
- 4 +/- 1.024 V
- 8 +/- 0.512 V
- 16 +/- 0.256 V (Highest accuracy)

Each use case and sensor will require a different gain setting, but such should always be the highest gain and accuracy possible maintaining all expected signals within its range. It is important to note that because the unit is powered by 3.3V, it cannot process signals higher than that.

IR Obstacle Detection Sensor - Wheel Speed

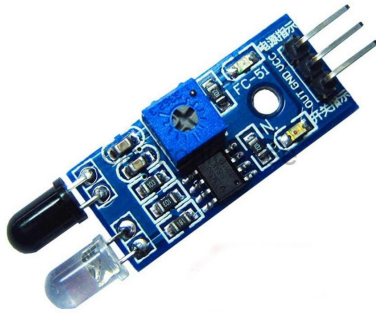


Figure 75: Infrared obstacle detection sensor

Datasheet: https://www.rhydolabz.com/documents/26/IR_line_obstacle_detection.pdf

VCC: 3.3V

Signal: Digital/GPIO - Sends 1 for obstacle detected and 0 for no obstacle.

Output: Whether or not it detects an object at its configured distance.

The obstacle detection sensor is used to detect whether or not something reflects its infrared light, with a variable sensitivity. This sensitivity is manually adjusted through the potentiometer on its board, which in turn changes the distance an object needs to be at to trigger the sensor signal. For the car, the sensor could be used for detecting obstacles on the track but it will primarily be used to compute wheel speed of all 4 wheels. It can do so with a surface extrusion being present somewhere in the wheel, that can be detected by the sensor on every rotation. Because of the sensor's accuracy, such extrusion can be only a few millimeters of the wheel plate. With that, the sensor can give us the interval between each full rotation, or the period. This algorithm can ultimately give us the wheel speed with good consistency. Calibration will be necessary to understand the optimal shape of the extrusion so that the sensor is the most accurate at various rotation speeds.

Understanding the rotation speed of each wheel is critical to evaluate traction on each wheel, power transmission through the drivetrain, and optimal gear configurations. In addition, it can also be used as a driver assisting tool, as wheel rotation is a main factor in gear shifting decision making. Finding the optimal windows to shift up and down gears, by looking at the rpm, can be a significant performance improvement for the car in the competition.

DHT11 - Temperature and humidity

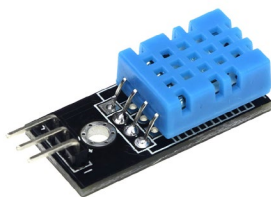


Figure 76: DHT11 Temperature and humidity sensor

Datasheet: <https://cdn-learn.adafruit.com/downloads/pdf/dht.pdf?timestamp=1589126511>

VCC: 5V

Signal: Digital/GPIO - Cyclic pattern of 1s and 0s indicate temperature and humidity.

Library: https://github.com/adafruit/Adafruit_CircuitPython_DHT

Output: Temperature in degrees celsius and humidity in saturation %.

The humidity and temperature sensor is one of the main components for understanding airflow and temperature distributions around the car. This sensor will primarily be used in the side pod next to the radiator but can also be placed next to the exhaust system. The humidity information is important as it can be directly correlated with the airflow in the area it is at, as more airflow leads to a smaller concentration of water particles in the air. This relationship is not yet understood fully however, and will require calibration when the car is running. If it turns out that the humidity information is not valuable in any place around the car, then this sensor can be replaced by thermistors only. To read this sensor, the python library provided by Adafruit can be used to build the driver. Readings can be done at any time interval desired by the design team, keeping in mind that the sensor has a small delay to respond to changes in the environment's temperature and humidity.

10K NTC Thermistor - Temperature



Figure 77: 10K NTC Thermistor with 50cm

Overview of NTC Thermistors: <http://www.resistorguide.com/ntc-thermistor/>

VCC: 3.3V

Signal: Analog - Used in voltage divider with 10K pull-up resistor - Processed through analog to digital converter.

Output: Temperature

The NTC (negative-temperature coefficient) thermistor works by having a resistance that changes based on its temperature. They are manufactured to have 10 k-ohms resistance at 25°C and have that resistance increase or decrease along with temperature on a non-linear behavior. Because of that, it needs to be calibrated with a thermometer or other temperature sensor, and using exponential regression. The calibration can be done to find the temperature in function of voltage on an amplifier gain of 1 and range of 0-3.3V, when in series with a 10K resistor as shown in the layout. Each thermistor uses around 0.165

mA which allows for multiple to be used in the car. With that flexibility, temperature can be read in multiple critical points around the engine, radiator, and driver.

SP2800 - Steering Position

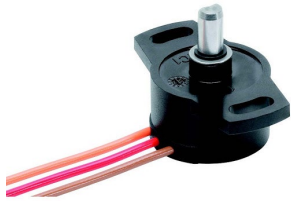


Figure 78: SP2800 Steering position sensor / potentiometer

Datasheet: <https://www.novotechnik.com/pdfs/SP2800.pdf>

VCC: 3.3V

Signal: Analog - Used in voltage divider with 5K pull-up resistor - Processed through analog to digital converter.

Output: Steering angle

The goal of this sensor is to record the driver's actions with the steering system, and how it turns the car as it drives. It mostly looks at driver performance but can also serve as an indication to adjustments to be made on the physical system such as changing the steering ratio between the wheel axis and steering wheel angles. Because it is a 5k ohms potentiometer, it is read by using a voltage divider with another 5k ohms resistor. The analog signal sent from the pair then, will vary between 0 and around 1.6V, in direct correlation with the angle being read by the potentiometer, from 0° to 360°.

Piezoelectric Sensor & Vibration Module - Area Pressure

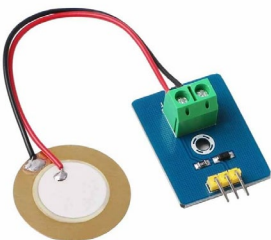


Figure 79: HiLetgo Piezoelectric Sensor Analog Ceramic Vibration Sensor Module

Datasheet: https://media.digikey.com/pdf/Data%20Sheets/DFRobot%20PDFs/DFR0052_Web.pdf

VCC: 3.3V

Signal: Analog - Processed through analog to digital converter

Output: Air pressure

The pressure and vibration sensor acts as a converter from air flow and its mechanical vibrations to voltage oscillations which are read through the analog signal. The attributes of air flow and its variability are critical for understanding how the car's body and other channels of air are performing. The interpretation of this sensor is based on the comparison of, say, high and low pressure scenarios. It can be calibrated with a barometer tool pressed against its plate at different levels.

Haltech - Speed, Gear, Brake Pressure, and Throttle Position

The Haltech is the current engine control system present in the car, which operates the gas line and engine shutoff, for example. The goal is to interface with it only to extract its data but not interfere with its functionality. From it, we would be able to retrieve the car's speed, gear, brake pressure, and throttle position. These are critical for understanding the car's linear movement, driver performance, and drivetrain performance. This integration was not finalized as of the writing of this report as the team lost access to the car and its tools given the COVID-19 pandemic shutdown.

The Network Connection and Read Concurrency

All sensors connected to the car will be interfaced with the main program in the RaspberryPi with their own driver, which internally manages read settings such as voltage gain in the case of analog signals, or the computation of wheel rotation interval when looking at the obstacle detector. These drivers have the outside interfacing functions to set up, read, and release the serial connection. Reading the serial connection will be done multiple times at the request of the main program. Currently these functions are synchronous but implementing them asynchronously would significantly improve performance. The read functions return the values read and the OS-time clock they were read. This guarantees that if any interrupts occur, the read is maintained true to when it corresponds to in the real world.

The main program's function is to loop over requests over all sensors over a specific time interval. Again, this time interval is defined by time elapsed in the OS-clock, and not on the program's clock. At the end of every block read, the main program organizes the block of data acquired and sends a request to the server with the information compacted. To improve performance of this function, the program can be split into two threads which share a buffer. While the main thread packs the sensor data and puts it into the buffer, the network connection thread maintains an http connection open, and constantly sends to the server any blocks of data from the buffer as they become available.

The server connection itself is done through a cellular network, provided by AT&T's IoT products. The LTE modem *Wistron NeWeb Corporation (WNC) MI4A2A* (Guide: http://cloudconnectkits.org/sites/default/files/GettingStartedGuide_Pi3_LTE_rv1-3_0_0.pdf) allows the Raspberry Pi to connect to an AT&T SIM card as shown below:

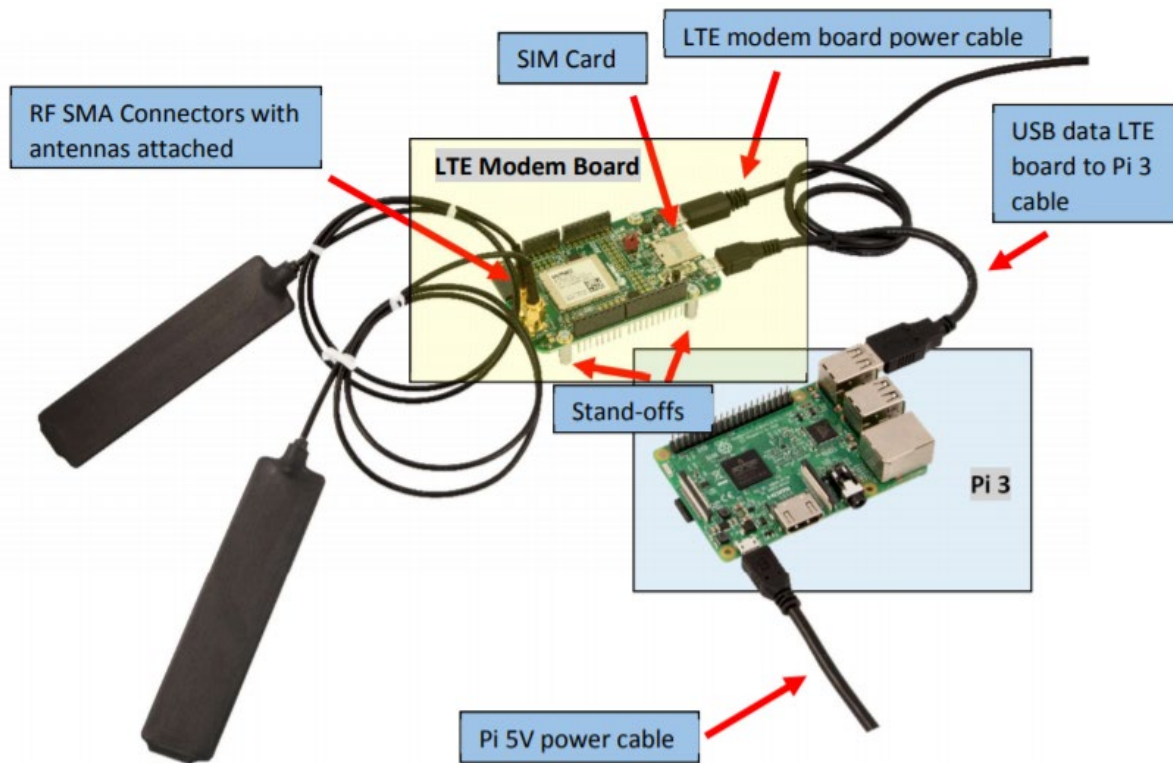


Figure 80: Connection layout between Raspberry Pi and LTE Modem Board

This setup allows the car's computer to access the internet from anywhere the AT&T LTE or IoT network reaches. While the LTE network is the same as we have on smartphones, the IoT network is a special product that provides increased range in exchange for lower speeds. Testing with the system integrated need to be done to access the network load of the sensor system, but analysis of the LTE network maps available at <https://www.att.com/maps/wireless-coverage.html> show that the LTE range would be sufficient to cover both the racetrack in Michigan and the WPI campus. The access to the cellular network also provides us with the car's location, which is useful from a data gathering perspective.

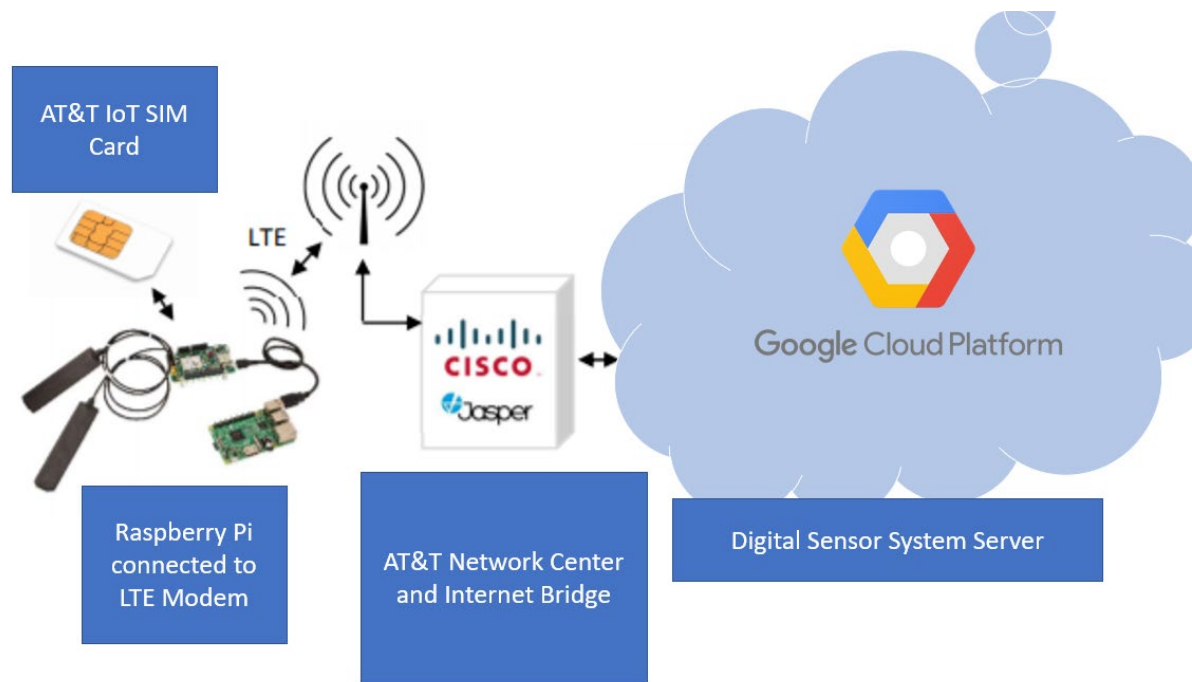


Figure 81: System layout between Raspberry Pi, LTE modem, and cloud network

The Server Architecture

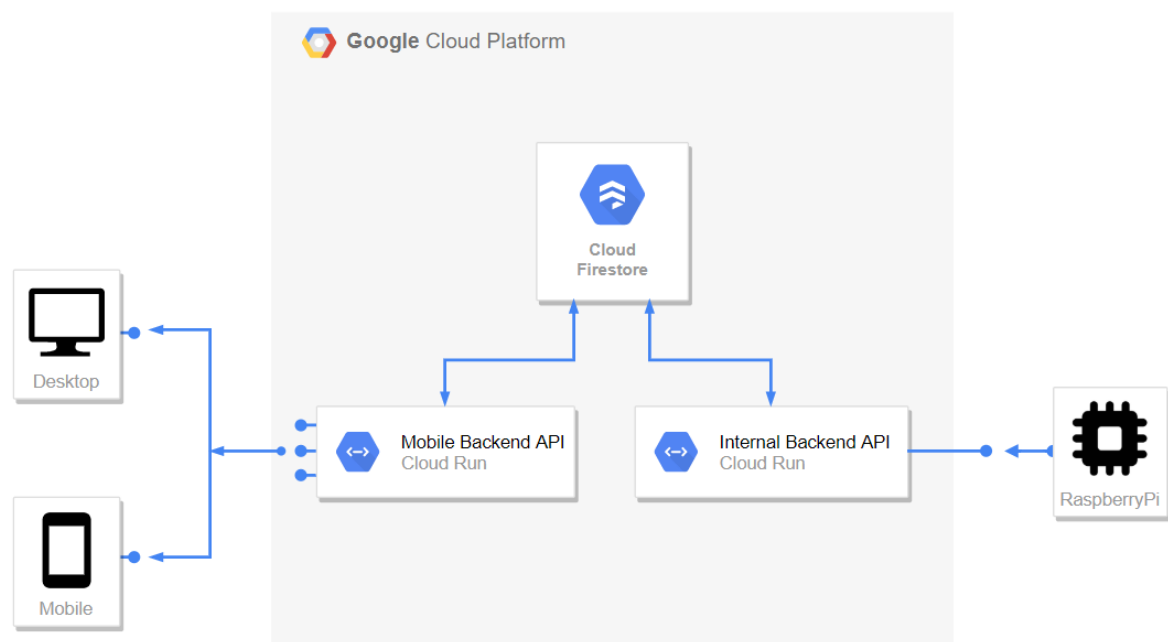


Figure 82: Server architecture for Google Cloud Platform instances

The layout above shows how the integration is done from the data generation in the car, to the

data storage in the cloud, and to the user interface. The technology stack used was provided by Google Cloud Platform, specifically *Cloud Firestore* and *Cloud Run*. These products are serverless and optimized for realtime updates on multiple platforms, ideal for the team's needs. The serverless aspects means it adjusts assigned computing power based on projected demand, costing less than options ran in servers and providing more reliability. Meanwhile, the realtime trait relates to the data storage ability to add, modify, and delete data on one end without locking the access from other clients or providing inaccurate "dirty" reads. In other words, it allows us the car to constantly send new sensors while any user in the visualization interface maintains access to reliable information.

The RaspberryPi will continuously send data to the cloud server maintaining an http connection open to the internal backend API (Application programming interface). This can be done with a single http connection over several seconds, or refreshing connections that send the data in chunked mode that are reopened every second or two. To the writing of this report, the connection between the RaspberryPi and API was not fully tested and optimized, and only used individual connections for each block of sensor readings.

The internal backend API is written in Node Js and built on a container for Google's Cloud Run service. The API has a single endpoint as it only expects the same request from the RaspberryPi with time stamped sensor data. The main role of this endpoint is to process and organize all data points, which come compressed and not ready for the user interface. It is its function to place it into the structure they are stored in the database, which is also ready for the user interface graphics. It also updates the metadata for the most up to date displayable data set. This endpoint is a singleton and will always maintain a single connection with a single car's computer, which is also more efficient to do the most intense data processing work.

The mobile backend API however, can have multiple instances, and then will have limited work to do with the data besides streaming it from the database to the client user interface. Currently, it uses usual HTTP requests to transmit the information, but it is highly recommended that the system is switched to HTTP 2.0 in order to make use of server push and stream multiple blocks of data in the same connections. This API initially only has one endpoint, which is used by the live user interface. It can, however, host endpoints in the future for other data visualization tools that might focus on a specific car system or on aggregate data.

The User Interface

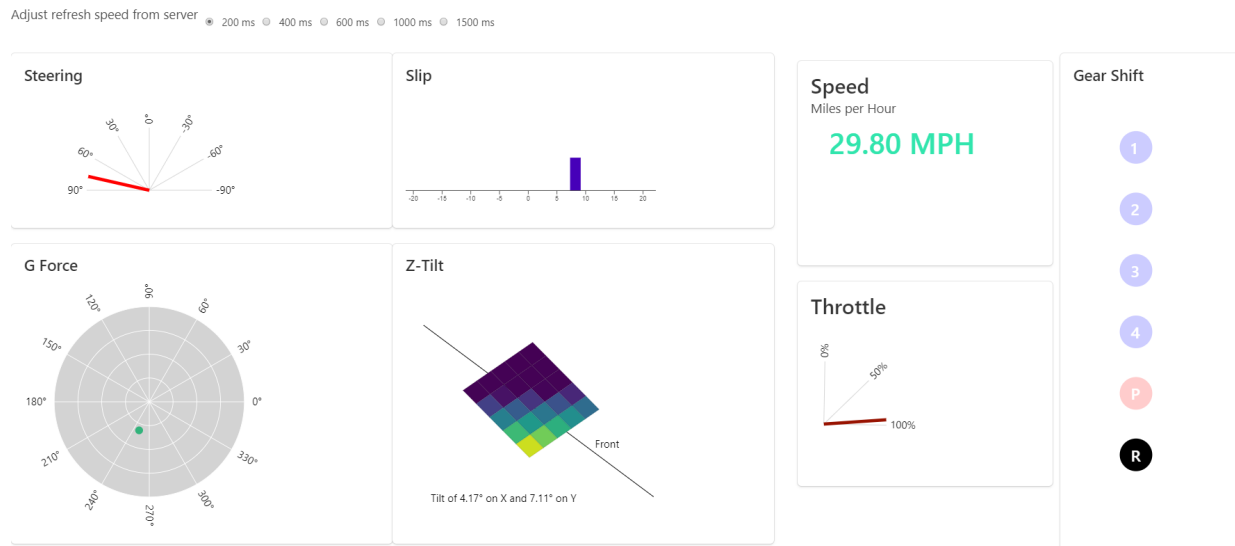


Figure 83: Partial screenshot of user interface

The user interface was built as a modular platform for live data visualization. While it implemented several graphical interfaces for different data points, it is flexible and built around modules that can be moved around and replaced. The main inspiration for the interface was from interfaces in car and airplane dashboard, primarily because of the primitives used to make reading so many graphs at once easier. This design evolved from that by focusing on key research questions:

- How can each data point be best represented to its scale?
- What are the graphical elements that highlight the key scales for each data type? (such as steering angle, tilt magnitude, etc)
- How do the graphical elements vary according to the scale?
- How do such changes perform under different refresh intervals?
- How are smaller or bigger changes to a value within a timed refresh get highlighted? (Such as slip angle increasing size and heat of primitives color)

With the project hosted in github pages, I was able to send them the link for it and get quick feedback. Not only were changes suggested to small details such as color scales and shapes, but users evaluating the platform also recommended adjustable refresh rates. Even though there might be new data from the car every X interval, a user might want to slow the graphics to only update every 3X interval. This was a simple toggle feature implemented on the top of the page which helped the accessibility of the interface.

The client itself was built mainly on Bulma and D3.js. Bulma was used broadly to build the layout of the page which allowed it to be modular and mobile ready. Bulma also helped with certain styling on the header of the page. The main tool used, however, was D3.js versions 4 and 5. The transition mechanism it provides was the critical piece of every interface when creating graphics that update constantly but don't require a page refresh. With all graphics following the same update procedure, their data was binded to a central client function which orchestrated the data requests to the server.

The Data Points and Visualization

Processed Data		Raw Data	
for the user interface	<i>units</i>	from the car	<i>units</i>
Acceleration (Magnitude on XY plane, Direction)	m/s^2	Acceleration (x,y,z)	m/s^2
Orientation on XY plane	<i>degrees</i>	Gyroscope (x,y,z)	<i>degrees</i>
Lateral tilt	<i>degrees</i>	Wheel rotation period (each)	<i>s</i>
Frontal tilt	<i>degrees</i>	Brake pressure (front and back)	<i>psi</i>
Wheel speed (each)	<i>rotations per minute</i>	Air pressure (each sensor)	<i>psi</i>
Brake use (front and back)	<i>degrees</i>	Temperature (each sensor)	<i>oC</i>
Air pressure for mapped locations	<i>psi</i>	Steering position	<i>degrees</i>
Temperature for mapped locations	<i>oC</i>	Throttle position	<i>degrees</i>
Steering position	<i>degrees</i>	Gear	<i>id</i>
Throttle position	<i>degrees</i>	GPS Position	<i>Lat, Long</i>
Gear	<i>id</i>	Speed	<i>m/s</i>
Path driven	<i>[Lat, Long]</i>		
Speed	<i>m/s</i>		
Traction (on each wheel)	<i>%</i>		
Slip angle	<i>degrees</i>		
Average wheel speed	<i>rotations per minute</i>		

Table 2: Data points for raw and processed API endpoints

The data from the RaspberryPi and the sensors described will come in the most compact and unprocessed way possible, to alleviate the load on its own memory but also the network connection. Such data will then be processed in the next steps server-side where computational power does not have the same limitations. The table above shows both the target processed data as well as what is provided by the RaspberryPi. Certain outputs are directly drawn from what is given from the car's computer, while others are computed from a combination of multiple or over a time series.

Acceleration (Magnitude on XY plane, Direction)

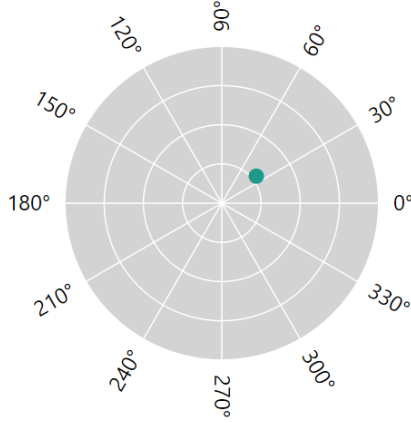


Figure 84: Acceleration / G force plot

An important data point to the car's dynamic, its acceleration, is displayed in a radial plot representing the view from above the car. The magnitude of the acceleration force in that plane is displayed by the distance of the plot point to the center and is calculated from the acceleration data on x and y axis:

$$a_{plot} = |proj_{xy}(a)| = \sqrt{a_x^2 + a_y^2}$$

Meanwhile, the angle the point is added on the radial plot is:

$$a_{\theta} = \theta \text{ in } \{asin(a_x/a_{plot})\} \cap \{acos(a_y/a_{plot})\}$$

Lastly the circles in the radial plot are a scale representing 1, 2, 3, and 4g, respectively (g being the gravitational constant approximated to 9.8m/s²).

Orientation on XY plane

The orientation of the car on the XY plane is a virtual compass for the car. A reference such as North or East should be calibrated as the 0 degree origin for the car, and the magnetometer will then provide this data point. The z axis of the magnetometer will, without processing, represent the car's orientation on the XY plane and act as a compass.

Lateral tilt & Frontal tilt

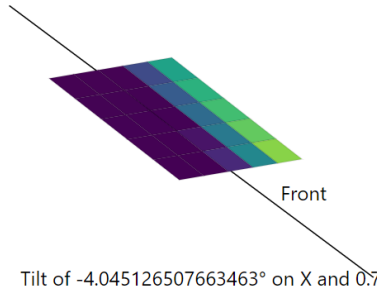


Figure 85: Tilt plot

The tilt graph will display the possible orientation the car might get on the tilt test itself or on racing, on its X and Y axis. The implementation of such was done in the user interface by applying the same tilt to a 3D plane and highlighting different positions with surface coloring. The equation was applied so that every point of the plane accounted for some X and Y tilt, depending on its distance from the center, the magnetometer.

$P_{tilted} = rot_y(\theta_{ytilt}) * rot_x(\theta_{xtilt}) * [P_x; P_y; 0]$ where P_x and P_y are all points of the surface before rotation and rot_x / rot_y are the 3D rotation matrices.

This approach allowed the highlighting of angles which are usually at a small scale in this orientation.

Wheel speed (individuals and average)

The wheel speed is processed from the interval/period between rotations calculated by the obstacle detection sensors in each wheel. These values are expected to be the same for all wheels but can vary if external conditions affect traction or reading. In order to improve the quality of the data, each wheel can have a running average of read values and discard reads that spike out of place (due to missing the rotation for example).

Brake use (front and back)

Data from the brake can be processed by understanding how much the driver is stepping on and using the brake. This is done by knowing the maximum and minimum operating pressures of the brake system, and finding where each reading fits in.

$$Brake\ use = 100\% * (B_{reading} - B_{minimum}) / (B_{maximum} - B_{minimum})$$

Air pressure for mapped locations

The most important factors from a data processing and visualization perspective will be mapping each data point to where in the car the sensor is and what have been the recorded maximums and minimums. For example, the user should be able to clearly see a reading of 12 psi next to the radiator, and that values there have ranged from 10 to 16 psi.

Temperature for mapped locations

Temperature readings are important to understand the status and performance of multiple parts of the car. On display, they are mapped to specific locations and linked to a history of running average in that location, as well as maximums and minimums. For example, the user should be able to clearly see a reading of 60°C around the exhaust, and that in the last 5 minutes of the engine running the average temperature was 58°C.

Steering position

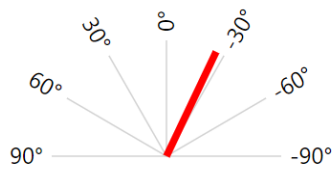


Figure 86: Steering position display

Steering position is the angle that the wheels of the car are turned at any moment in time. The graphic is bounded by the turning ratio of the car itself. This data point is directly calculated from the steering position sensor in the car, which after calibration should need no processing to give the platform the angle for graphing. The interface shows angle with the semi-circle plot shown above, where the red bar moves to the corresponding angle..

Throttle position

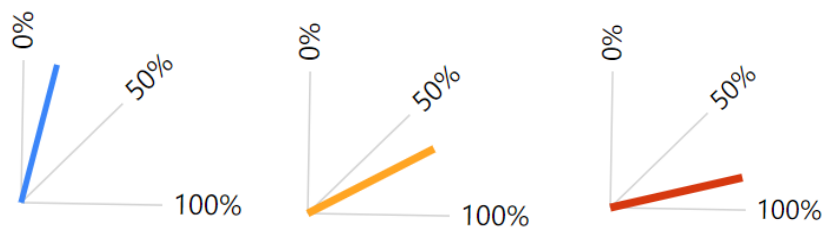


Figure 87: Three instances of the throttle position display

Throttle position is displayed based on the amount the driver is stepping on the throttle, from its lowest and maximum operating positions. The graph uses a quarter-circle and a bar that changes color with different values, on top of indicating the angle. The 0% mark is high in the middle and the 100% on the bottom to represent the position of the throttle pedal in each situation.

Gear

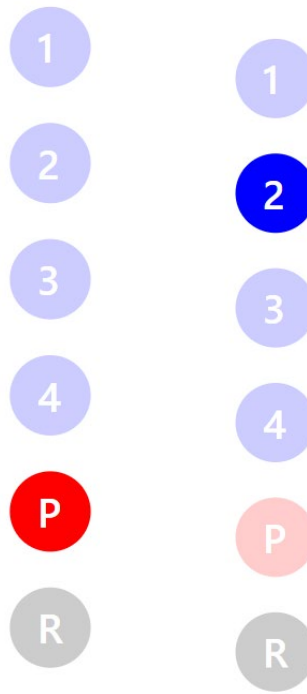


Figure 88: Two instances of the Gear display

The gear graphic is a discrete display of which gear the car is in at the moment. The data comes from the haltech and is directly sent to the platform with no need for processing. It is displayed by having all possible gears as lights that “turn on” when active, with parking (P) and reverse (R) gears having different colors.

Path driven

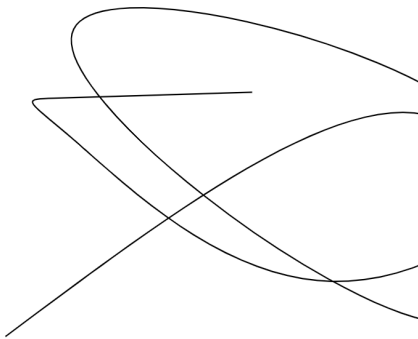


Figure 89: Screenshot of the path driven plot

The path driven is a cumulative interpolation of multiple latitude and longitude readings over time. It intends to show the user in the interface where the car has been relative to its current position, but

most importantly, what kind of sections it has driven through (straight line, elbow curve, etc). The current position of the car in the path is always in the center of the graph, with the entire graph and path driven through moving in response. The computation of the path is done with the update of an array of car positions, from most recent to furthest. This array can have a limit in size so the entire path driven so far is not shown, but only the recent. Additionally, to reduce the load on the network connection, this is the only graphic that caches the previous data on the client side. This allows the server to only send the most up-to-date position, instead of always resending the entire path driven through.

Speed

12.52 MPH 67.05 MPH

Figure 90: Two instances of the speed display

The speed display focuses on the numerical value of the linear speed of the car, given by the Haltech engine control system. On top of the numerical value, the speed value changes the color it is displayed at, as shown above. The color scale starts from blue (lowest values) and goes to orange, then red (highest values).

Traction

Traction will be a metric displayed for each wheel, representing the power transmission between the tires and ground. It is percentage based, where 100% means there is no loss of energy from the wheel rotating and the ground being pushed back relative to the car. Alternatively, 0% represents complete tire slip and no movement being applied to the ground. Traction for each wheel is computed from comparing the wheel speed with the car's linear speed.

$Traction = 100\% * v_{car} / (\omega_{wheel} * (1 \text{ min}/60s) * 2\pi * r_{wheel})$ given
wheel speed ω_{wheel} in rpm and wheel radius r_{wheel} in meters.

Slip angle

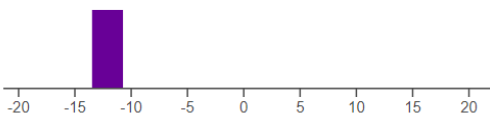


Figure 91: Slip angle graphic

The slip angle display shows the angle between the direction the front wheels are pointing at and the direction of travel. The graphic uses a vertical bar that moves left and right on its scale, with 0° of slip being in the middle. The bar increases width and gets a darker color as it moves away from the middle, in

order to visually highlight changes as well. The slip angle is computed combining acceleration, gyroscope, and steering position data. By constantly integrating the values from the accelerometer, the current velocity vector can be always updated. At the same time, the direction the wheels are pointing at are a combination of the steering position and gyroscope on the z axis. The angle difference between both vectors is then the slip angle.

$$V_t = V_{t-1} + a_{t-1} \text{ for } t \text{ in seconds}$$

$$\text{Wheel Angle } \theta = \beta_{\text{steering position}} + \gamma_{\text{Gyroscope } Z}$$

$$V_\delta = \delta \text{ in } \{\sin(V_x/|V|)\} \cap \{\cos(V_y/|V|)\} \text{ where } |V| = \sqrt{V_x^2 + V_y^2}$$

$$\text{Then, } \alpha_{\text{slip}} = V_\delta - \text{Wheel}_\theta$$

Conclusion & Results - Digital Sensor System

The design and implementation processes of the digital sensor system for the car highlighted several challenges and opportunities. Over the last few years, there hasn't been a fully integrated digital sensor system in WPI's formula SAE car. This is not only due to the obstacles of combining computer science and computer engineering into an already fast paced project, but also because it is a relatively new feature for these cars to have. Most of the existing technology that connects sensors all the way to live visualization platforms is proprietary to car manufacturers and professional racing teams. The work done on the digital sensor system at WPI this year can represent a significant step for our team to have powerful capabilities in the future. Not only does it let engineers understand their car in ways they couldn't before, but it helps the team make more efficient use of their resources. Being a university hosted team, the effort to make the most out of budgets, sponsorships, and team members' availability is one of the highest priorities.

Technical roadblocks throughout the year but especially the COVID-19 pandemic did not allow for the system described in this report to be fully implemented and tested. The Raspberry Pi and each sensor used by it was wired and tested individually successfully. They displayed results as expected and were calibrated to the environment they were in. It is important to note that initially the goal was to use the Rust programming language for the sensor drivers and concurrency management. Rust is a relatively new language with several advantages regarding memory management and thread safety. Over time, however, it started presenting internal compatibility issues that would have had to wait for an update. Because of that, the implementation of the sensors and any system on the Raspberry Pi was done based on Python and its libraries. *The source code for the python client on the Raspberry Pi is available at https://github.com/Oporto/mqp_fsae_digital/tree/master/python-client.*

The hardware for this system on the car was not fully integrated. Due to restricted access to the lab after the state and federal shutdown, the Haltech control system of the engine was not connected to the Raspberry Pi. The cellular network modem was also not configured with the rest of the system as it was of lower priority given the current development context and that other systems took longer than expected to

be finalized. This was done in a way that the SIM card for AT&T was not yet activated and the credit that it comes with not consumed.

The server side of the system, on Google's Cloud Platform, was built and tested. While the mobile API endpoints to the user interface are developed, the internal endpoint to the RaspberryPi will need some adjusting as the integration is done in the future. The network connection between the Cloud Run container and the Firestore instance is secured and established using IAM (Identity and Access Management). This allows for any interactions to be then created between the endpoints and the data itself, be it simply inserting/extracting or processing. The API endpoints and container files were all built using Node.js and the Express package, with the source code being available at:

https://github.com/Oporto/mqp_fsae_digital/tree/master/server/rawdata_endpoints_nodejs.

The user interface, and live data visualization platform, was developed and deployed at <https://oporto.github.io/final>. While it would already display the data from several sensors, it is missing the implementation for some such as wheel speed and traction. The insight from this visualization also depends on the validity of the data it is showing in real-time. Because there is no driving car in our team connected to the sensors yet, the data displayed is random. The use of colors and scale make it easy for a user to notice important changes on different displays at the same time. When it comes to improving the visualization, studies can be performed to validate the specific color choices and display positions. Another example of possible future change, is that the track display can implement a fade where the oldest points added to the path are faded out, in order to facilitate viewing the current path when the old ones overlap. The source code for the user interface is available at:

https://github.com/Oporto/mqp_fsae_digital/tree/master/ui-live.

The current state of the entire digital sensor system has significant room for improvement and flexibility. It does not restrict itself to one car, location, or number of data points to be gathered. The technologies chosen are able to scale effectively and are accessible so that future teams can continue this work. This system can also be replicated into multiple cars, as the WPI formula SAE team moves to finalizing the combustion engine one but also to start a formula electric next year. Looking at the challenge of migrating to the electric powered race car in the future, this digital system has the potential to be a powerful tool in accelerating our learning and improving communication between teams.

Appendix A: SOLIDWORKS Studies

Pedal Box Version 1

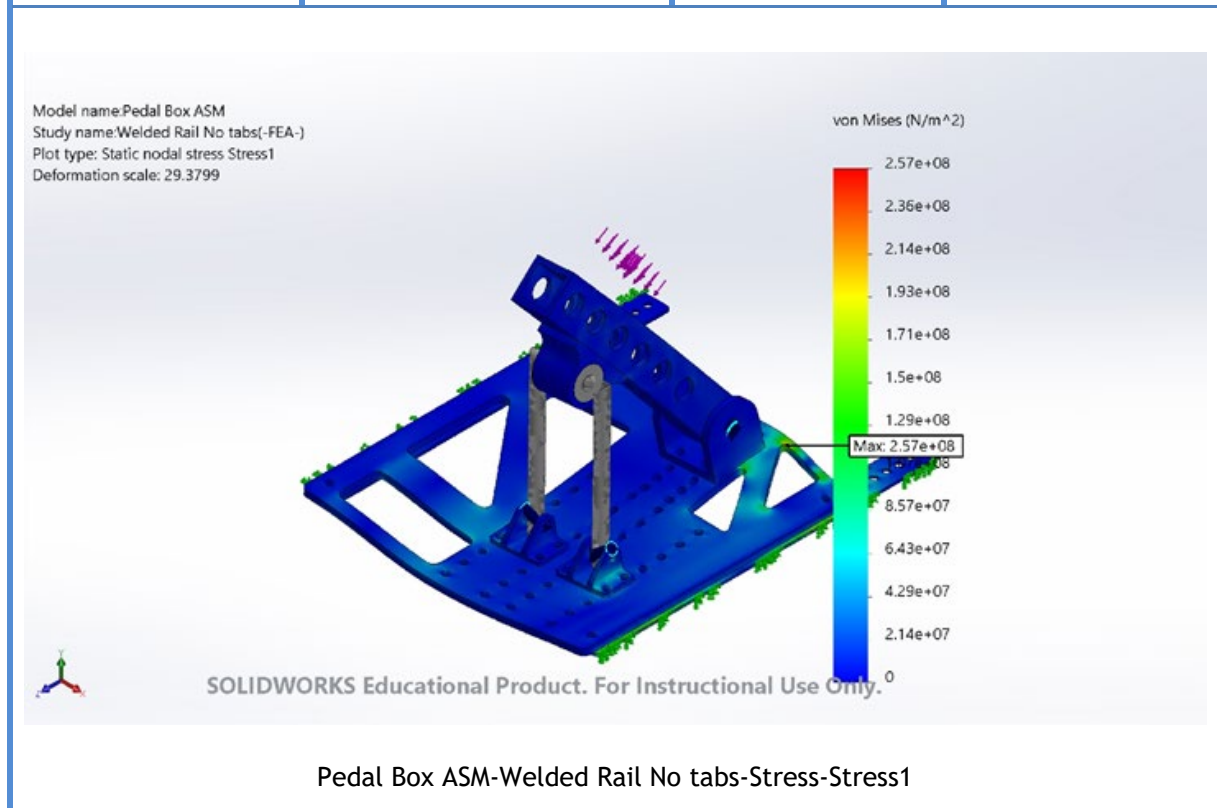
Reaction forces

Selection set	Units	Sum X	Sum Y	Sum Z	Resultant
Entire Model	N	0.000163615	711.465	-1,128.99	1,334.47

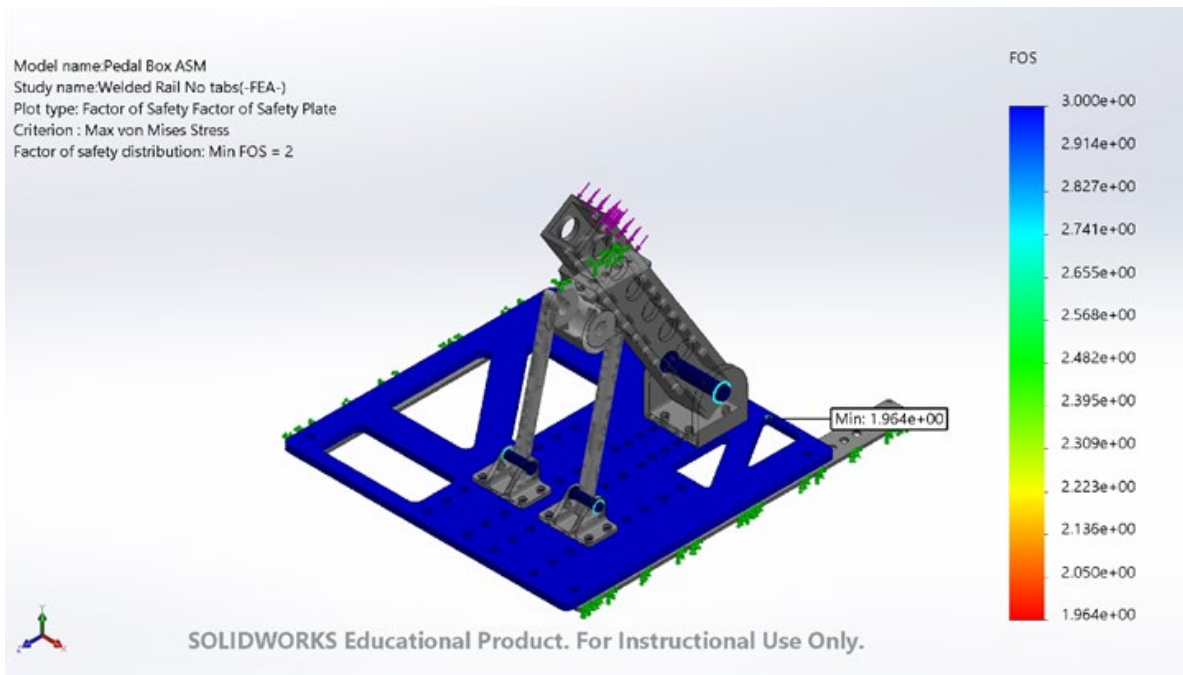
Reaction Moments

Selection set	Units	Sum X	Sum Y	Sum Z	Resultant
Entire Model	N.m	0	0	0	1e-33

Name	Type	Min	Max
Stress1	VON: von Mises Stress	0N/m ²	2.57e+08 N/m ²
		Node: 115601	Node: 35824



Name	Type	Min	Max
Factor of Safety Plate	Max von Mises Stress	1.964e+00	3.000e+00
		Node: 35824	Node: 23464



Pedal Box ASM-Welded Rail No tabs-Factor of Safety-Factor of Safety Plate

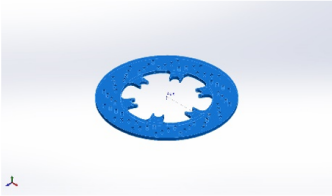
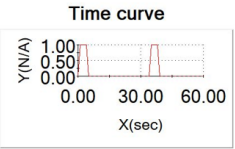
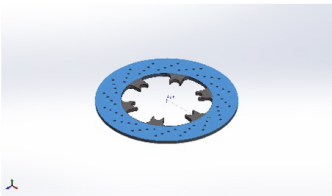
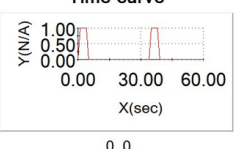
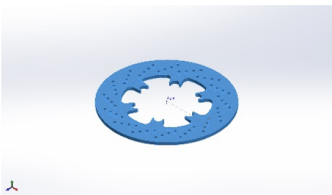
Drilled Brake Rotor

Material Properties

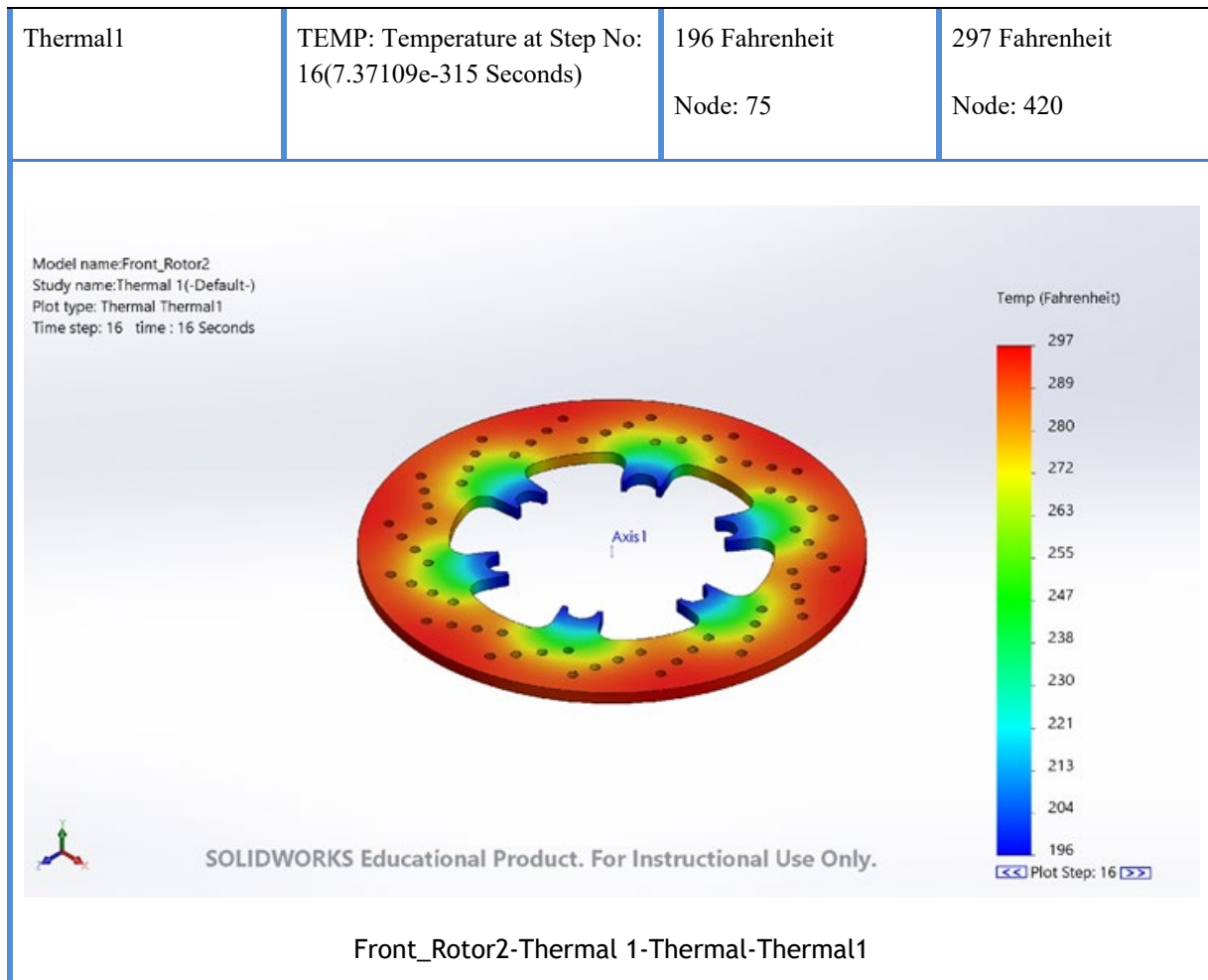
Model Reference	Properties	Components
-----------------	------------	------------

			SolidBody 1(Split Line1)(Front_ Rotor2)
	Name:	KAZ Ductile Iron	
	Model type:	Linear Elastic Isotropic	
	Default failure criterion:	Unknown	
	Thermal conductivity:	53.3 W/(m.K)	
	Specific heat:	510 J/(kg.K)	
	Mass density:	7,200 kg/m ³	

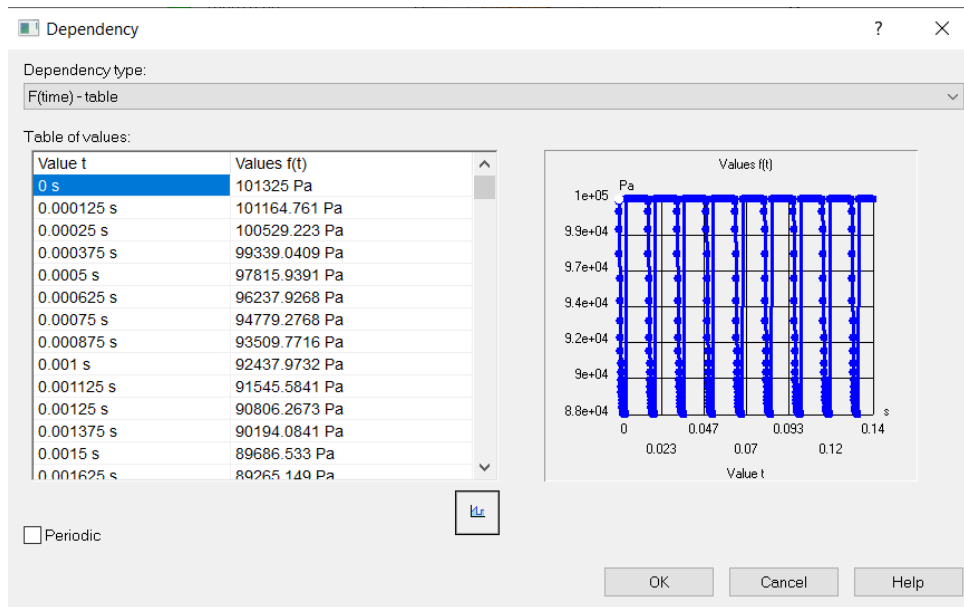
Thermal Loads

Load name	Load Image	Load Details	Function Curve
Convection-1		Entities: 117 face(s) Convection Coefficient: W/(m ² .K) Time variation: On Temperature variation: Off Bulk Ambient Temperature: 293 Kelvin Time variation: Off	 Time curve 0, 0
Heat Power-1		Entities: 2 face(s) Heat Power Value: 5050.06 W Time variation: on	 Time curve 0, 0
Temperature-1		Entities: 1 Solid Body (s) Initial temperature: 293 Kelvin	

Name	Type	Min	Max
------	------	-----	-----



Plenum Input Conditions



Appendix B: Status of Components

Intake System

Component	Status	Next Steps
3D printed intake components	Manufactured	<ul style="list-style-type: none">• Coat all components with XTC-3D, and assemble the plenum with epoxy and carbon fiber to be one complete piece

Exhaust System

Component	Status	Next Steps
Tubing	Delivered	<ul style="list-style-type: none">• Cutting of components and welding into place

Engine Mounts

Component	Status	Next Steps
Front Mounts	Done	
Rear Mounts	Done	
Engine Mount Spacers	Length determined in SolidWorks model	<ul style="list-style-type: none">• Purchase Material• Manufacture on lathe
Engine Mount Threaded Rod	Correct size threaded rod is acquired. Reuse the same nuts.	<ul style="list-style-type: none">• Cut threaded rods to correct length

Brake System

Component	Status	Next Steps
Pedal Plate	Done	
Pedal Plate Rails	Done	

Brake Pedal	V2 Design Complete	Manufacturing <ul style="list-style-type: none"> • Waterjet pedal body • Make end plate out of square tube cut out or equivalent thickness sheet metal
Brake Rotors	Two designs complete (drilled and solid)	Manufacturing <ul style="list-style-type: none"> • Rotor blanks need to be machined to the correct thickness • The shape of each iteration can then be waterjet • The rotors should be surface ground or turned to final thickness
Brake Master Cylinder Brackets	Design done, manufacturing in progress	Finish manufacturing (CNC machine)
Brake Pedal Bracket	Design done, manufacturing in progress	Finish manufacturing (CNC machine)
Throttle Pedal Mount	Design Required	Needs to be designed and manufactured

Suspension

Component	Status	Next Steps
Front Upright	Design done, material ordered	Finish manufacturing (CNC machine)
Rear Upright	Design done, manufacturing in progress	Manufacturing <ul style="list-style-type: none"> • Drill upper and lower ball joint holes • Drill toe link hole • Drill and tap brake caliper holes • Drill pushrod hole
Front Rockers	Design done, material ordered, bearings ordered	Finish manufacturing (CNC machine)
Rear Rockers	Design done, material ordered, bearings ordered	Finish manufacturing (CNC machine)

Front Upper Control Arms	Final design not complete, material ordered	Adjustments need to be made based on the finalized mounting points.
Front Lower Control Arms	Final design not complete, material ordered	Adjustments need to be made based on the finalized mounting points.
Rear Upper Control Arms	Final design not complete, material ordered	Adjustments need to be made based on the finalized mounting points.
Rear Lower Control Arms	Final design not complete, material ordered	Adjustments need to be made based on the finalized mounting points.
Control Arm Clevises	Manufacturing for the initial design is complete but the final design was changed.	Finish manufacturing (CNC machine)

Bodywork

Component	Status	Next Steps
Nosecone	Design done, mold manufacturing in progress	Manufacturing <ul style="list-style-type: none"> • Finish mold (seal and sand) • Vacuum bagging using mold
Side pod(s)	Design of right side pod done	Design <ul style="list-style-type: none"> • Left side pod around exhaust (optional) Manufacturing <ul style="list-style-type: none"> • Mold(s) • Vacuum bagging using mold(s)
Side panels	Design done	Manufacturing <ul style="list-style-type: none"> • Vacuum bagging of flat sheet cut to size • Curve sheet to frame shape when epoxy is nearly cured
Floor panel	Not started	Design <ul style="list-style-type: none"> • Measure dimensions of floor area

		Manufacturing <ul style="list-style-type: none"> ● Vacuum bagging of flat sheet cut to size
Fastening system	Type and rough placement selected	<ul style="list-style-type: none"> ● Determine final locations ● Purchase fasteners ● Manufacture tabs ● Drill holes for fasteners in panels ● Trim panels as necessary

Appendix C: Calculations

Brake System: Front

Assumptions:

Vehicle Weight (W)= 550 lb.

Acceleration (x direction) (a_x)=1.6 g=coefficient of friction between tire and road (μ_{tire})

Center of gravity height (h)=12 in.

Car length (l)= 60 in.

Rotor effective radius (r_{rotor})= 3 in.

Coefficient of friction between pad and rotor (μ_{pad})=0.42

Brake bias (b)=0.5

Pedal ratio (pr)= 2.48

Calculate total weight transfer in x direction:

$$\Delta W_x = \frac{h}{l} * (W * a_x)$$

ΔW_x = 176.19 lb.

Calculate total weight that must be stopped by front wheels:

$$W_{total\ front} = \Delta W_x + \frac{W}{2}$$

$W_{total\ front}$ = 451.19 lb.f

Calculate required front braking torque to lock front wheels:

Tire radius (r) = 8 in.

Required front braking torque $\tau_{front} = r * W_{total\ front} * \mu_{tire}$

$$\tau_{front} = 5775.21 \text{ in}\cdot\text{lb.}$$

$$\text{Torque per front wheel } (\tau_{front \text{ per wheel}}) = 5775.21/2 = 2887.6 \text{ in}\cdot\text{lb.}$$

Next, parameters in an Excel spreadsheet were adjusted to arrive at the desired driver lockup pedal force range of 90 to 100 lb. f:

Calculate master cylinder and piston areas:

$$\text{Master cylinder bore (MC}_{\text{bore front}}) = 0.625 \text{ in.}$$

$$\text{MC}_{\text{area front}} = ((\text{MC}_{\text{bore front}}/2)^2) * \pi = 0.31 \text{ in.}^2$$

$$\text{Piston diameter (D}_{\text{piston}}) = 0.98 \text{ in.}$$

$$\text{Number of pistons} = 4 \text{ per caliper}$$

$$\text{Piston area (A}_{\text{piston}}) = ((\text{D}_{\text{piston}}/2)^2) * \pi * \text{number of pistons}$$

$$\text{A}_{\text{piston}} = 3.04 \text{ in.}^2$$

Calculate force required on pedal for lockup:

$$\text{Force required by driver (F}_{\text{driver}}) = \left(\frac{\tau_{front \text{ per wheel}}}{\text{MC}_{\text{bore front}}} \right) / (2 * r_{\text{rotor}} * \mu_{\text{pad}} * \text{A}_{\text{piston}}) / (pr * b)$$

$$\text{F}_{\text{driver}} = 93.24 \text{ lb. f}$$

Calculate line pressure:

$$\text{Front line pressure (P}_{\text{front}}) = (\text{F}_{\text{driver}} * pr * b) / \text{MC}_{\text{area front}}$$

$$\text{P}_{\text{front}} = 375.73 \text{ psi}$$

Brake System: Rear

Assumptions:

Vehicle Weight (W)= 550 lb.

Acceleration (x direction) (a_x)=1.6 g=coefficient of friction between tire and road (μ_{tire})

Center of gravity height (h)=12 in.

Car length (l)= 60 in.

Rotor effective radius (r_{rotor})= 3 in.

Coefficient of friction between pad and rotor (μ_{pad})=0.42

Brake bias (b)=0.5

Pedal ratio (pr)= 2.48

Calculate total weight transfer in x direction:

$$\Delta W_x = \frac{h}{l} * (W * a_x)$$

$$\Delta W_x = 176.19 \text{ lb.}$$

Calculate total weight that must be stopped by rear wheels:

$$W_{\text{total rear}} = \frac{W}{2} - \Delta W_x$$

$$W_{\text{total rear}} = 98.81 \text{ lb.f}$$

Calculate required rear braking torque to lock rear wheels:

Tire radius (r) = 8 in.

Required front braking torque $\tau_{rear} = r * W_{\text{total rear}} * \mu_{tire}$

$$\tau_{rear} = 1264.79 \text{ in*lb.}$$

Torque per rear wheel ($\tau_{rear \text{ per wheel}}$)= $1264.79/2 = 632.39 \text{ in*lb.}$

Next, parameters in an Excel spreadsheet were adjusted to arrive at the desired driver lockup pedal force range of 90 to 100 lb. f:

Calculate master cylinder and piston areas:

Master cylinder bore (MC_{bore rear})= 1 in.

$$MC_{\text{area rear}} = ((MC_{\text{bore rear}}/2)^2) * \pi = 0.79 \text{ in.}^2$$

Piston diameter (D_{piston})= 0.98 in.

Number of pistons= 2 per caliper

Piston area (A_{piston})= ((D_{piston})/2)^2 * π * number of pistons

$$A_{\text{piston}} = 1.52 \text{ in.}^2$$

Calculate force required on pedal for lockup:

Force required by driver ($F_{\text{driver}} = \frac{\tau_{\text{rear per wheel}}}{MC_{\text{bore rear}}} / (2 * r_{\text{rotor}} * \mu_{\text{pad}} * A_{\text{piston}}) / (pr * b)$)

$F_{\text{driver}} = 104.55 \text{ lb. f}$

Calculate line pressure:

Rear line pressure ($P_{\text{rear}} = (F_{\text{driver}} * pr * b) / MC_{\text{area rear}}$)

$P_{\text{front}} = 164.13 \text{ psi}$

Appendix D: References:

1. Antanaitis, D. and Rifici, A., "The Effect of Rotor Crossdrilling on Brake Performance," SAE Technical Paper 2006-01-0691, 2006, <https://doi.org/10.4271/2006-01-0691>.
2. D. L. M. William F. Milliken, Race Car Vehicle Dynamics, Warrendale, PA: SAE International, 1995.
3. B. Beckman, The Physics of Racing, Burbank, CA, 1991
4. M. Giaraffa, "Tech Tip: Springs and Dampers, Part one," [Online]. Available: <https://optimung.com/springsdampers1/>. [Accessed 17 January 2019]
5. M. Giaraffa, "Tech Tip: Springs and Dampers, Part Two," [Online]. Available: <https://optimung.com/springs-dampers-part-two/>. [Accessed 17 January 2019]
6. M. Giaraffa, "Tech Tip: Springs and Dampers, Part Three," [Online]. Available: <https://optimung.com/tech-tip-springs-dampers-part-three/>. [Accessed 17 January 2019]
7. M. Giaraffa, "Tech Tip: Springs and Dampers, Part Four," [Online]. Available: <https://optimung.com/spring-dampers-part-four/>. [Accessed 17 January 2019]
8. M. Giaraffa, "Tech Tip: Springs and Dampers, Part Five," [Online]. Available: <https://optimung.com/spring-dampers-part-five/>. [Accessed 17 January 2019]
9. M. Giaraffa, "Tech Tip: Springs and Dampers, Part Six," [Online]. Available: <https://optimung.com/spring-dampers-part-six/>. [Accessed 17 January 2019]